

# Current developments in electromagnetic induction methods

Heinrich Brasse

Universidad Libre de Berlín

# A possible classification of the geoelectric methods with regard to frequency

## 1) DC-methods

DC geoelectrics (DCR, VES)

Method of induced polarization (IP)

Self or spontaneous potential method (SP)

Magnetometric Resistivity (MMR)



## 2) Electromagnetic methods with low frequencies (induction methods)

Magnetotellurics (MT), geomagnetic deep sounding (GDS)  
Particularly: Audio Magnetotellurics (AMT), Controlled  
Source AMT (CSAMT),  
VLF, VLF-R, Radio Magnetotellurics (RMT)  
*Unimportant today: Tellurics, AFMAG*

„Real“ electromagnetic induction methods, classified in  
frequency domain and time domain methods (FD, TD)  
Many FD-methods, e.g., Slingram, Turam  
TDEM- or TEM- (Transient-EM) methods

SNMR Surface Nuclear Magnetic Resonance

### 3) ground-penetrating-radar (EMR, GPR)

All methods can be utilized in boreholes and offshore

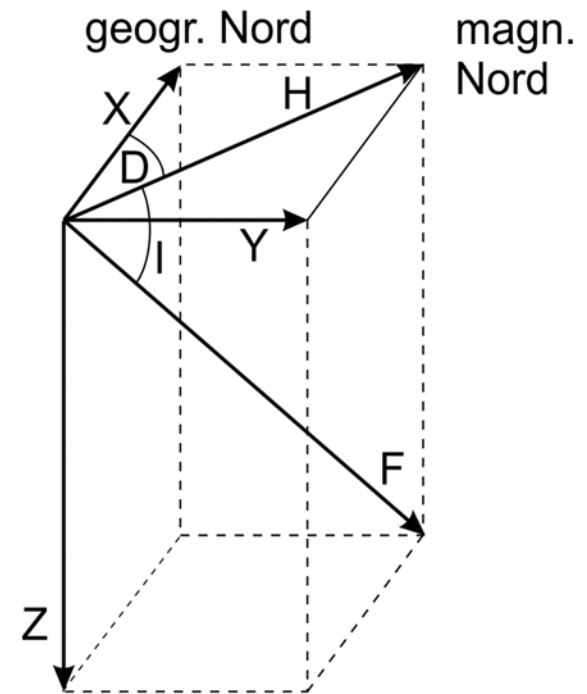
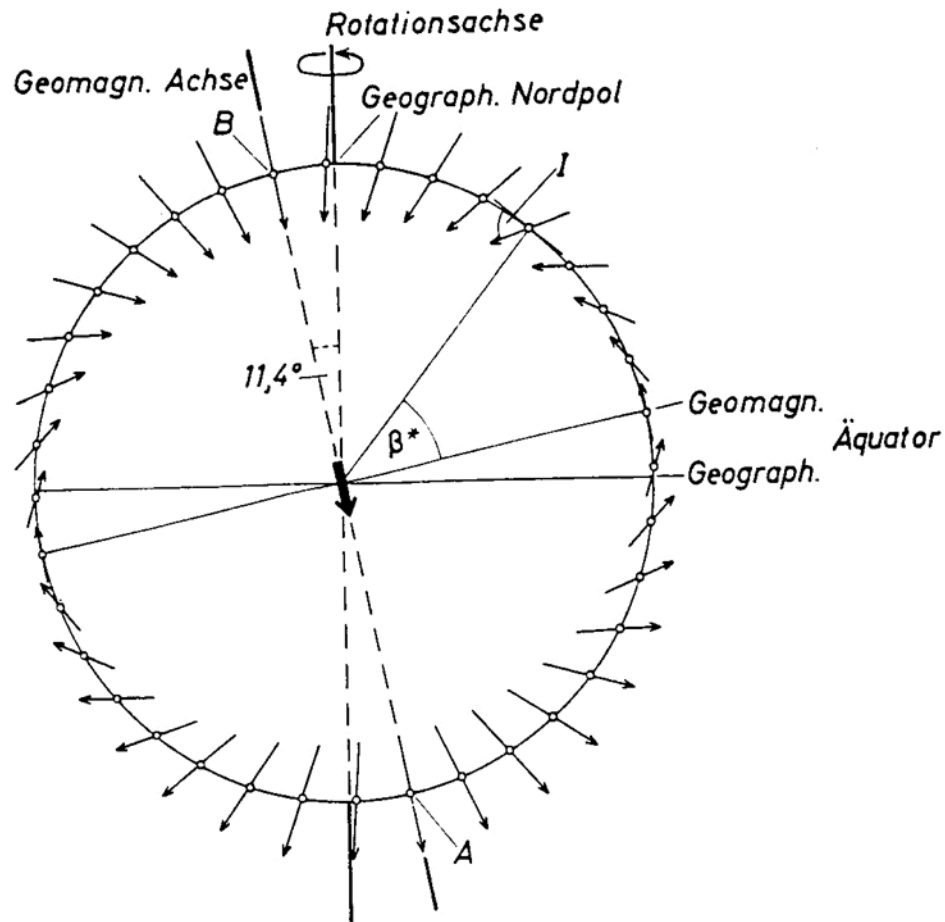
If only magnetic fields are utilized → aero geophysical methods

Depth range: upper meters to upper mantle !

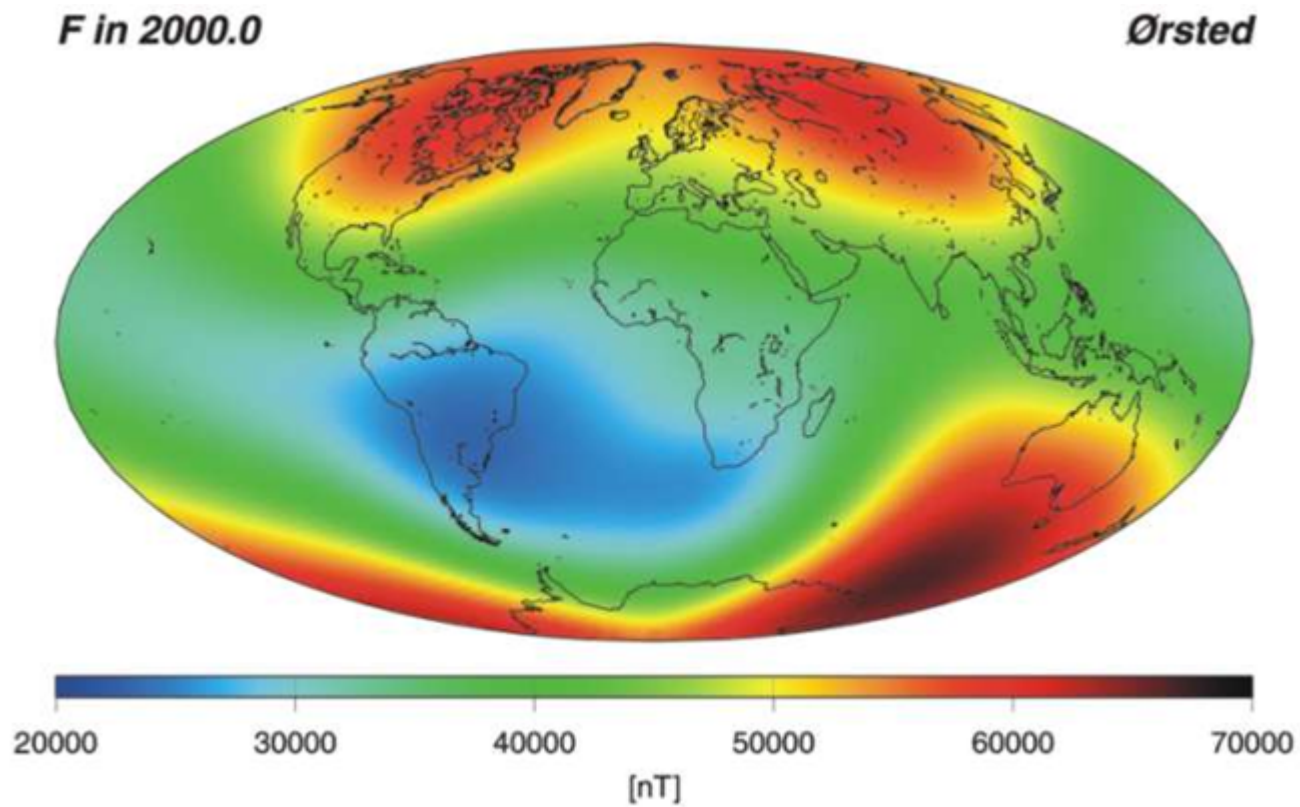
# Applications

- environmental geophysics;
- hydrology and hydrogeology, permafrost, geothermal resources;
- archaeology;
- exploration munitions or similar (UXO = unexploded ordnance);
- exploration of minerals;
- exploration of sedimentary basins, sub-salt structures;
- exploration of mineral deposits;
- tectonic questions, shear zones and
- study of the deeper crust and the upper mantle.

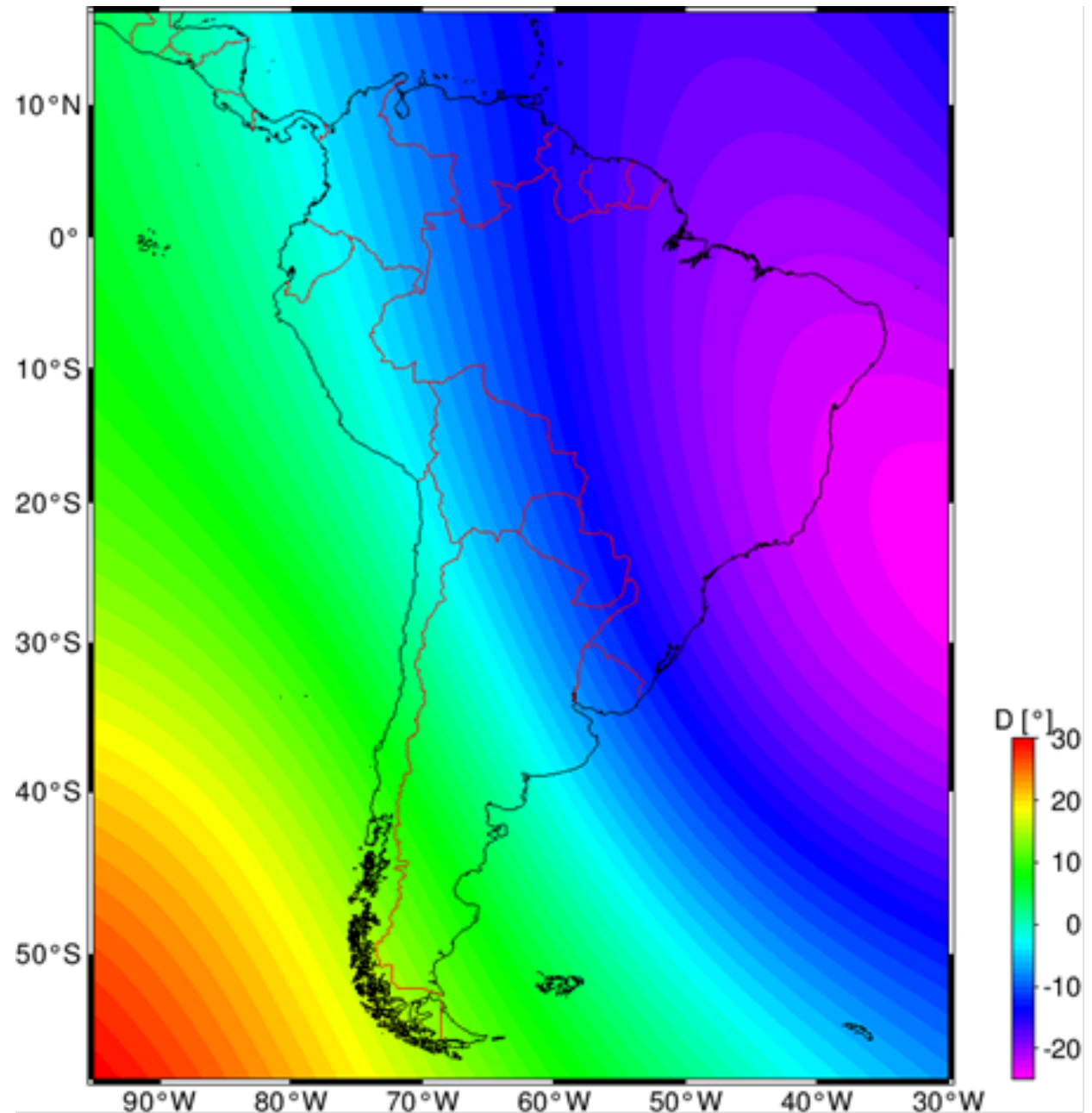
# Earth's magnetic main field, magnetic elements



The main field is not a dipole field



Declination in  
South America,  
epoch 2005.0  
from IGRF



# EM $\neq$ magnetic exploration

- In **magnetics**, we utilize the static geomagnetic field and remove secular and faster variations as perturbances.
- In **electromagnetics**, we are not interested in the static geomagnetic field. We either don't measure it at all or remove it during data evaluation.

# Basic literature (text books) and further reading

- Berdichevsky, M.N. & Dimitriev, V.I. (2002): Magnetotellurics in the context of ill-posed problems, Society of Exploration Geophysicists, Tulsa.
- Chave, A. & Jones, A.G. (2012): The Magnetotelluric Method, Cambridge University Press, Cambridge.
- Grant, F.S. & West, G.F. (1965): Interpretation Theory in Applied Geophysics, McGraw-Hill, New York.
- Nabighian, M.N. (ed., 1987 und 1991): Electromagnetic Methods in Applied Geophysics, Vol. 1 + 2, Society of Exploration Geophysicists, Tulsa.
- Simpson, F. & Bahr, K. (2005): Practical Magnetotellurics, Cambridge Univ. Press.
- Telford, W.M., Geldart, L.P. & Sheriff, R.E. (1992): Applied Geophysics, 2nd edition, Cambridge University Press, Cambridge.
- Zhdanov, M.S. (2009): Geophysical Electromagnetic Theory and Methods, Methods in Geochemistry and Geophysics, 43, Elsevier.

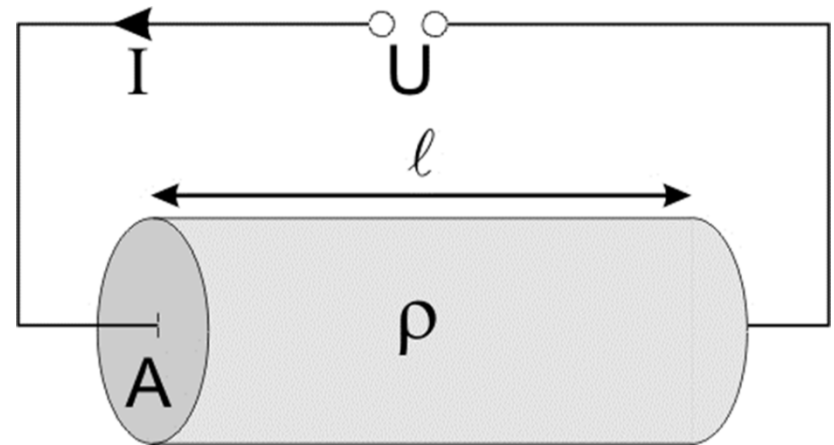
<http://userpage.fu-berlin.de/~hbrasse/Vorlesungsmanuskripte.html>



# Basics

$$R = \rho \frac{\ell}{A}$$

$$\sigma = \frac{1}{\rho}$$



The *resistivity*  $\rho$  is a material property; it is measured in  $\Omega\text{m}$ .

Its reciprocal is *conductivity*  $\sigma$ ,  
in units of  $1/\Omega\text{m} = \text{S/m}$  (S = Siemens)

# Dar Zarrouk Parameters

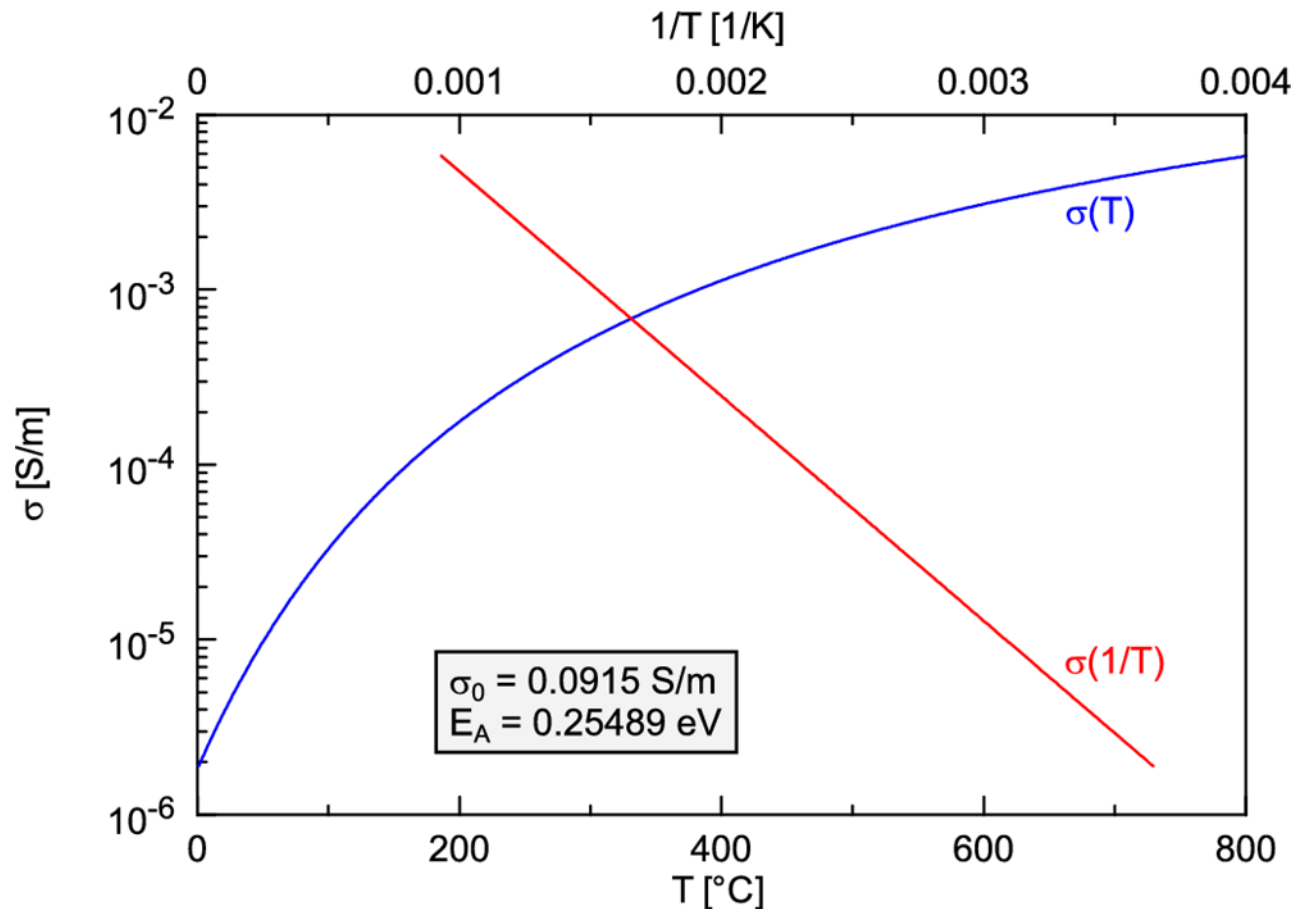
Conductance or integrated conductivity (in Siemens)

$$\tau = \int_{z_1}^{z_2} \sigma(z) dz \qquad \tau = \sum_{i=1}^n \sigma_i \Delta z_i$$

Transversal resistivity (in  $\Omega\text{m}^2$ )

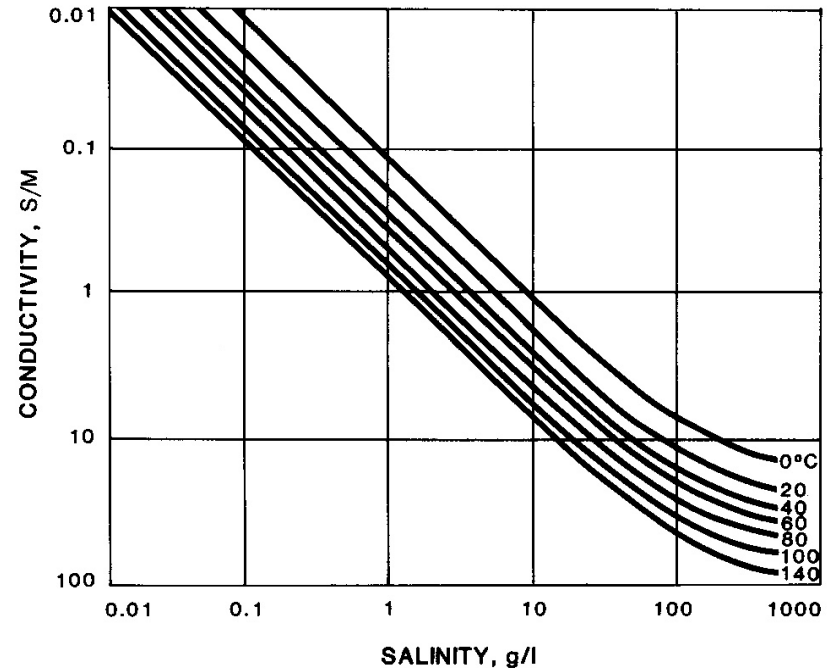
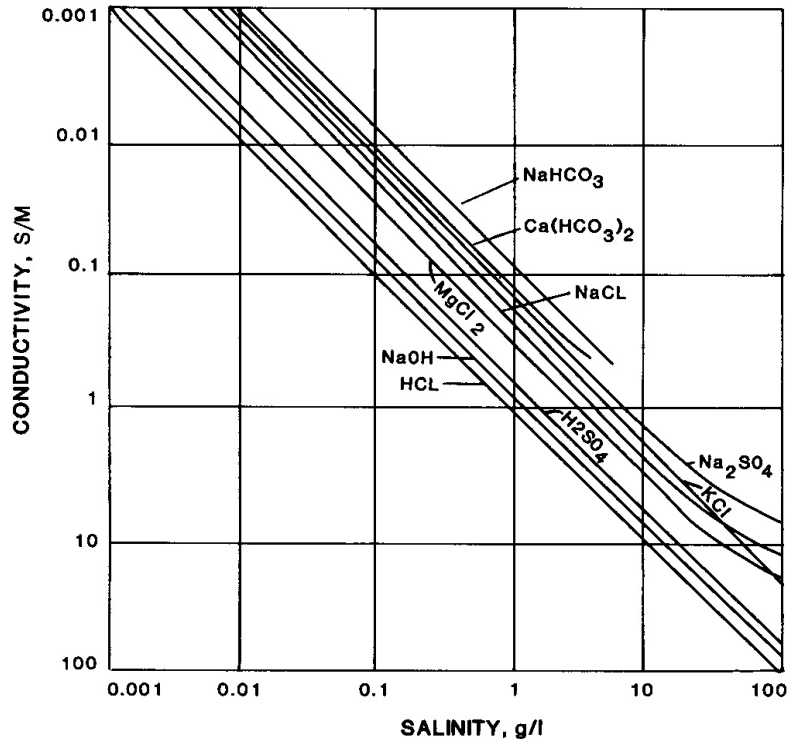
$$T = \int_{z_1}^{z_2} \rho(z) dz \qquad T = \sum_{i=1}^n \rho_i \Delta z_i$$

# Semiconductors: Arrhenius law $\sigma = \sigma_0 \exp\left(-\frac{E_A}{kT}\right)$



Temperature dependence of electrical conductivity, here for a dry granulite. Constants have been determined in laboratory experiments (Glover & Vine 1995). Therefore electrical anomalies with  $\sigma$  over 0.1 S/m in the earth's crust cannot be explained by higher temperatures.

Electrolytic and/or electronic constituents are needed to explain high conductivities



Conductivity as salinity function for varying solutions (left) and varying temperatures of a mixed solution (right). After Palacky (1987)

# Mixing laws for two-phase systems

$$\rho_G = F \rho_f = a \Phi^n S^m \rho_f \quad \text{Archie's law (1942)}$$

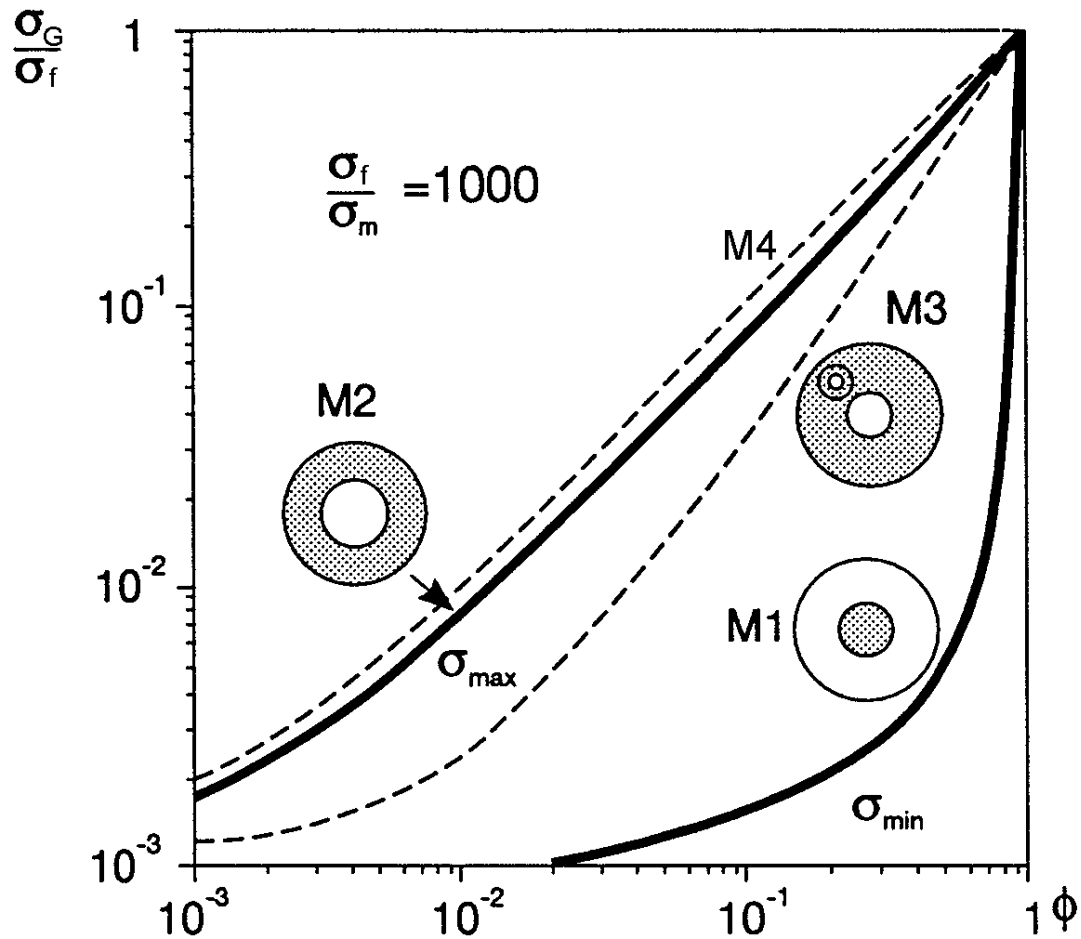
$$\sigma_{\max} = \sigma_f \left( 1 - \frac{3(1-\phi)(\sigma_f - \sigma_m)}{3\sigma_f - \phi(\sigma_f - \sigma_m)} \right)$$
$$\sigma_{\min} = \sigma_m \left( 1 + \frac{3\phi(\sigma_f - \sigma_m)}{3\sigma_m + (1-\phi)(\sigma_f - \sigma_m)} \right)$$

Hashin-Shtrikman  
upper and lower  
bound (1962)

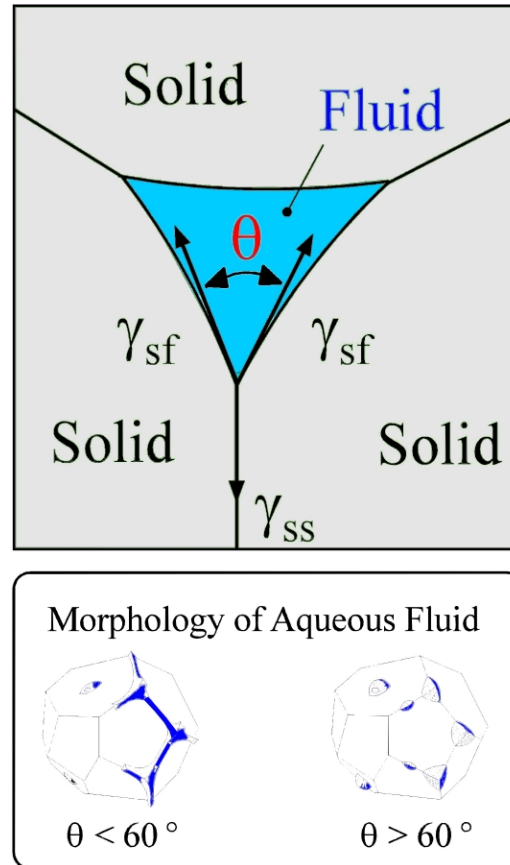
$$\sigma_{\max} = \phi \sigma_f + (1-\phi) \sigma_m$$

$$\sigma_{\min} = \left( \frac{\phi}{\sigma_f} + \frac{1-\phi}{\sigma_m} \right)^{-1}$$

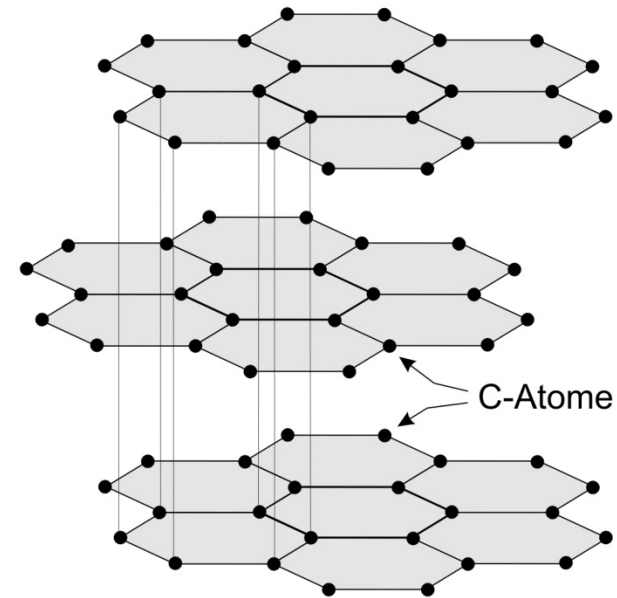
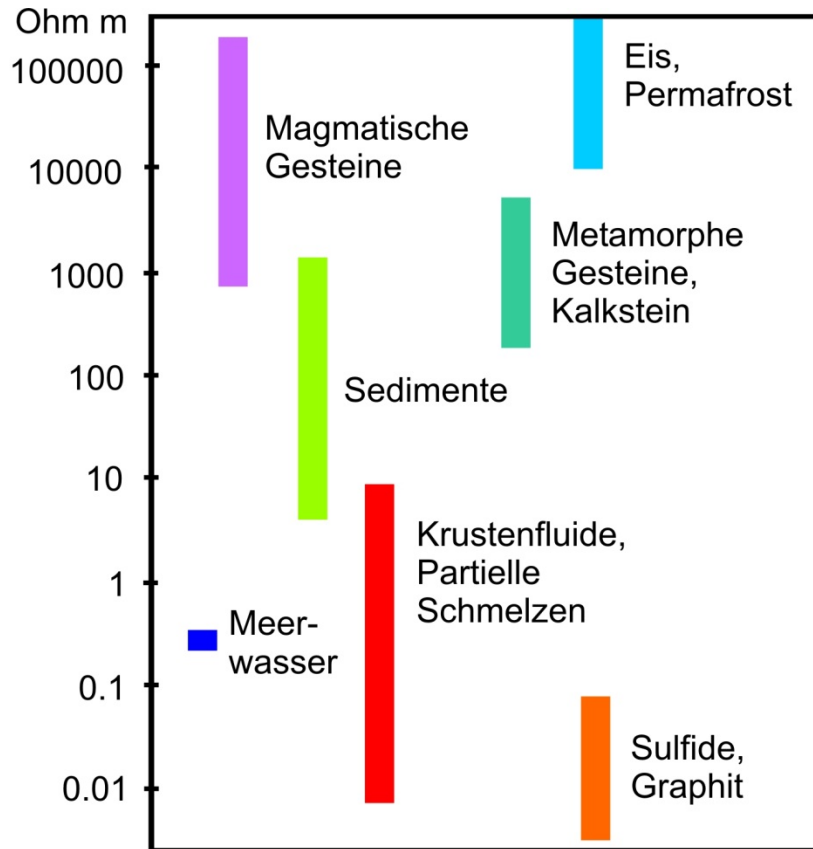
Parallel or serial  
connection of fluid phase



Extremal models according to Hashin-Shtrikman and Sen, calculated for a conductivity proportion of 1:1000. M1: HS lower bound, M2: Hs upper bound, M3: according to Sen, M4 (upper broken line): anisotropic (ellipsoids) model. Fig. from Weidelt, in: Knödel et al. (1997).



Dihedral (wetting) angle (according to Mibe, 2000).



Typical resistivity of some rocks and minerals. The resistivity of freshwater is about 10-100  $\Omega\text{m}$ , that of dry ice and (potash) salt over  $10^6 \Omega\text{m}$ . In the case of mineralization the conductivity largely depends on the mineral; only a small amount is needed to raise the conductivity of pyrrhotite, while there has to be a proportion of at least 60% in the rock matrix of pyrite. Right: Lattice structure of graphite.



# Anisotropy

$$\underline{\underline{\sigma}} = \begin{pmatrix} \sigma_{xx} & \sigma_{xy} & \sigma_{xz} \\ \sigma_{yx} & \sigma_{yy} & \sigma_{yz} \\ \sigma_{zx} & \sigma_{zy} & \sigma_{zz} \end{pmatrix}$$

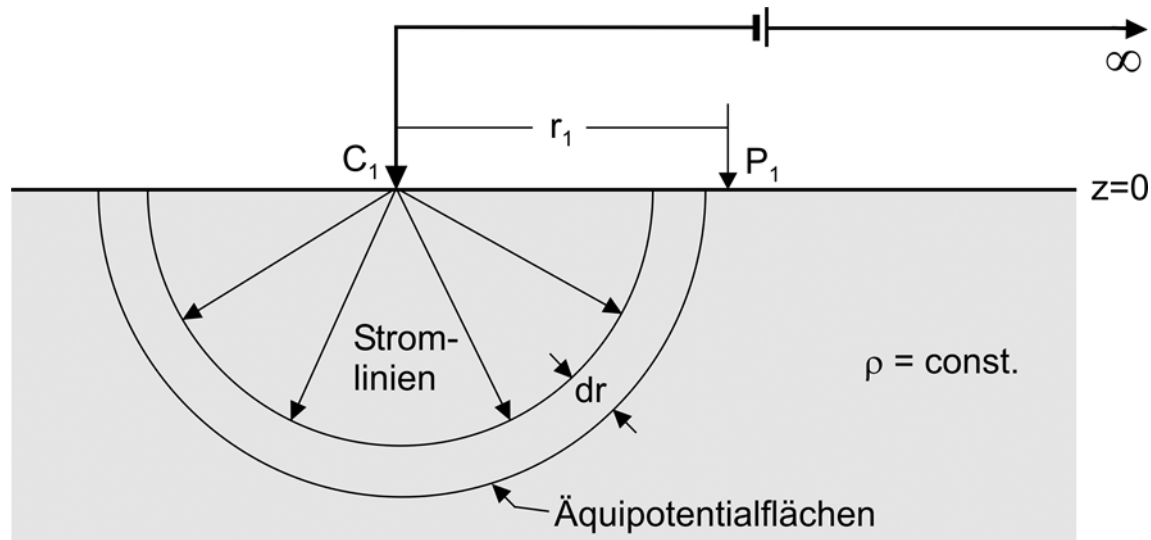
Conductivity is now a tensor

$$\underline{\underline{\sigma}} = \begin{pmatrix} \sigma_1 & 0 & 0 \\ 0 & \sigma_2 & 0 \\ 0 & 0 & \sigma_3 \end{pmatrix}$$

Axis transformation:  
3 conductivities and 3 angles  
(strike, dip and slant)

Many rocks are inherently anisotropic, e.g., paragneiss, lacustric sediments, etc. Anisotropy coefficients  $\sigma_{\max}/\sigma_{\min}$  are usually in the range 2-5. This is often ignored in applied geophysics for the time being due to its complexity.

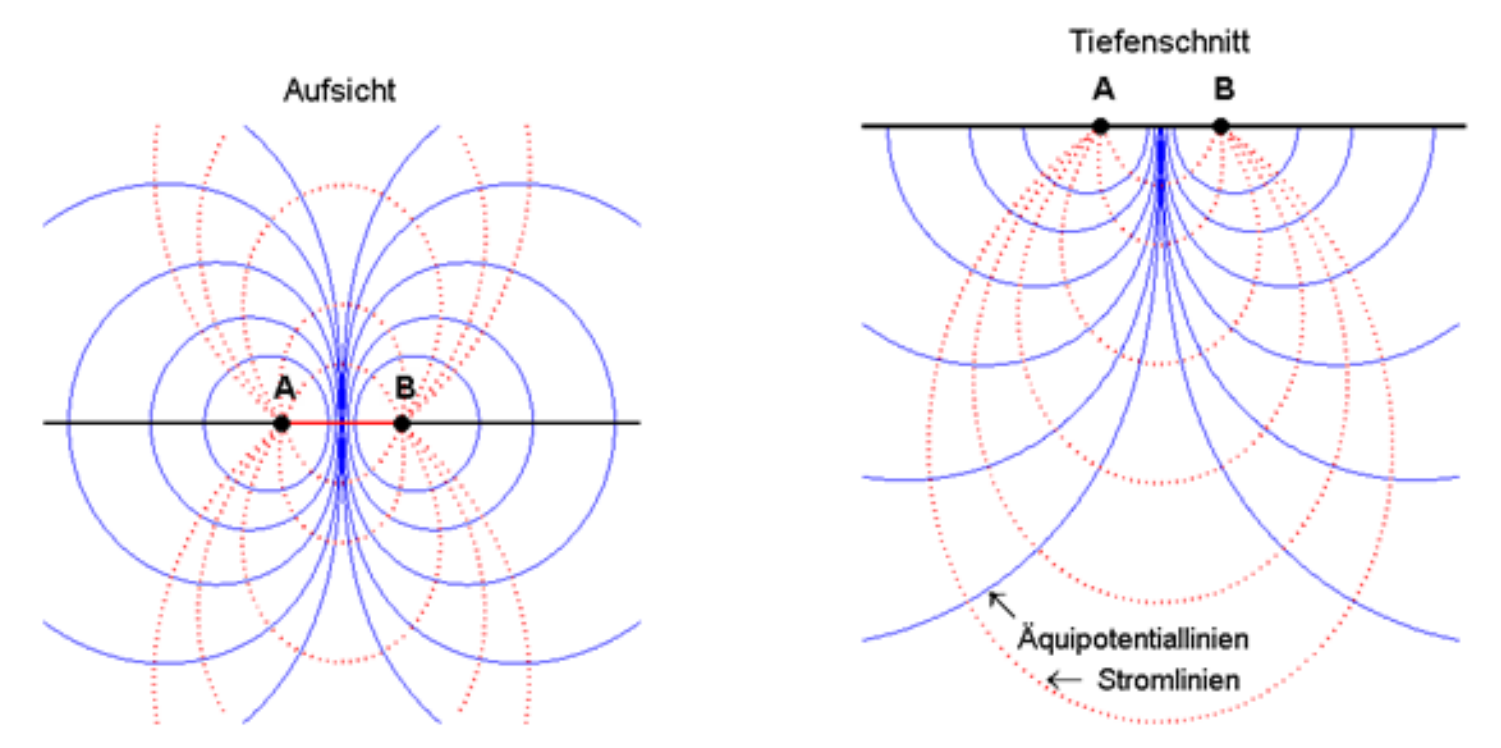
# Let's begin with DC geoelectrics



Current distribution in a homogeneous half space for injection by a point electrode; the 2nd electrode is thought at infinity.

$$U(r) = \frac{I\rho}{2\pi r}$$

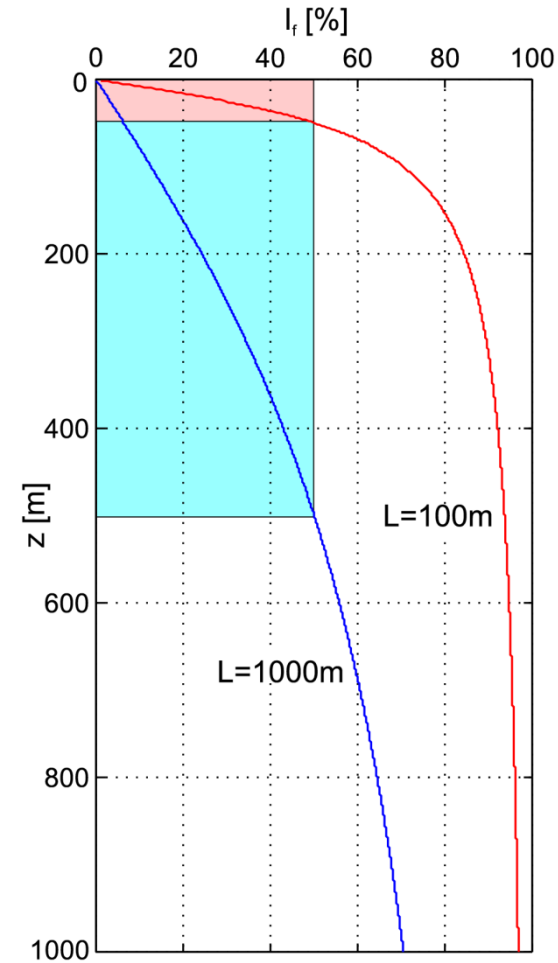
## 2-point layout

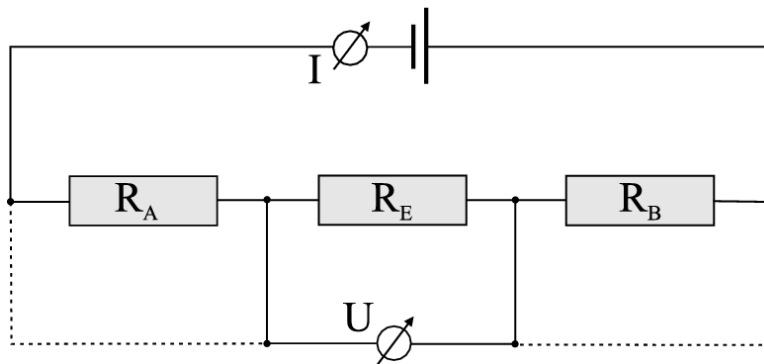


$$U(P) = U_1(P) + U_2(P) = \frac{\rho I}{2\pi r_1} + \left( -\frac{\rho I}{2\pi r_2} \right) = \frac{\rho I}{2\pi} \left( \frac{1}{r_1} - \frac{1}{r_2} \right)$$

Portion of the current system in %, which flows above a depth  $z$ , plotted for electrode separations of  $L=100\text{m}$  and  $L=1000\text{m}$ .

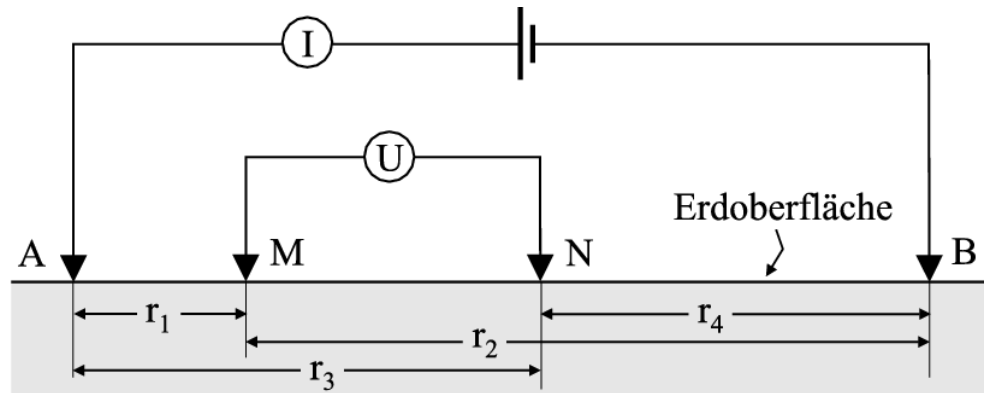
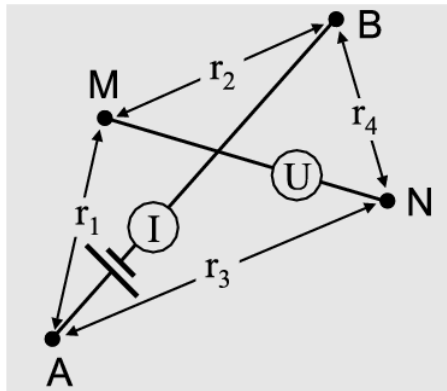
$$I_f = \frac{2}{\pi} \arctan \left( \frac{z}{L/2} \right)$$





4-point layout

Auxiliary circuit diagram for 2- and 4-point configuration.



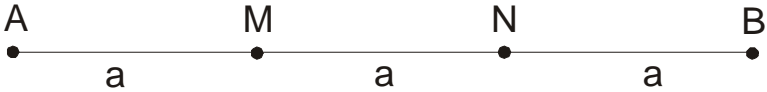
$$\rho = \frac{2\pi \Delta U}{I} \left( \frac{1}{r_1} - \frac{1}{r_2} - \frac{1}{r_3} + \frac{1}{r_4} \right)^{-1} = G \frac{\Delta U}{I}$$

G = geometry factor

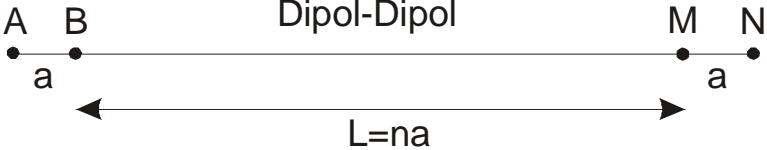
# Common 4-point layouts of DC resistivity.



Wenner



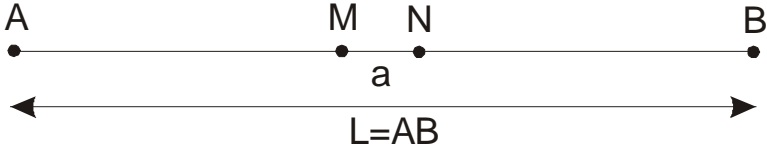
Dipol-Dipol



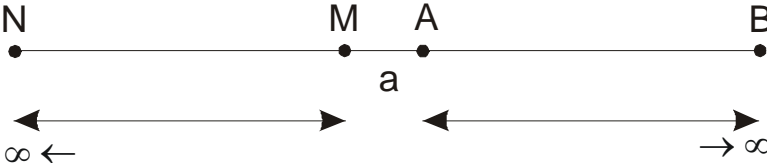
Pol-Dipol

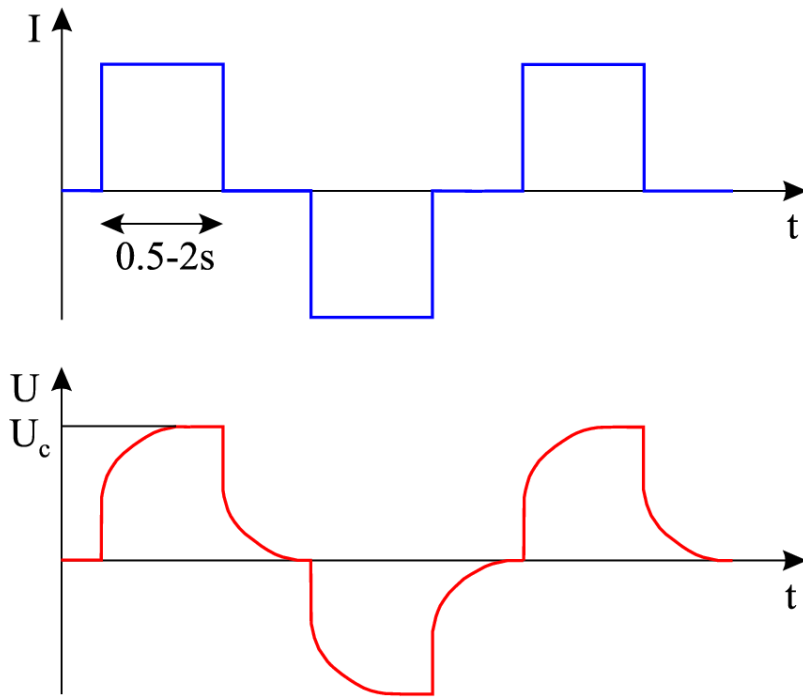


Schlumberger

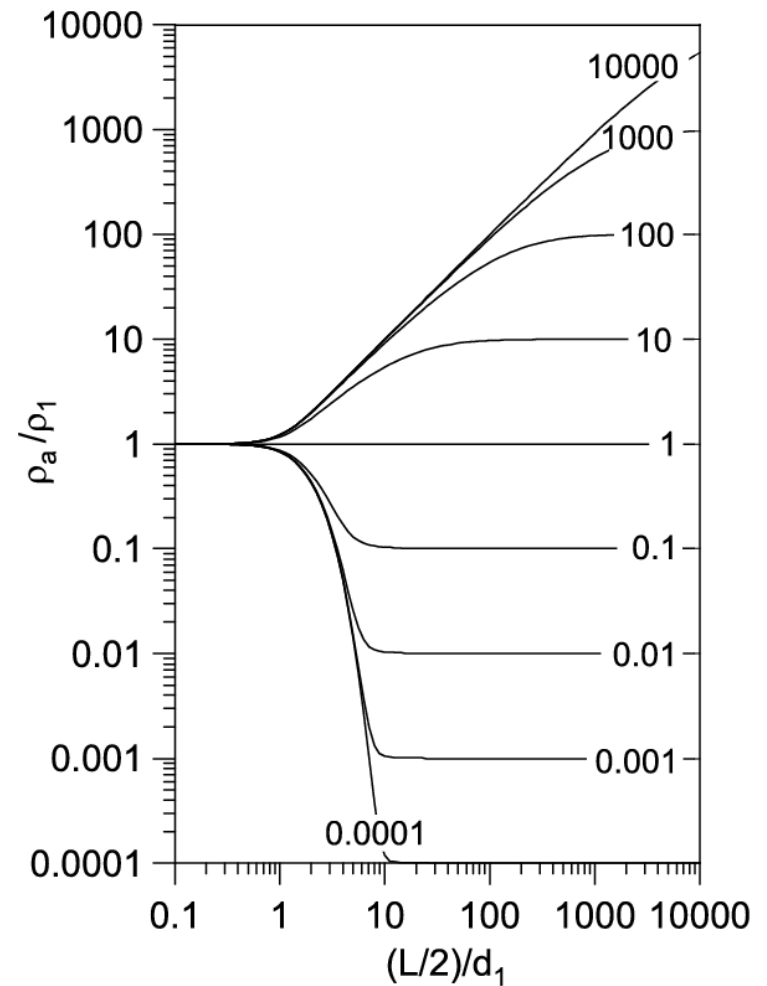


Pol-Pol



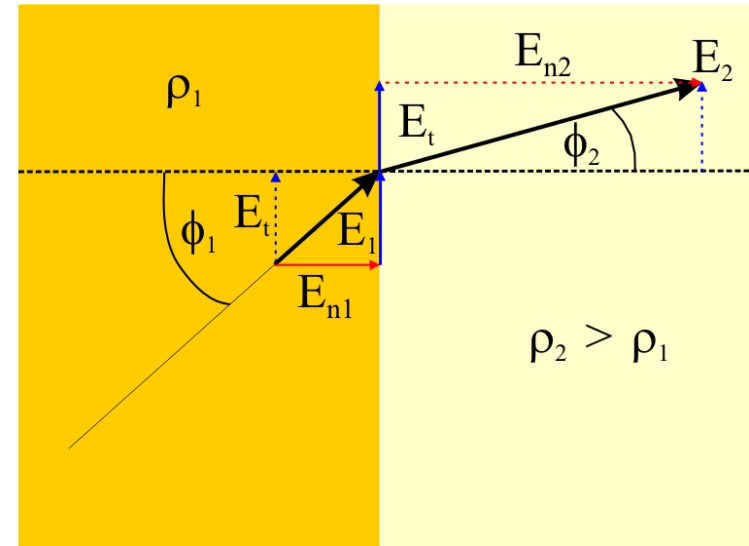
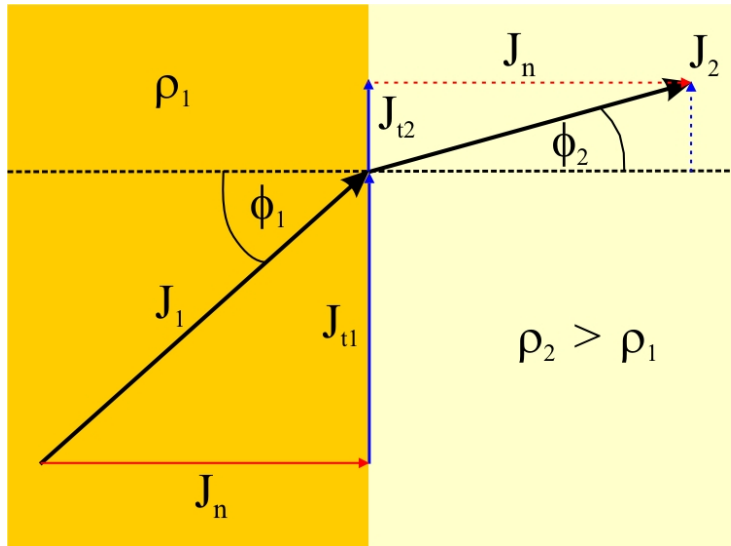


Temporal course of an alternating "direct" current (top). Below: Measured voltage with IP effects.



Example of a set of master curves for the 2-layer case.

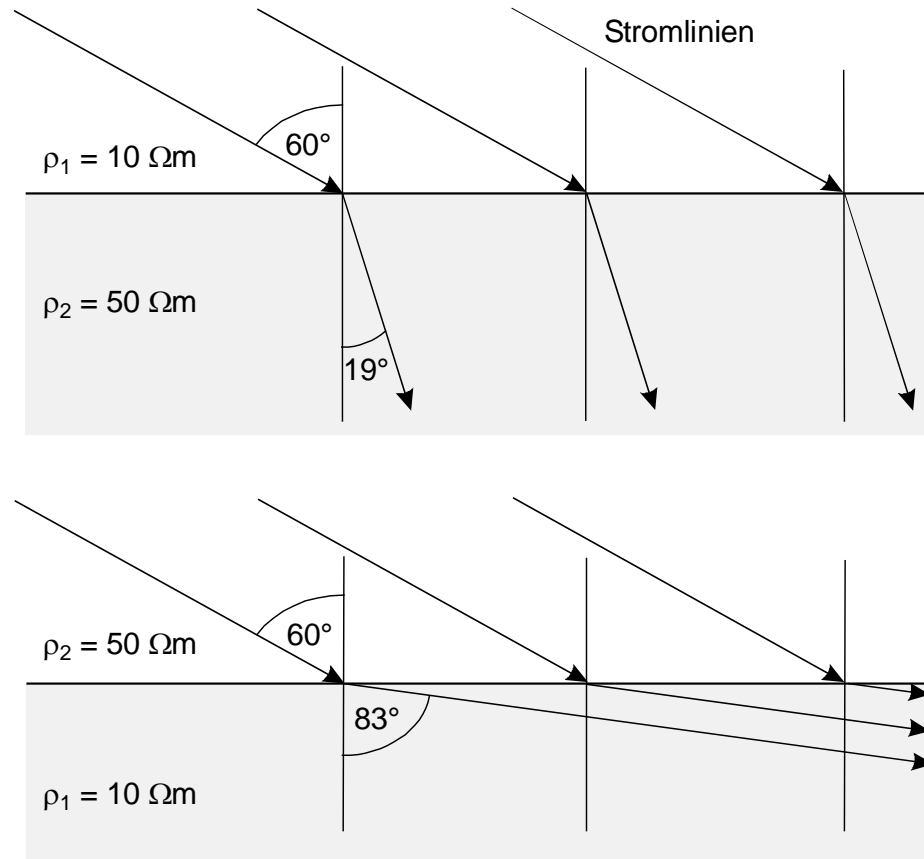
# Layered half space or lateral discontinuities: boundary conditions



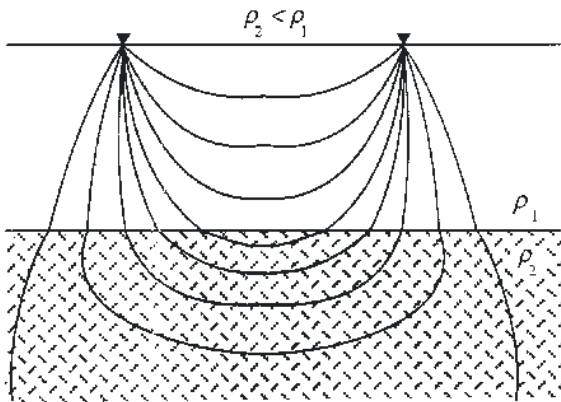
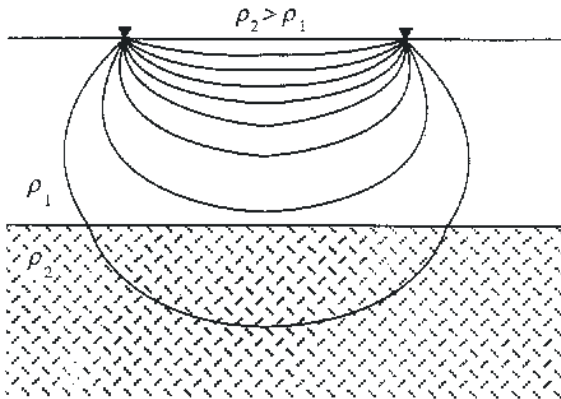
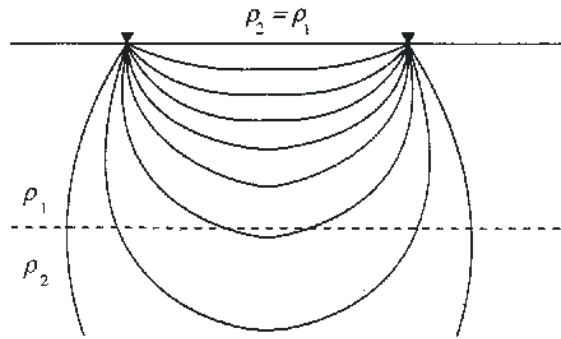
law of refraction of the current lines

$$\frac{\sigma_1}{\sigma_2} = \frac{\rho_2}{\rho_1} = \frac{\tan \phi_1}{\tan \phi_2}$$

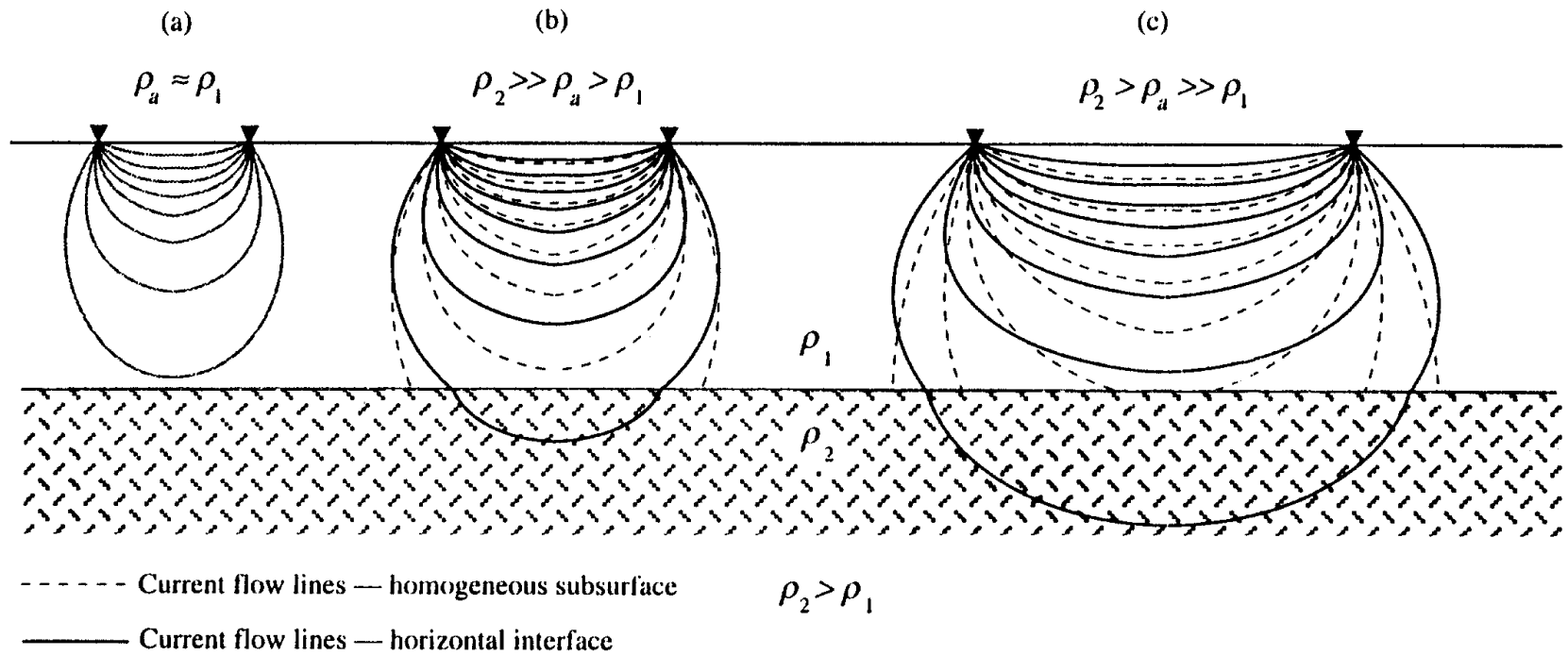




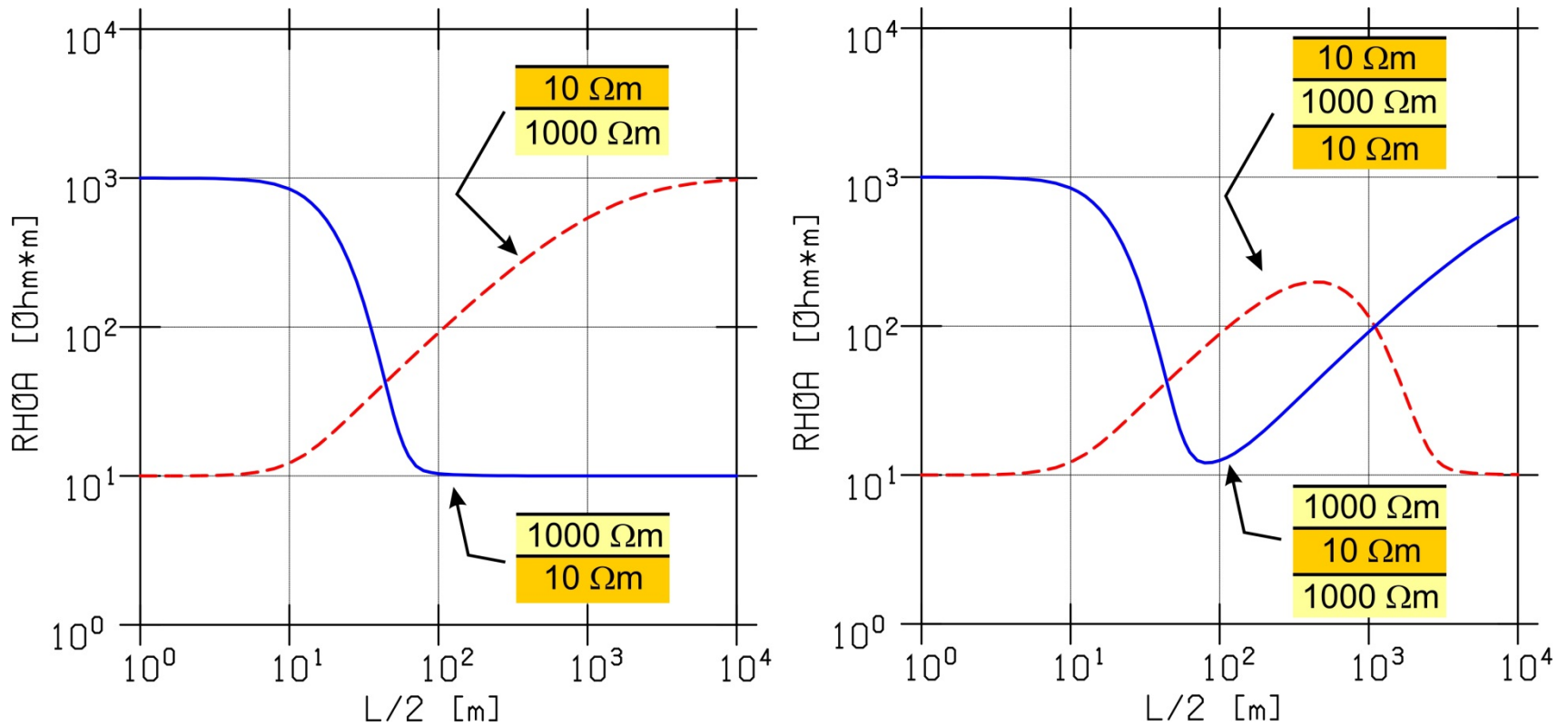
Refraction of current lines at a boundary, the angle of incidence is each time  $60^\circ$ . Above: Poor conductor beneath good conductor, the refraction angle is  $19^\circ$  and the current lines penetrate deeper into the resistor. Bottom: If the current lines penetrate into a good conductor, a current concentration results at the boundary, the refraction angle is  $83^\circ$ .



*Current system in two-layered subsoil with varying resistivity of the substrate. From P. Kearey, M. Brooks, I. Hill (2002): An introduction into geophysical exploration, Wiley-Blackwell.*



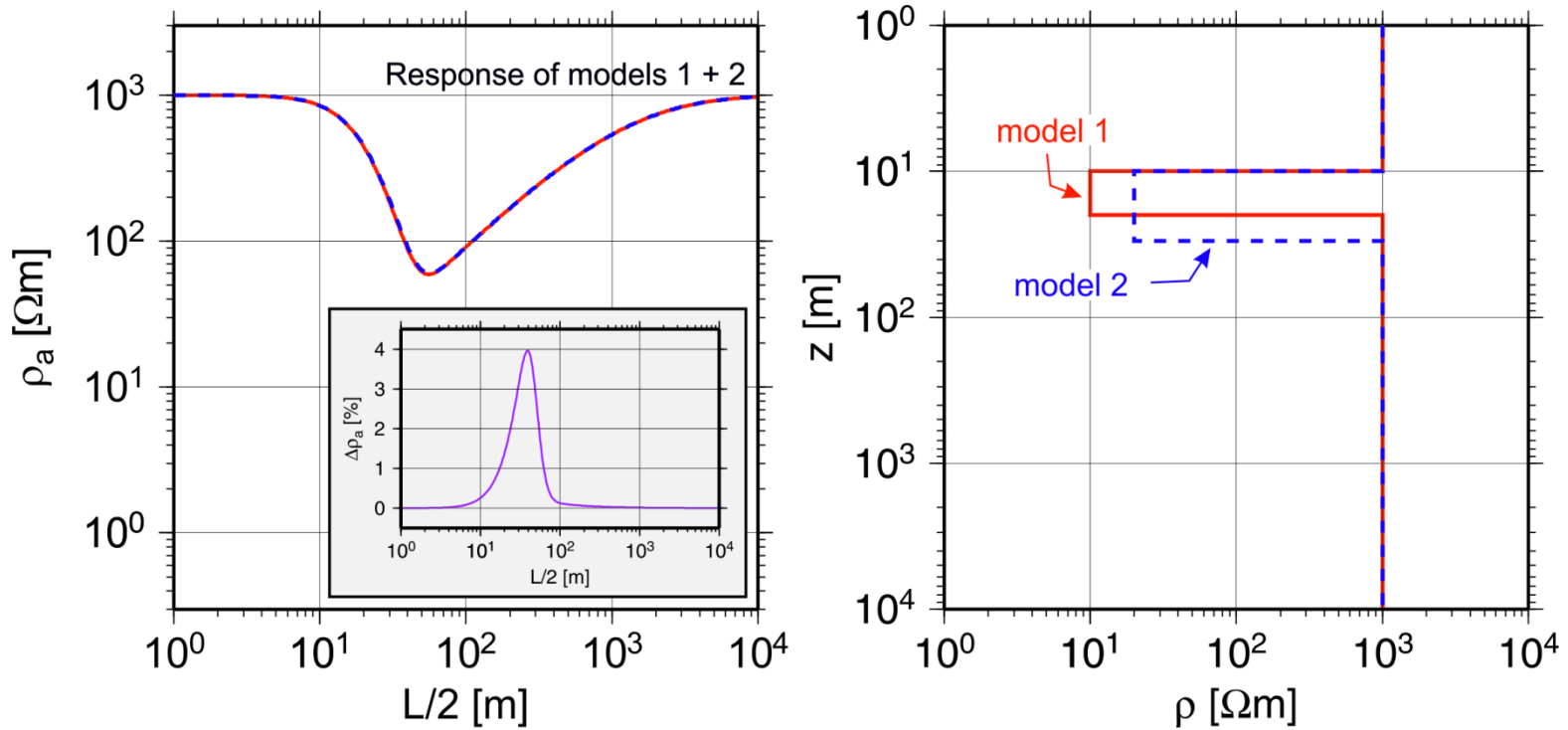
Current system and apparent resistivity for a 2-layer case when the spread is expanded.



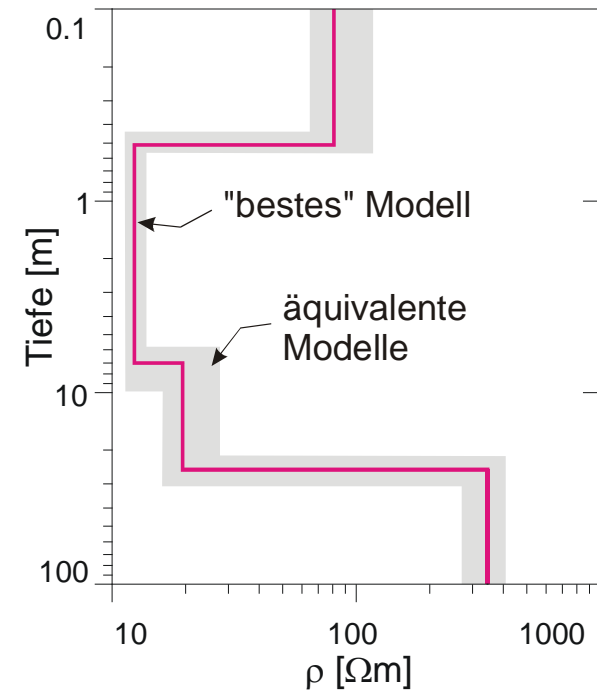
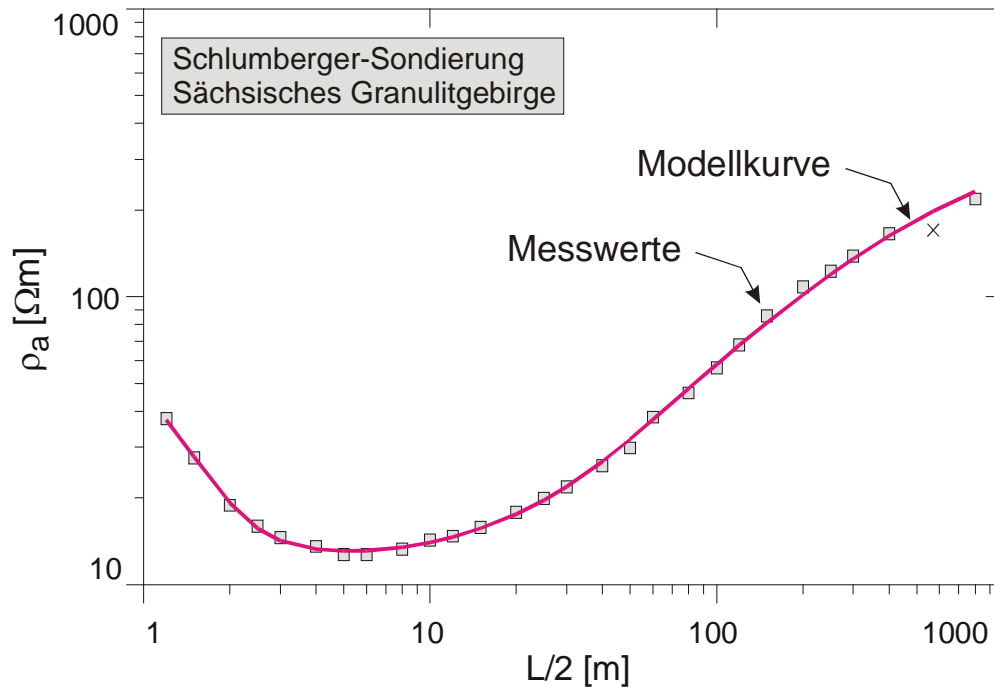
$\rho_a$  curves for 2- (left) and 3-layer (right) cases for a Schlumberger array. Layer thicknesses are 10 m for the overburden and 100 m for the intermediate layer on the right hand side.

<http://userpage.fu-berlin.de/~mtag/ves1d/VES-Java.html>

# The big drawback: principle of equivalence and suppression of layers

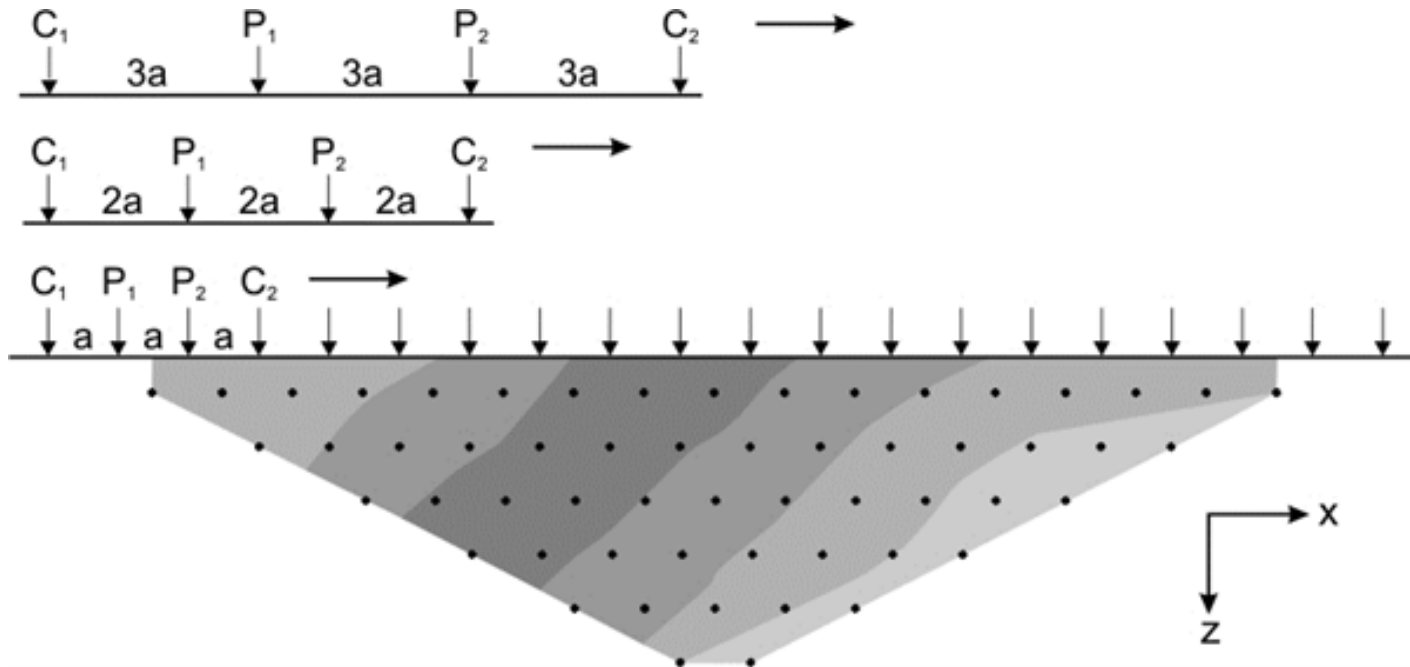


Model response (left) for two equivalent 3-layer models (right): Model 1:  $\rho_2 = 10 \Omega\text{m}$ ,  $d_2 = 10$  m; Model 2:  $\rho_2 = 20 \Omega\text{m}$ ,  $d_2 = 20$  m. Conductance of the 2nd layer is 1 S in both cases.



A practical example: The equivalent models surround the "best" model approximately like an envelope. One recognizes specifically the poor resolution of the second layer boundary.

# Geoelectrical tomography



Scheme to construct a geoelectric pseudo section, shown here for a Wenner configuration. The data points – i.e.  $\rho_a(x,z)$  – are plotted below the centers of each individual array; depth of these points is proportional to the spread and somehow arbitrary. Through relocation of the arrays (which happens electronically with the help of a computer program after all electrodes have been set and connected) a continuous coverage is achieved. Modern array instruments allow the connection of 64-256 electrodes.

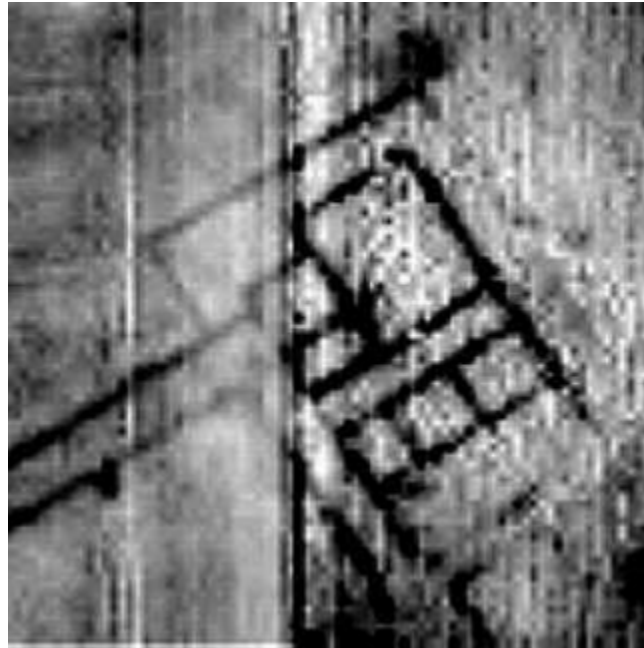
# Software

<http://www.geoelectrical.com>

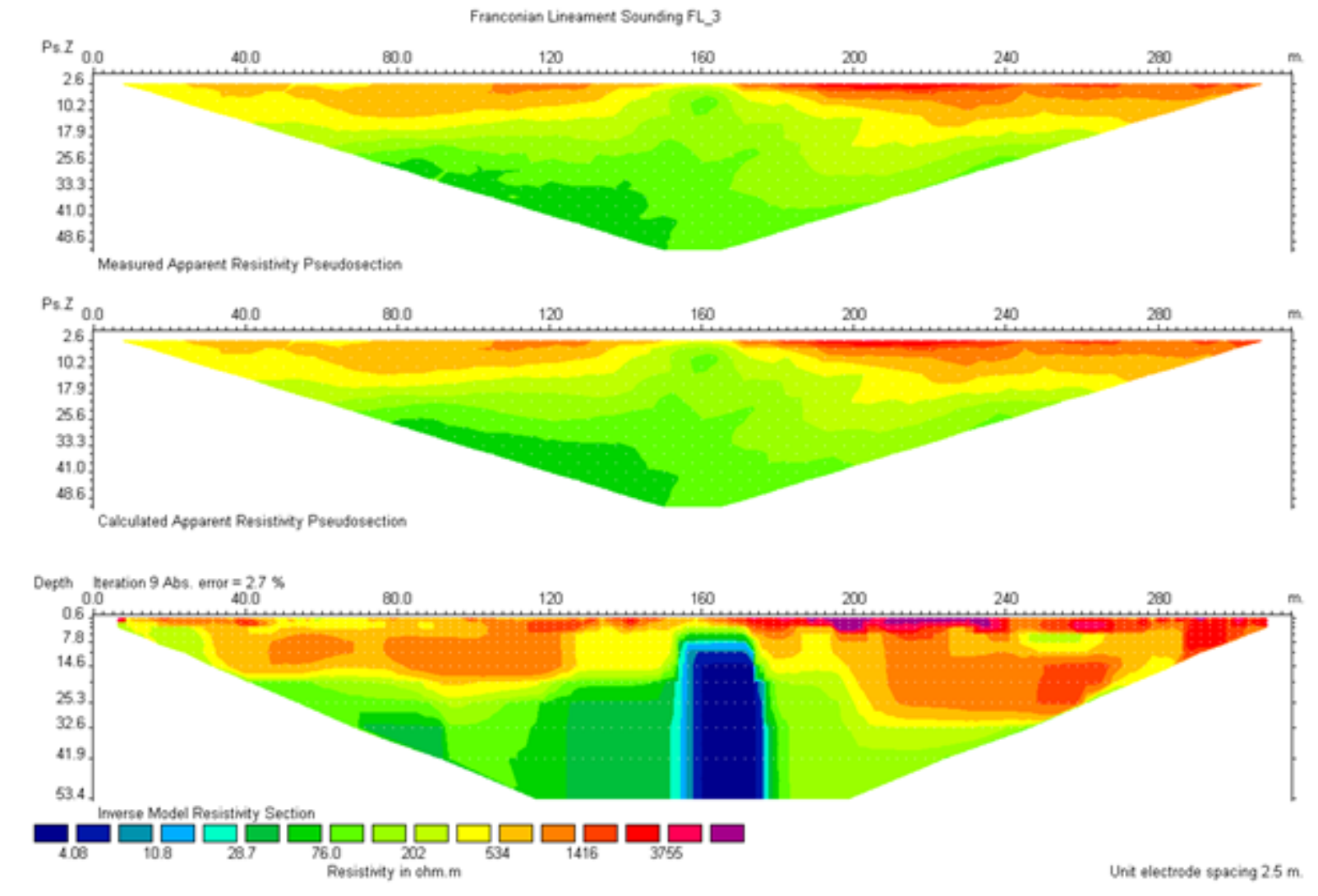
<http://www.resistivity.net>



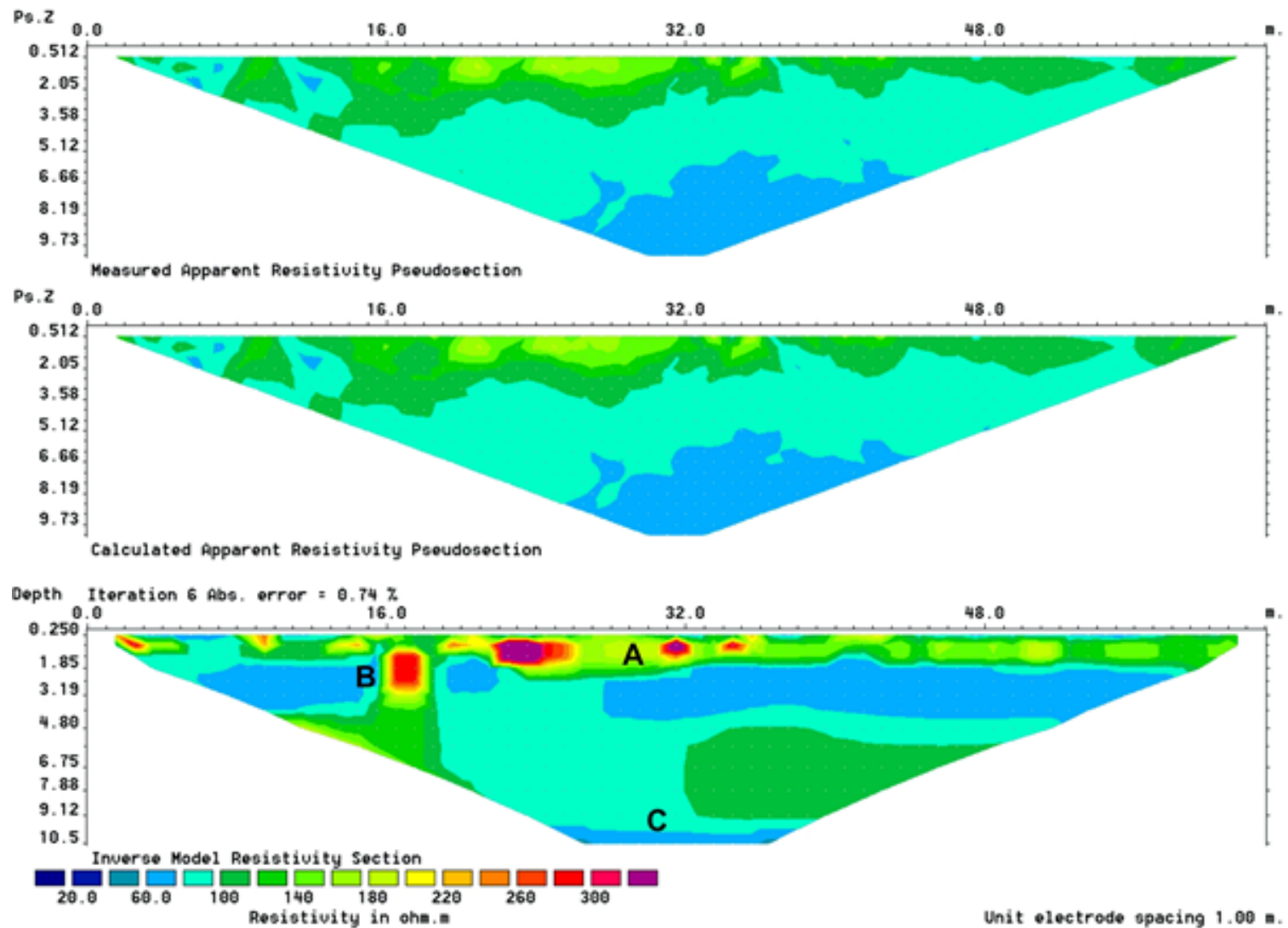
## Some examples



Example of a profiling for the walls of an old Roman villa in Austria (source: web site University of Vienna).



*An example of 2-D inversion of data from the Franconian Line in Bavaria, carried out with the program res2dinv by Loke and Barker (1996). Top: pseudo section of a Wenner- $\alpha$  measurement, center: model response, bottom: resistivity model. The very good conductor (in blue) is caused by graphitized shear planes, a sub-fault of the Franconian Line system. This conductor is also responsible for a strong self-potential anomaly (see later). Data were collected during a geophysical field excursion of the Free University in 2002.*



Geoelectric tomography on the sport field of the Free University campus in the district of Lankwitz. A: Near-surface inhomogeneities due to gravel fillings of the field. B: Tunnel from pre-world war II times. C: Aquifer at  $z \approx 10\text{m}$  (thus much deeper than downtown). The tunnel, once found could also be accessed directly and its location was determined precisely; due to its small cross section ( $\sim 1.40\text{ m}^2$ ) it's resolved only as a moderately poor conductor. Data were collected during a geophysical practical course in 2004.



En el túnel

Berlín durante la guerra  
(Campus de la Geociencia)



1603





## Maxwell's equations

$$\nabla \times \underline{\underline{H}} = \frac{\partial \underline{\underline{D}}}{\partial t} + \underline{\underline{J}}$$

$$\nabla \times \underline{\underline{E}} = -\frac{\partial \underline{\underline{B}}}{\partial t}$$

$$\nabla \cdot \underline{\underline{B}} = 0$$

$$\nabla \cdot \underline{\underline{D}} = Q$$

Furthermore:

$$\underline{\underline{D}} = \epsilon_r \epsilon_0 \underline{\underline{E}}$$

$$\underline{\underline{B}} = \mu_r \mu_0 \underline{\underline{H}}$$

The permeability  $\mu_r$  differs significantly from 1 only for some titanium-magnetites. In most electromagnetic applications, however, we can set it to 1 and neglect it.

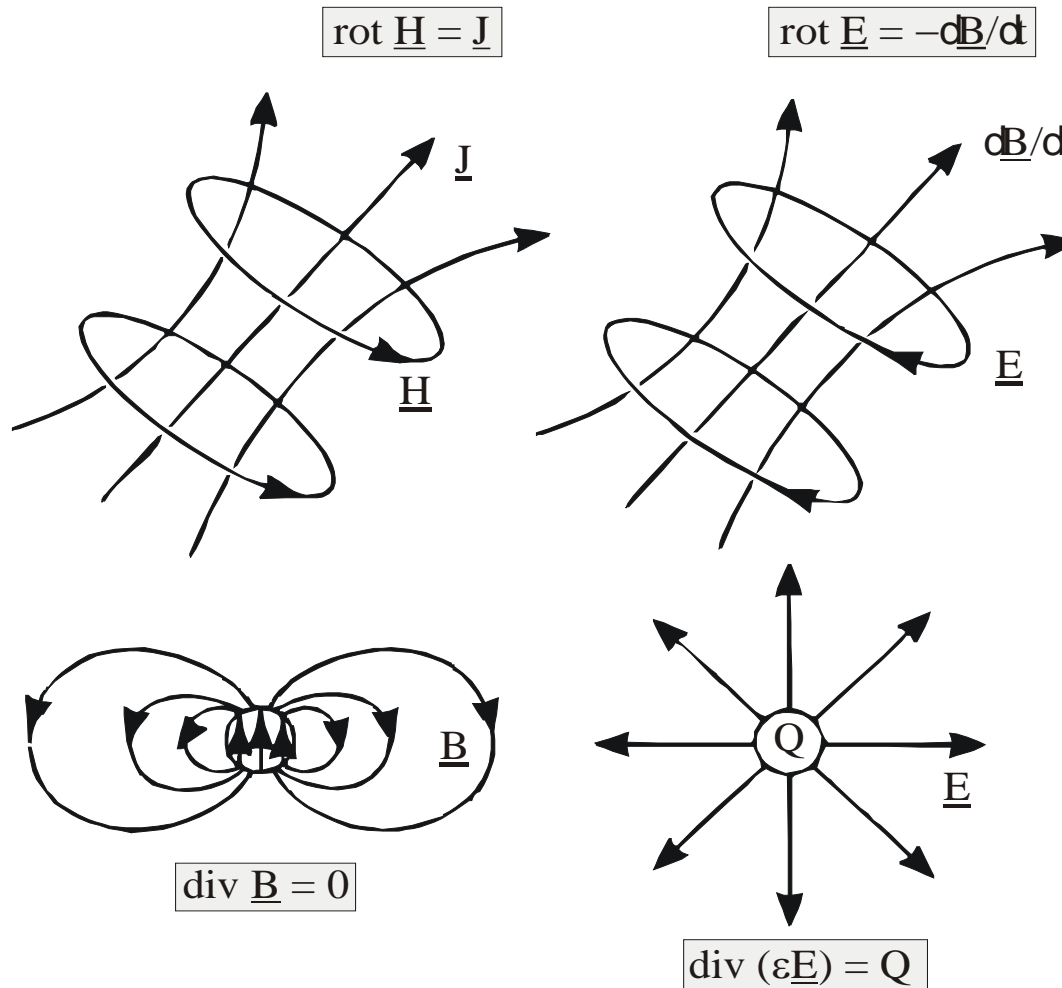


*Illustration of Maxwell's equations. Upper left: an electric current causes a magnetic eddy current; upper right: a time varying magnetic field causes an electric eddy field; lower left: no magnetic monopoles exist; lower right: the electric charges are sources of the electric field.*

## Telegrapher's equation

$$\nabla^2 \underline{F} = \mu\sigma \frac{\partial \underline{F}}{\partial t} + \mu\varepsilon \frac{\partial^2 \underline{F}}{\partial t^2}$$

Let field  $F$  have a periodic space and time dependency  
→ Helmholtz equation

$$\frac{\partial^2 \underline{F}}{\partial z^2} = \gamma^2 \underline{F}$$

Complex propagation constant

$$\gamma^2 = v^2 + i\omega\mu\sigma - \mu\varepsilon\omega^2 = v^2 + k^2 - \kappa^2$$



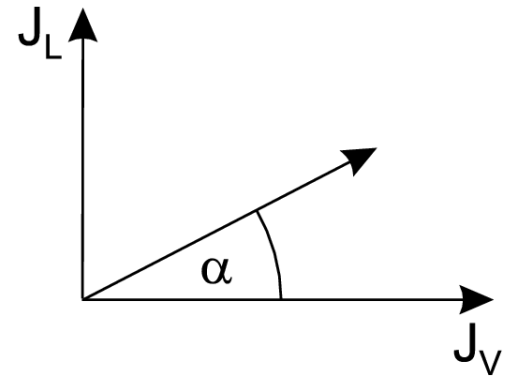
$$\gamma^2 = \nu^2 + i\omega\mu\sigma - \mu\epsilon\omega^2 = \nu^2 + k^2 - \kappa^2$$

$\nu > 0$  for near-field methods,  $\nu = 0$  for plane waves

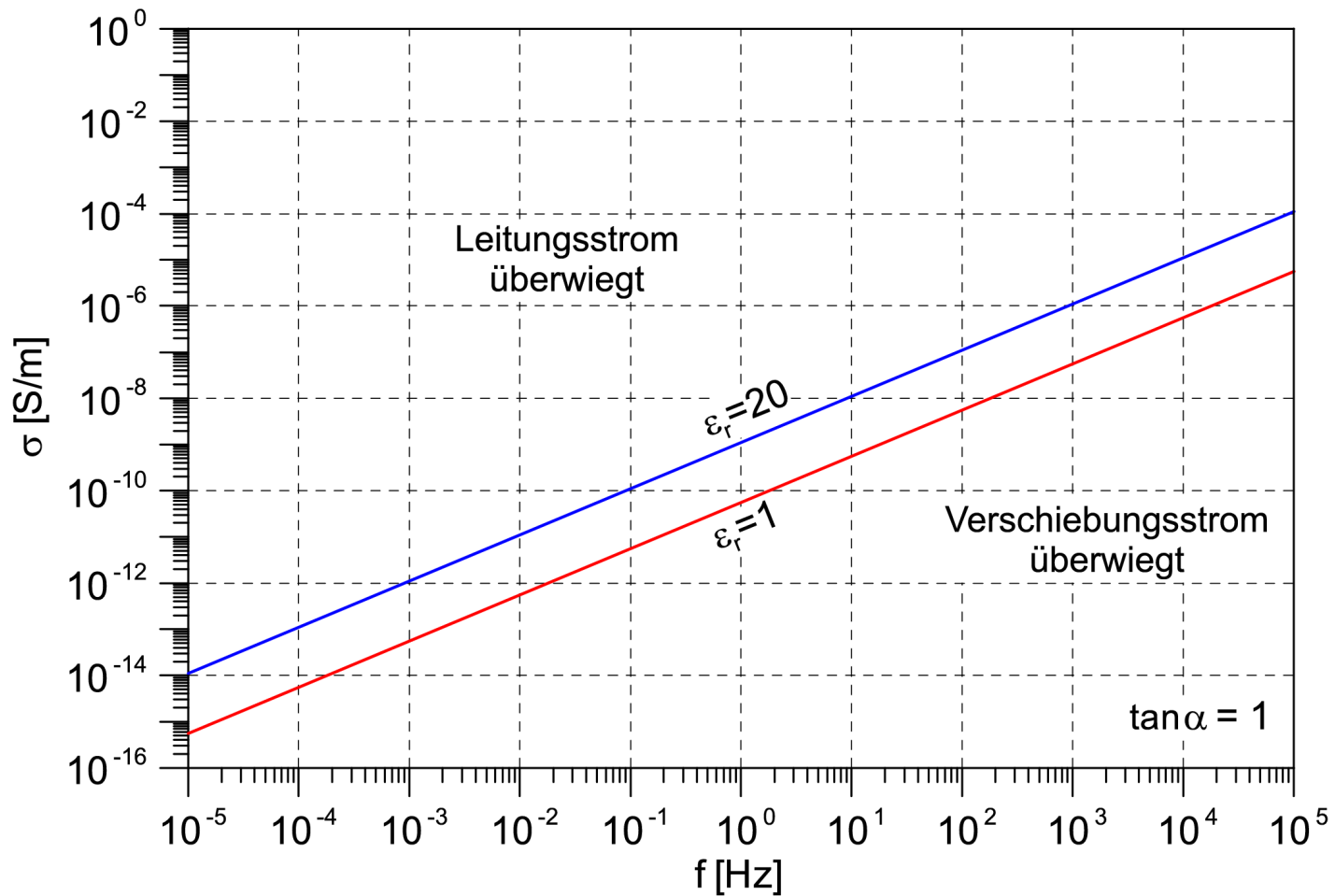
Relative weight of  $k$  and  $\kappa$  (induction vs. displacement current):

$$\tan \alpha = \frac{J_L}{|J_V|} = \frac{\sigma}{\epsilon \omega} = 1.8 \times 10^{10} \frac{\sigma}{\epsilon_r f}$$

Loss tangent;  $\alpha$  is called a loss angle  
(because of Ohmic losses when  $J_L \neq 0$ .)



If  $\tan \alpha \ll 1$ , then we have the case of GPR (generally  $f > 50$  MHz). If  $\tan \alpha \gg 1$ , then we talk of induction methods.



*The relation between diffusion current and displacement current ( $\tan \alpha = 1$ ) for different dielectric constants  $\epsilon_r$*

Diffusion term only

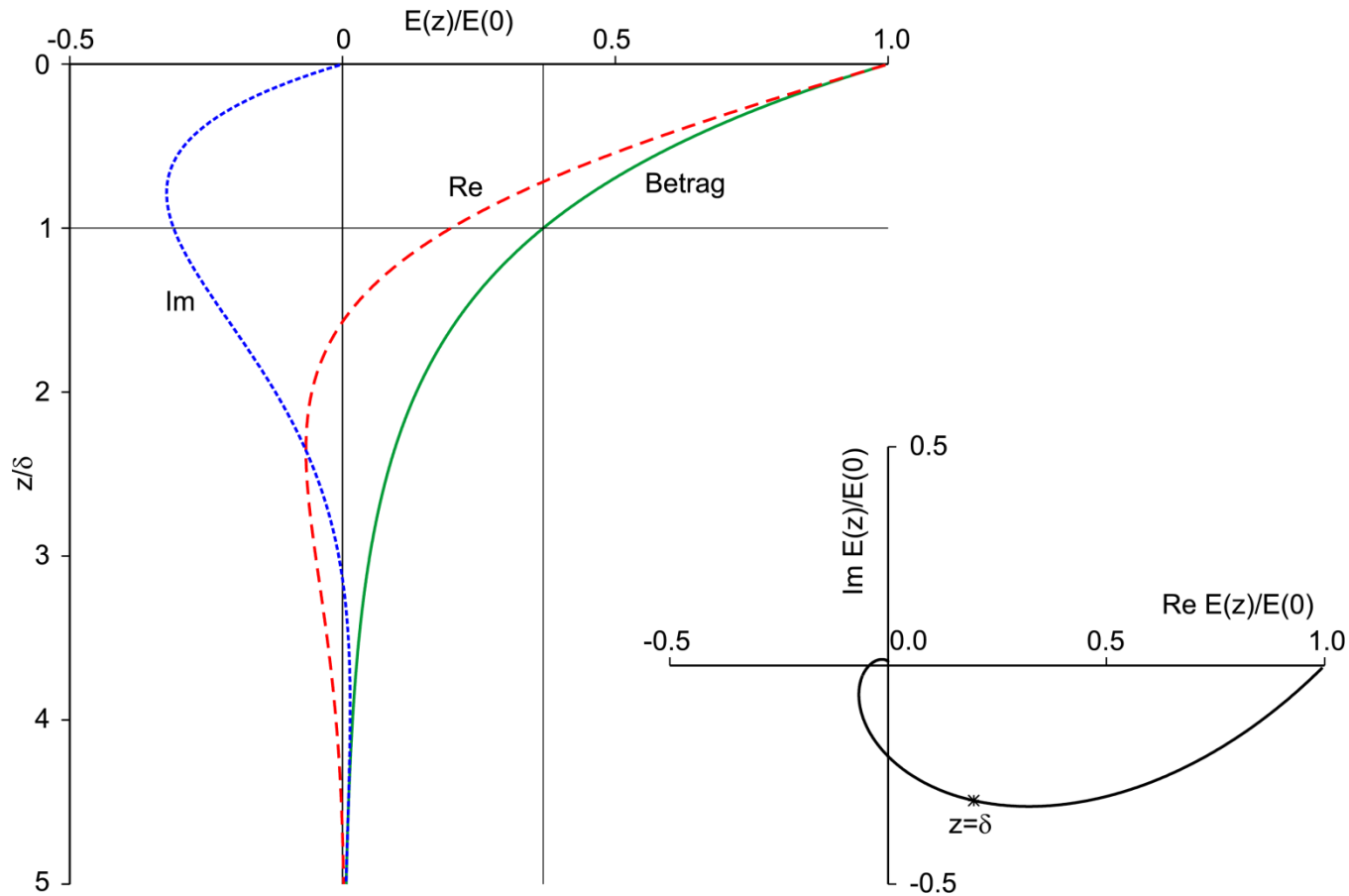
$$\frac{\partial^2 \underline{F}}{\partial z^2} = k^2 \underline{F} \quad k = \sqrt{i\omega\mu\sigma} \quad \text{complex wave number}$$

$$\underline{F}(z) = \underline{F}_0 e^{-kz} + \underline{F}_1 e^{+kz}$$

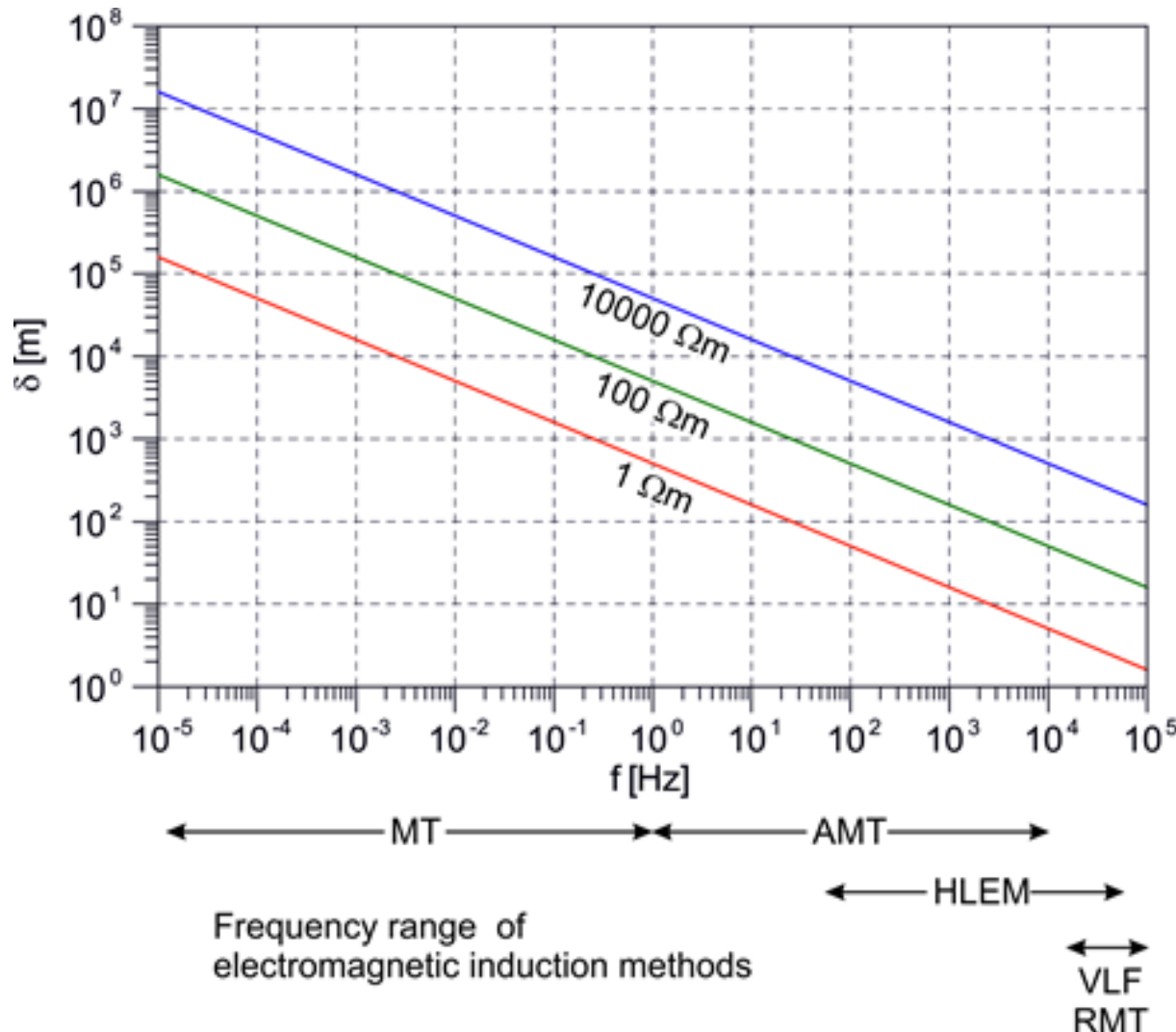
$$\delta = \sqrt{\frac{2}{\mu\omega\sigma}} \quad \text{Skin depth or depth of penetration}$$

$$\delta \approx 0.5 \sqrt{\rho T} \quad \text{oder} \quad \delta \approx 0.5 \sqrt{\rho / f} \quad [\text{km}]$$

# Exponential decay



Only diffusion term is valid for a wide range of frequencies



# “Waves” in MT ?

Incoming wave at  $T = 10^4$  s

$$\sigma = 0 \text{ S/m}$$

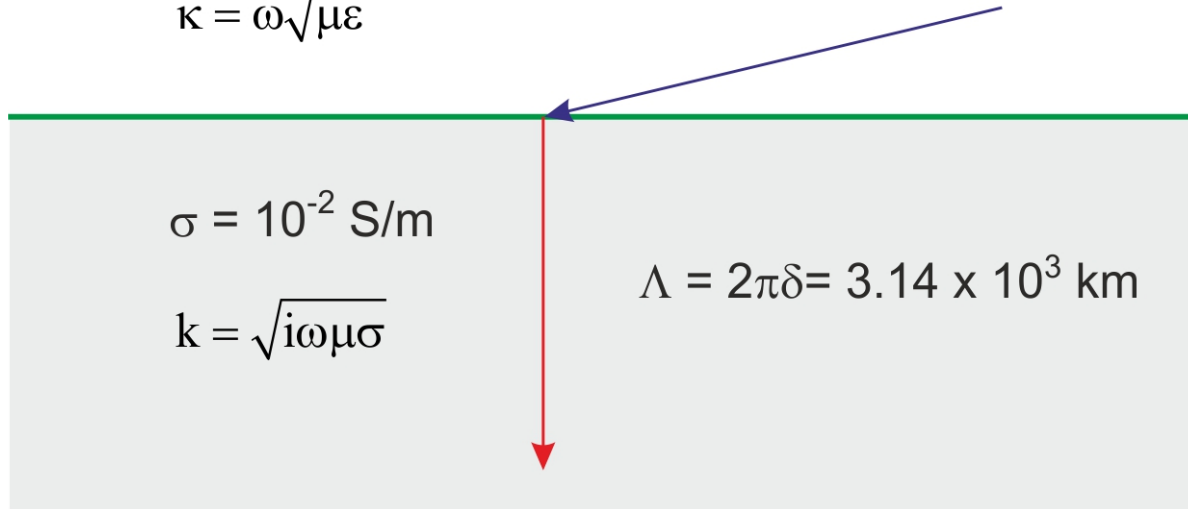
$$\lambda = c_0 T = 3 \times 10^9 \text{ km}$$

$$\kappa = \omega \sqrt{\mu \epsilon}$$

$$\sigma = 10^{-2} \text{ S/m}$$

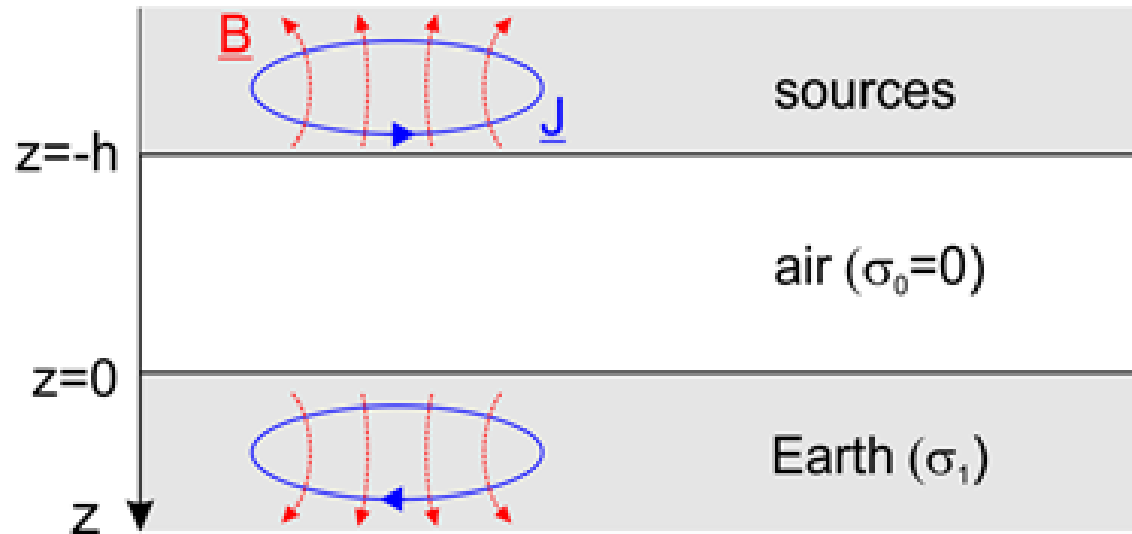
$$k = \sqrt{i \omega \mu \sigma}$$

$$\Lambda = 2\pi\delta = 3.14 \times 10^3 \text{ km}$$



An incoming wave is always refracted perpendicularly into the ground due to the huge conductivity contrast between air and the earth

# The general model of geomagnetic induction without wave analogy



## The magnetotelluric impedance

$$B_y = B_{y0} e^{-kz}$$

$$\frac{\partial E_x}{\partial z} = -E_{x0} k e^{-kz} = -i \omega B_y = -i \omega B_{y0} e^{-kz}$$

$$Z = Z(\omega) = \frac{E_{x0}}{B_{y0}} = \frac{i\omega}{k} = \frac{i\omega}{\sqrt{i\omega\mu\sigma}} = \sqrt{\frac{i\omega}{\mu\sigma}} = \sqrt{\frac{\omega}{\mu\sigma}} \sqrt{i}$$

$$Z(\omega) = -\frac{E_{y0}}{B_{x0}}$$



## Apparent resistivity and phase

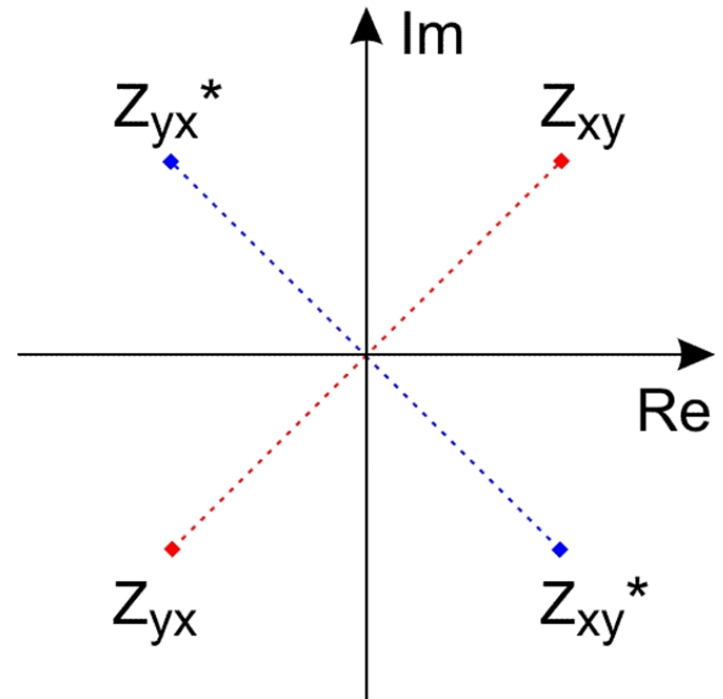
$$|Z| = \sqrt{\frac{\omega}{\mu\sigma}}$$

$$\rho = \rho(\omega) = \frac{\mu}{\omega} |Z|^2 \quad \rho = \rho(T) = 0.2 T |Z|^2$$

$$\varphi = \varphi(T) = e^{i\pi/4} = 45^\circ$$

$$\begin{pmatrix} E_x \\ E_y \end{pmatrix} = \begin{pmatrix} Z_{xx} & Z_{xy} \\ Z_{yx} & Z_{yy} \end{pmatrix} \begin{pmatrix} B_x \\ B_y \end{pmatrix}$$

Impedance tensor



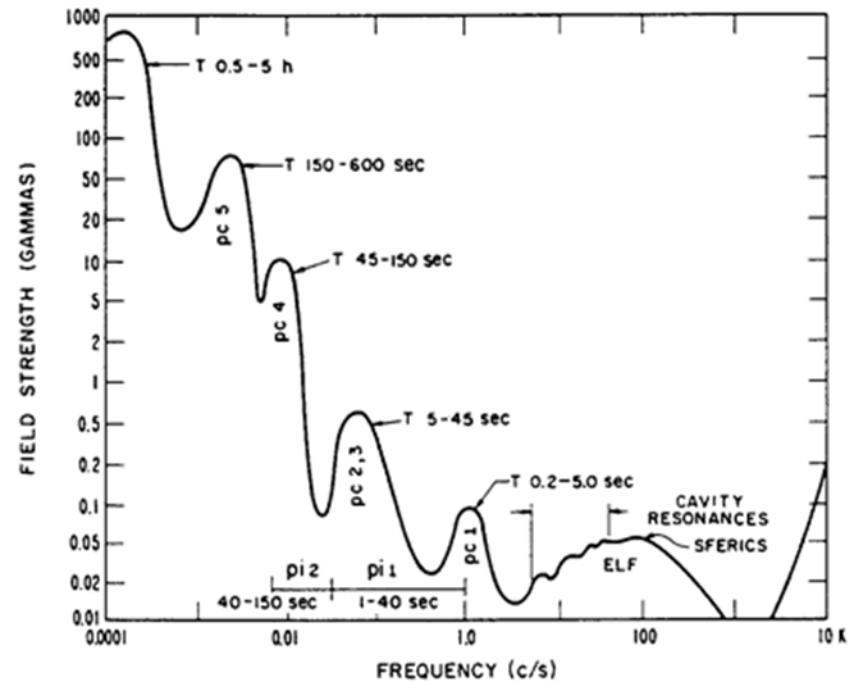
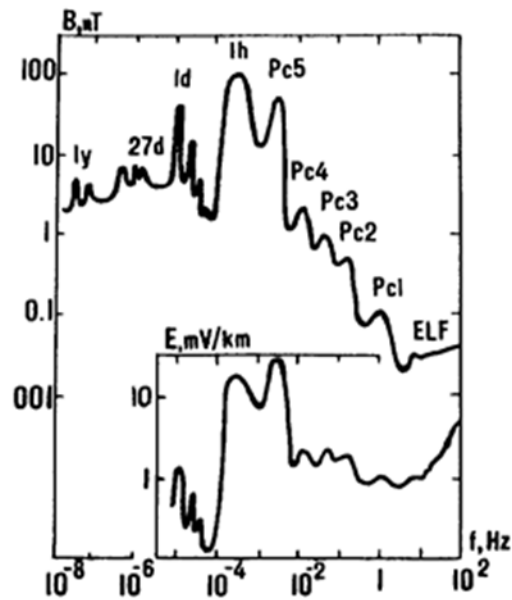
# Magnetotellurics: a passive EM method

So MT relies on the occurrence of natural signals in a broad frequency range from approx.  $10^{-4} < f < 10^4$  Hz.

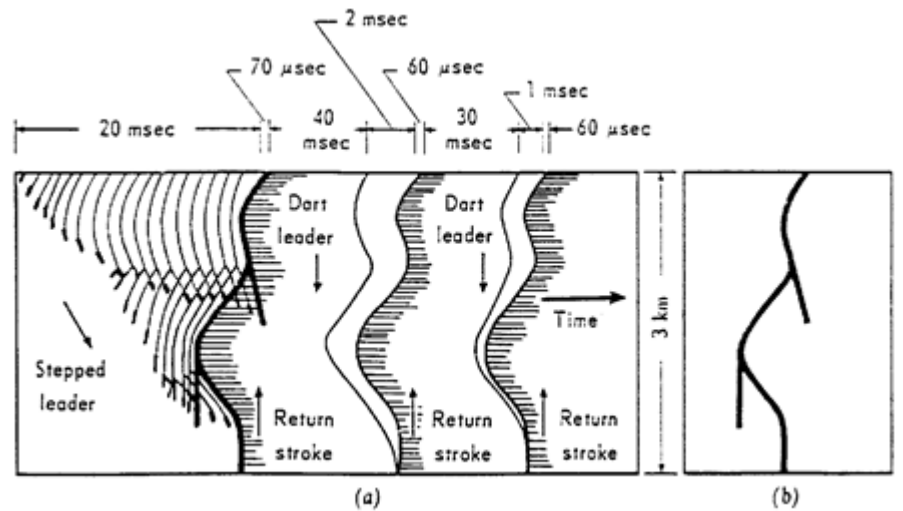
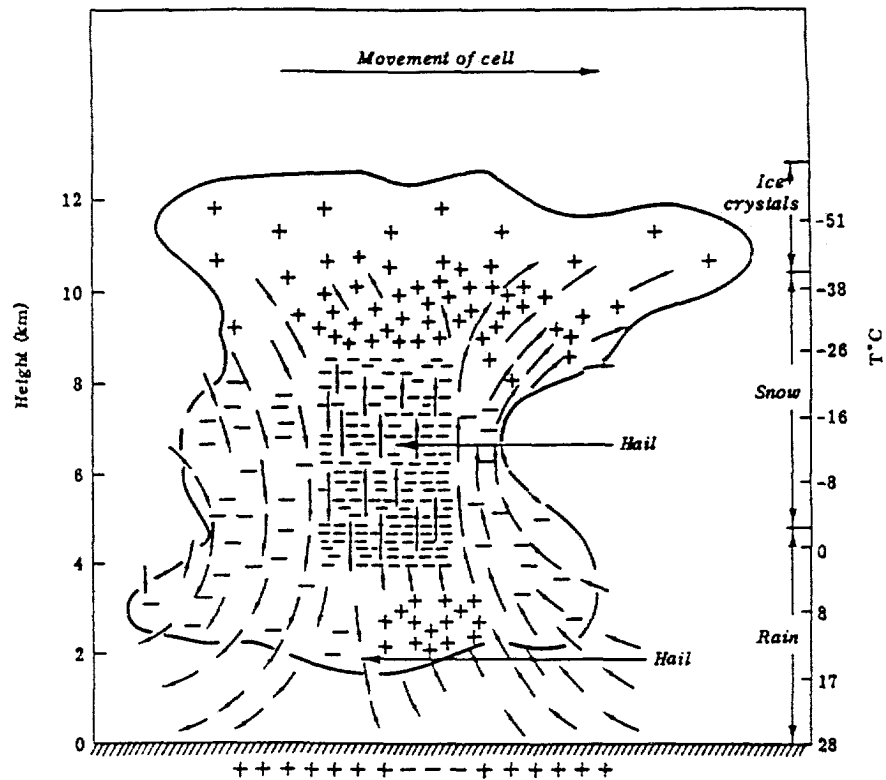
But does this natural excitation exist reliably? Fortunately yes!

- $f > 1$  Hz: Radiation from lightnings, propagation worldwide in the waveguide earth/ionosphere, Schumann resonances → **Audiomagnetotellurics (AMT)**
- $f < 1$  Hz: Variations of the solar wind, frozen magnetic field, interaction with magnetosphere → **long-period magnetotellurics (LMT)**
- Since modern induction coil magnetometers cover a broad frequency range → **broad-band magnetotellurics (BBMT)**

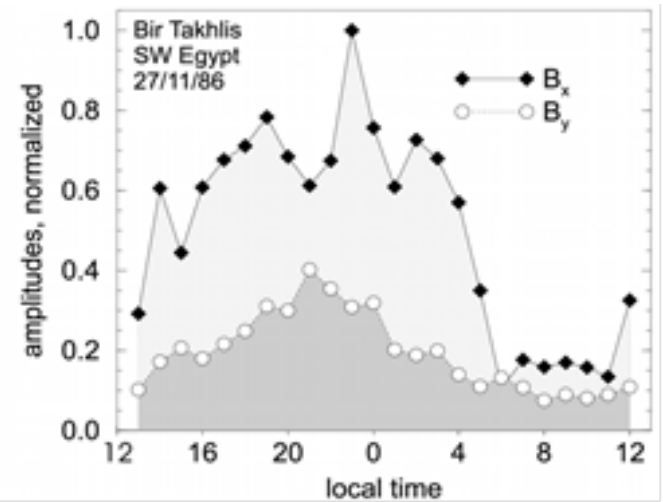
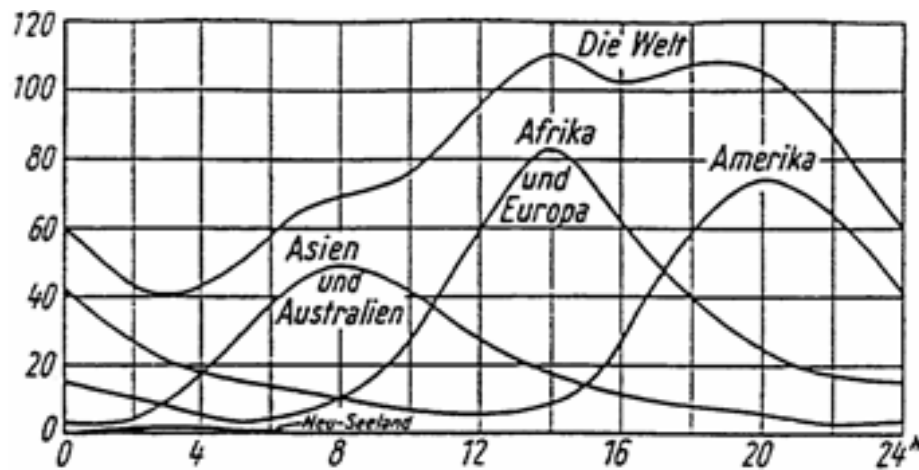
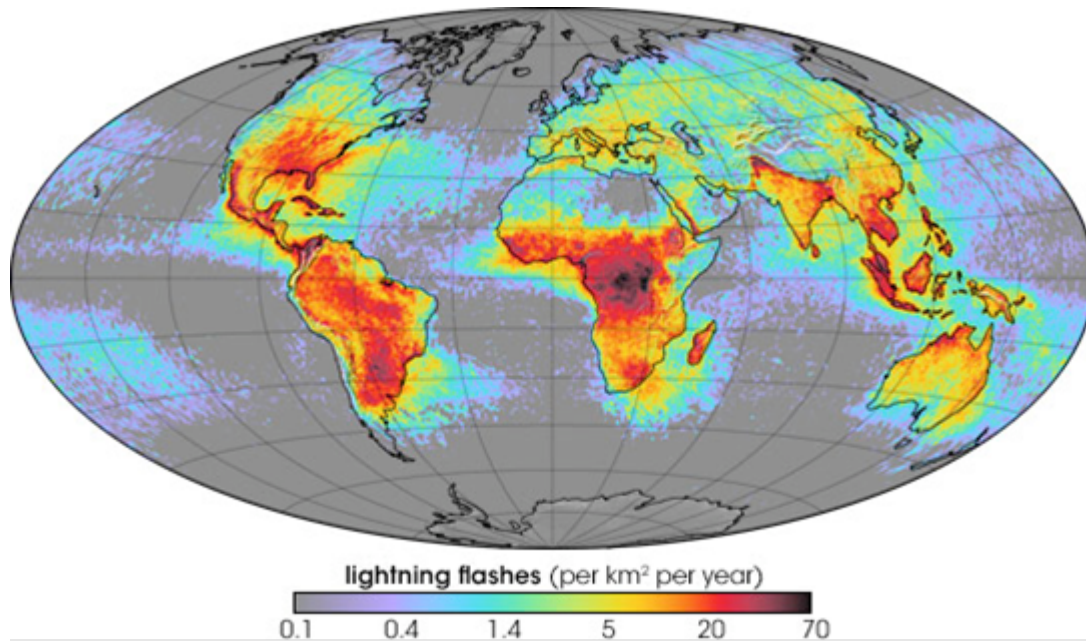
# Geomagnetic variations – an overview



# Lightnings



# Frequency of lightnings

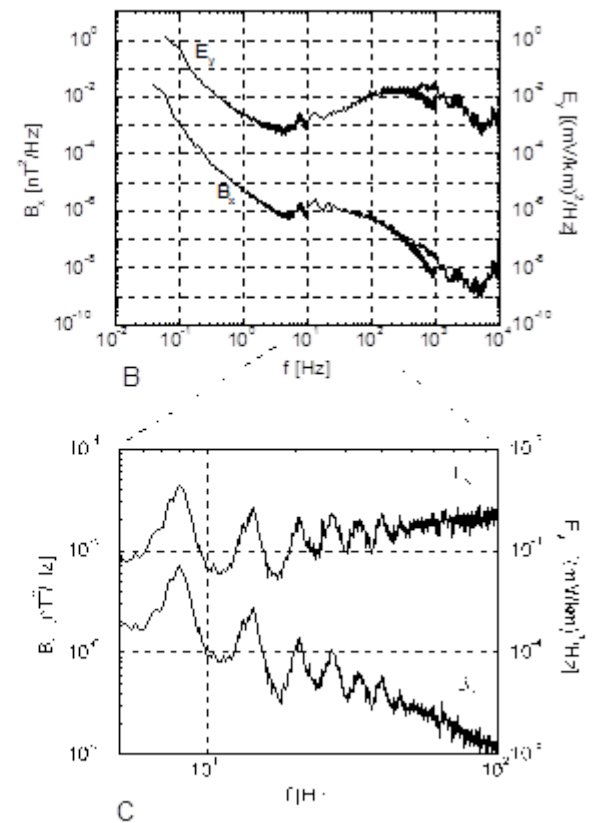
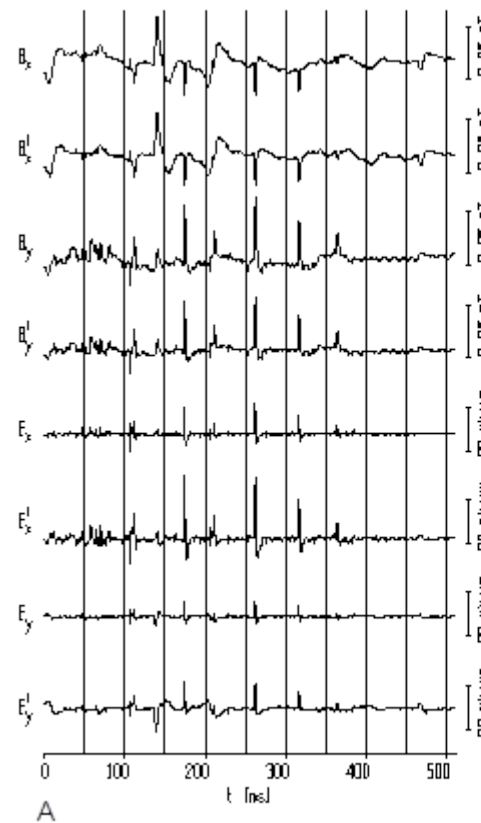
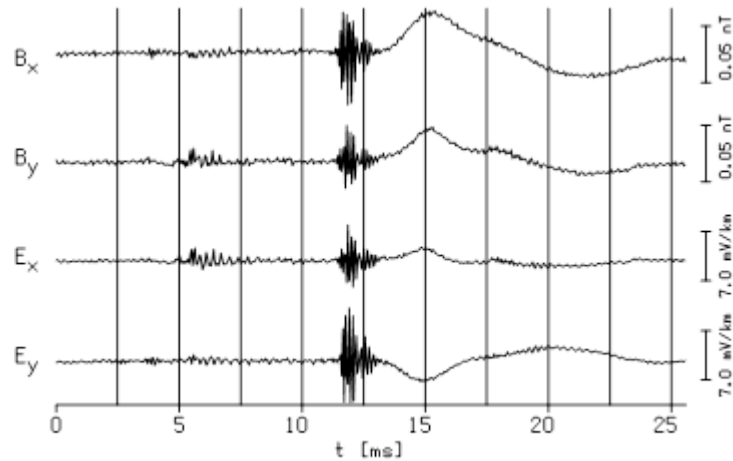


# Exotic sources



Chaitén 2008 eruption ([nature.com](http://nature.com))

# Some atmospherics and Schumann resonances in a noise-free environment (Eastern Sahara)

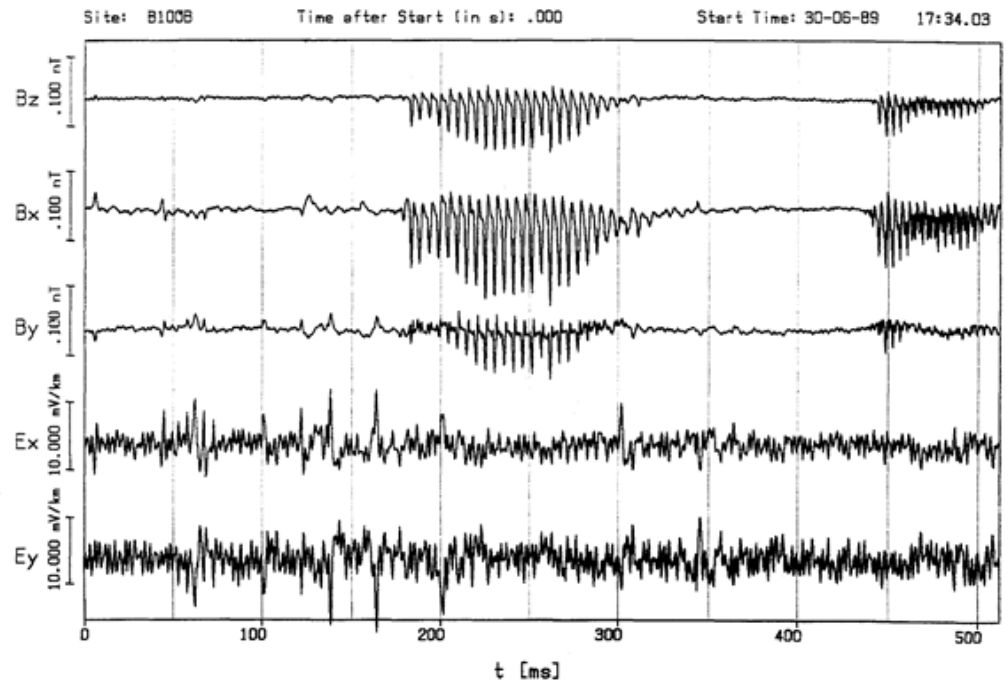
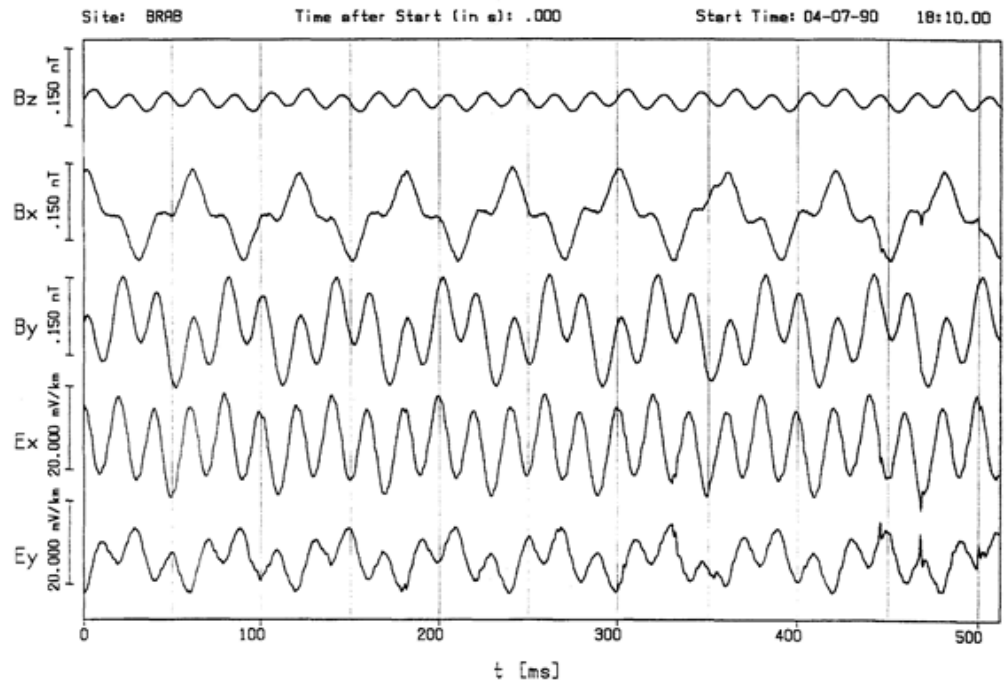


# Perturbances

Railway (DC, 16.7 Hz) and  
power line networks (50 or 60  
Hz plus harmonics)

Worst noise comes from DC  
sources.

But if one knows the current,  
one may utilize this as CSEM  
or TEM source!





# Long-period variations

Link to Niemegk observatory:

[http://www-app3.gfz-potsdam.de/Magnetogramme/Niemegk/niemegk\\_dhz\\_e.html](http://www-app3.gfz-potsdam.de/Magnetogramme/Niemegk/niemegk_dhz_e.html)

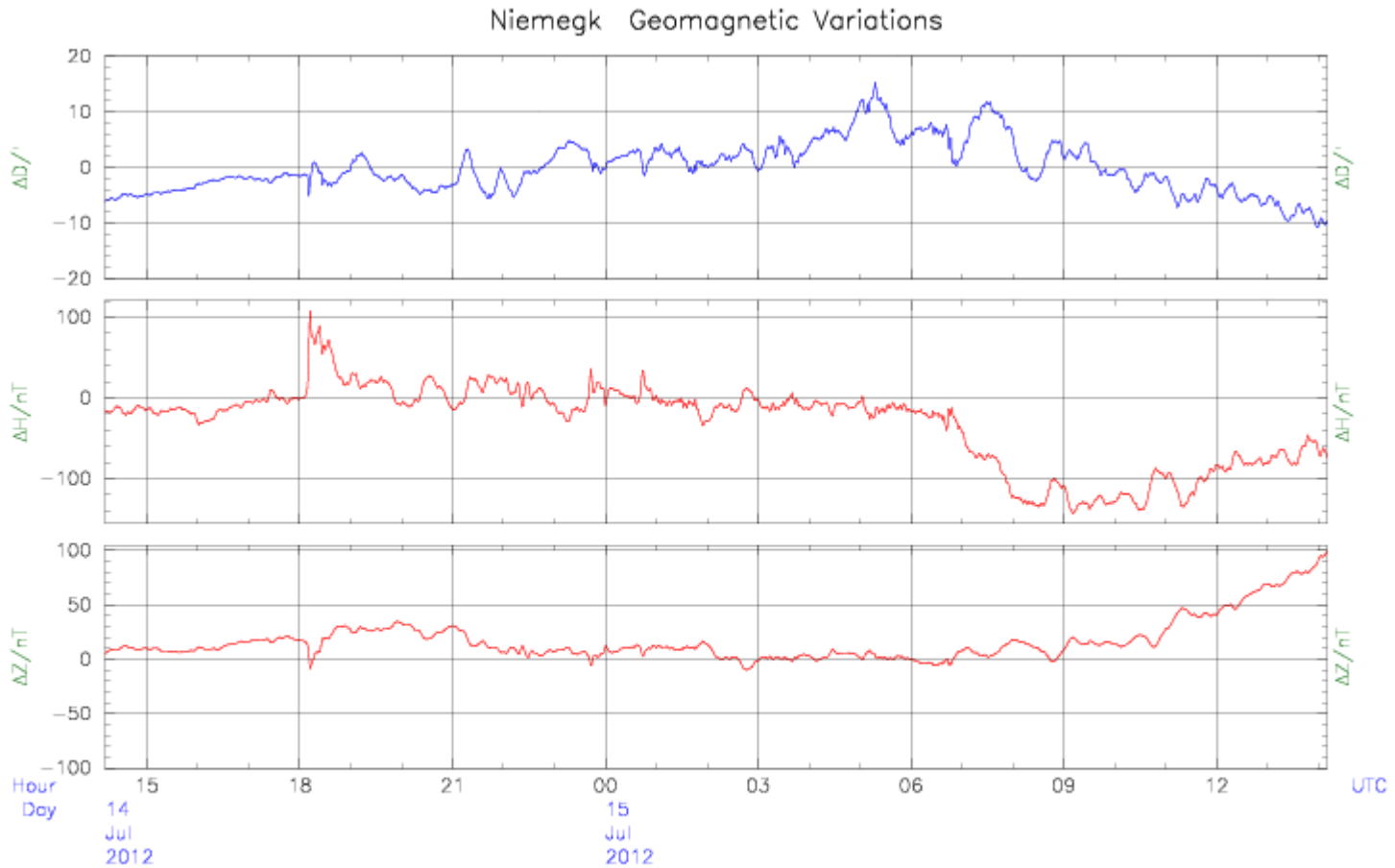
[http://www-app3.gfz-potsdam.de/Magnetogramme/Niemegk/niemegk\\_k\\_e.html](http://www-app3.gfz-potsdam.de/Magnetogramme/Niemegk/niemegk_k_e.html)

Space weather:

[www.spaceweather.com](http://www.spaceweather.com)

<http://www.swpc.noaa.gov/SWN/>

# Last days (small) geomagnetic storm



Determination of the absolute values:  $D = 172' + \Delta D$ ,  $H = 18894 \text{ nT} + \Delta H$ ,  $Z = 45470 \text{ nT} + \Delta Z$

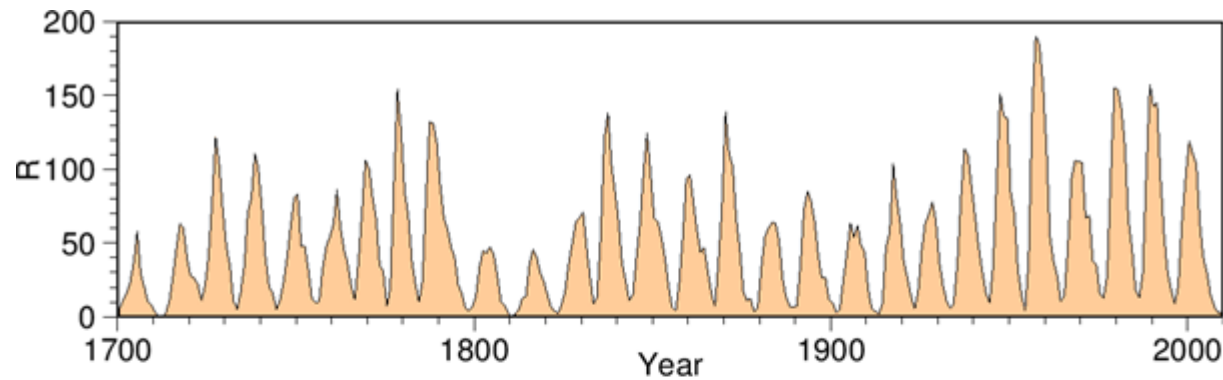


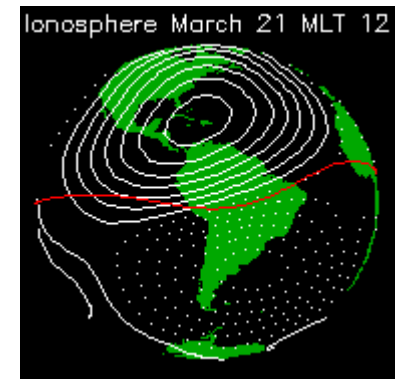
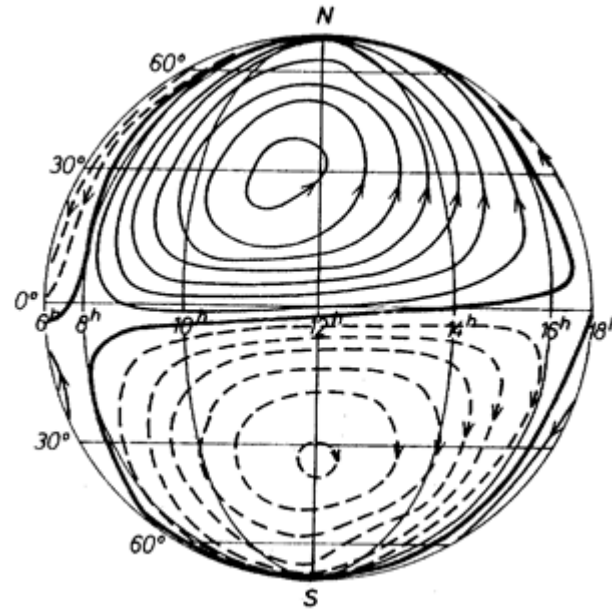
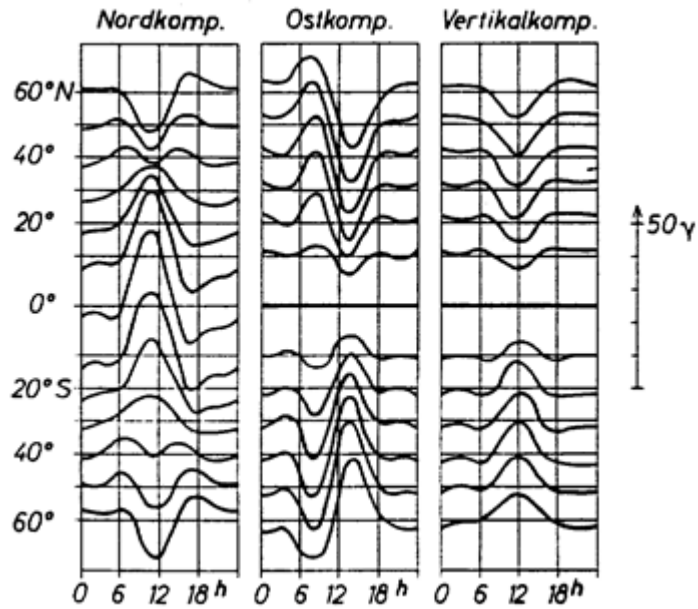
*Fig. 3.15a: Relative number of sunspots  $R$  to measure solar activity from 1700-2010. Plotted from data of the World Data Center for the Sunspot Index, Royal Observatory of Belgium (<http://sidc.oma.be/>). In the second half of the 17th century hardly any spots could be observed (Maunder minimum). This correlated with a global cooling of the earth.*

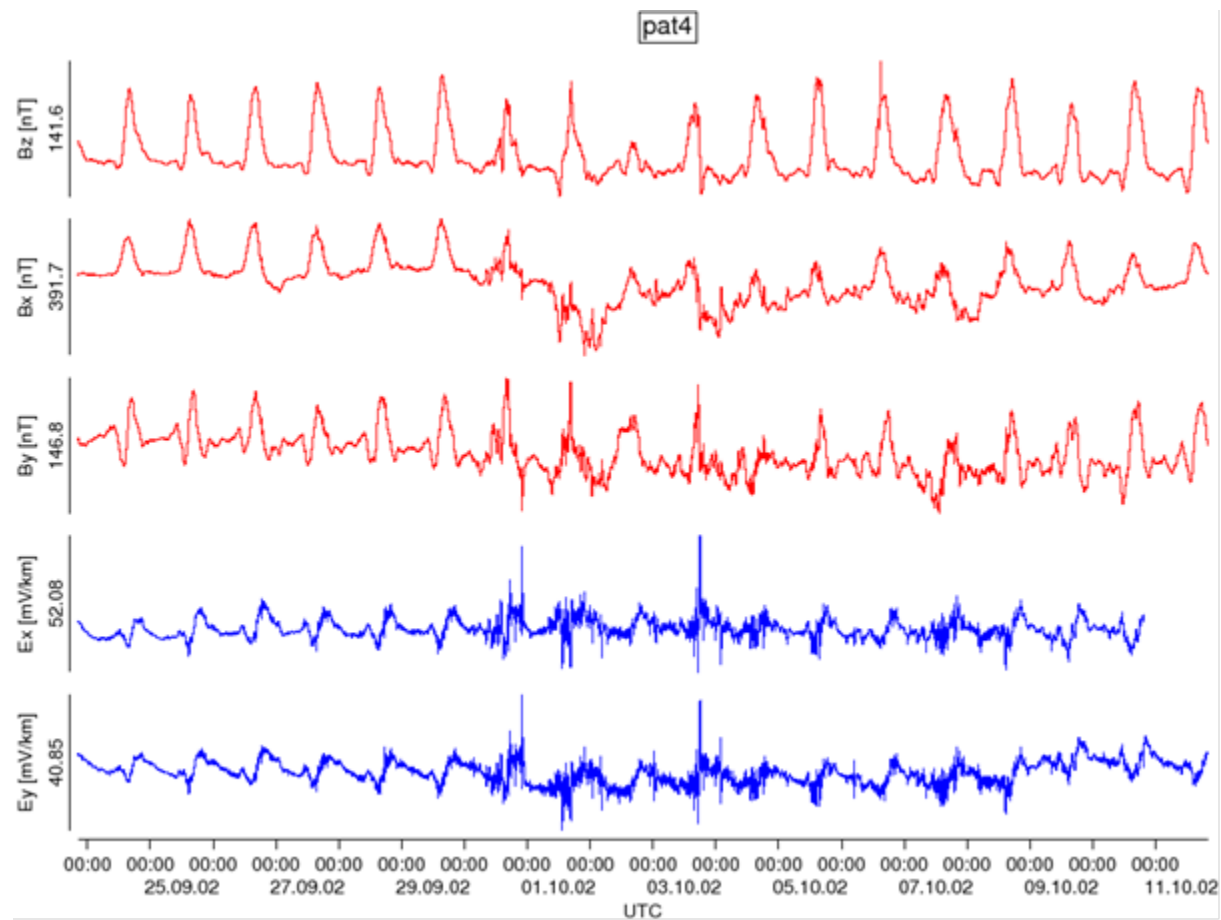


*Fig. 3.15b: Several large spot groups on the surface of the sun in October 2003. Source: NASA.*

### 3.4 Sq-Variations

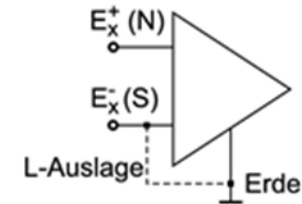
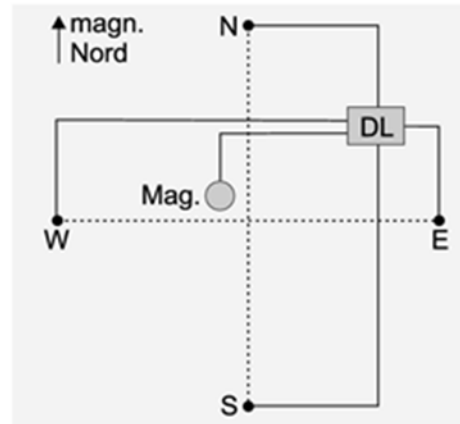
4.2.1.1.1.1.1.1 Variations with periods of one day ( $T = 24\text{h} + \text{harmonics}$ ) can be observed on days without magnetic perturbations. For this reason they are called Sq (solar quiet). They are the result of current eddies in the ionosphere on the day side and they strongly depend on the latitude. These variations are an inhomogeneous source for normal magnetotellurics. Fig. 3.19 shows a registration example





# Modern measurement systems

- Unpolarizable electrodes
- Cable length 50-100m
- Data acquisition standard today: 24bit ADC
- GPS controlled – many sites operate simultaneously



- Operation times: 3-4 days BBMT, 2 weeks LMT. More offshore
- Remote reference is standard now
- Interstation functions (magneto-variation method)



*Fig. 4.1: Above left: Fundamental layout in the field (DL: data logger). The probes are in a cross layout. Above right: Connection of the telluric probes at the input of an operational amplifier. Below left: Layout of telluric cables. Below right: View on data logger, electronics for controlling the fluxgate magnetometer, external GPS for time synchronization and solar*

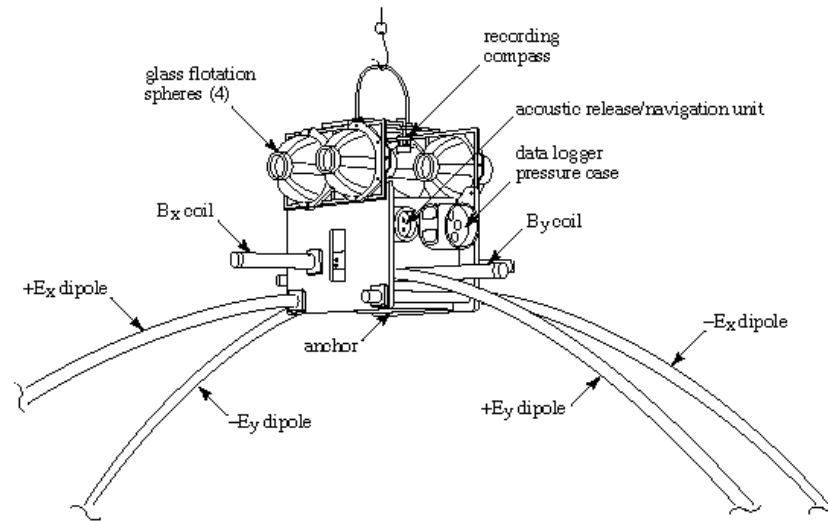


Fig. 4.2: Scheme and deployment of an instrument for the sea bottom, in this version with induction coils.  
 Source: Web site Scripps Institution of Oceanography, S. Constable

*Induction coil magnetometers* basically consist of a large number of windings wrapped around a highly-permeable  $\mu$ -metal core. The induced voltage in a single loop is

$$U = -nA \frac{\partial B}{\partial t} \cos \vartheta \quad . \quad (4.1)$$

Consequently, voltage is proportional to frequency. In (4.1)  $n$  indicates the number of coils,  $A$  the enclosed area and  $\vartheta$  is the angle of the surface normal to the magnetic field lines. A simple estimation with  $B = 1 \text{ nT}$ ,  $T = 1 \text{ s}$ ,  $\vartheta = 0^\circ$ ,  $n = 1$  and  $A = 0.01 \text{ m}^2$  results in a voltage  $U = 10^{-11} \text{ V}$ ! However, voltages in the order of mV are necessary. For this reason, in practice, coils with  $10^4$  to  $10^5$  windings are used. It is not possible to extend the area  $A$  significantly, but the same effect can be achieved by coiling on a highly permeable core (superpermalloy). Instead of (4.1) and with  $\vartheta = 0^\circ$ , then follows:

$$U \approx -nA \frac{\partial B}{\partial t} \mu_r \quad , \quad (4.2)$$

with  $\mu_r$  that can reach values of up to  $10^5$  (superpermalloy).

The number of turns cannot be extended at will because they increase the inner resistance and the capacity of the coils which result in a characteristic resonance curve (see Fig. 4.3) with the following resonance frequency:

$$\omega_0 = \sqrt{\frac{1 + R/R_e}{LC}} \quad , \quad (4.3).$$

Here  $R_e$  indicates the input resistance of the instrument.

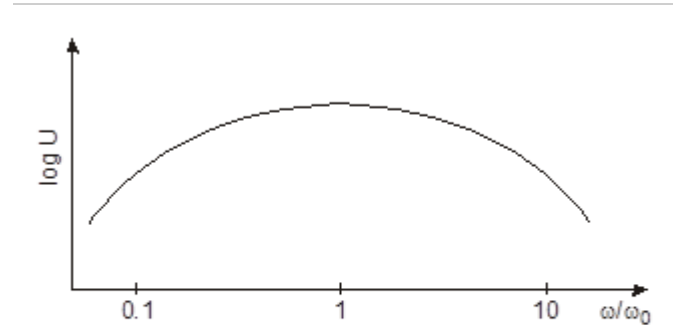


*Fig. 4.3: Fundamental course of the resonance curve of an induction coil.*



Of course, we prefer a flat curve, i.e. a constant sensitivity for a large frequency range (Fig. 4.4). This can be achieved by an additional bucking coil. Using an electronic *chopper*- or *lock-in-amplifier* it is possible to extend the frequency range of induction coils far into the range of long periods. In this case the weak low-frequency signal is modulated (multiplied by an alternating rectangle function), intensified, demodulated and finally filtered with a low-pass filter.

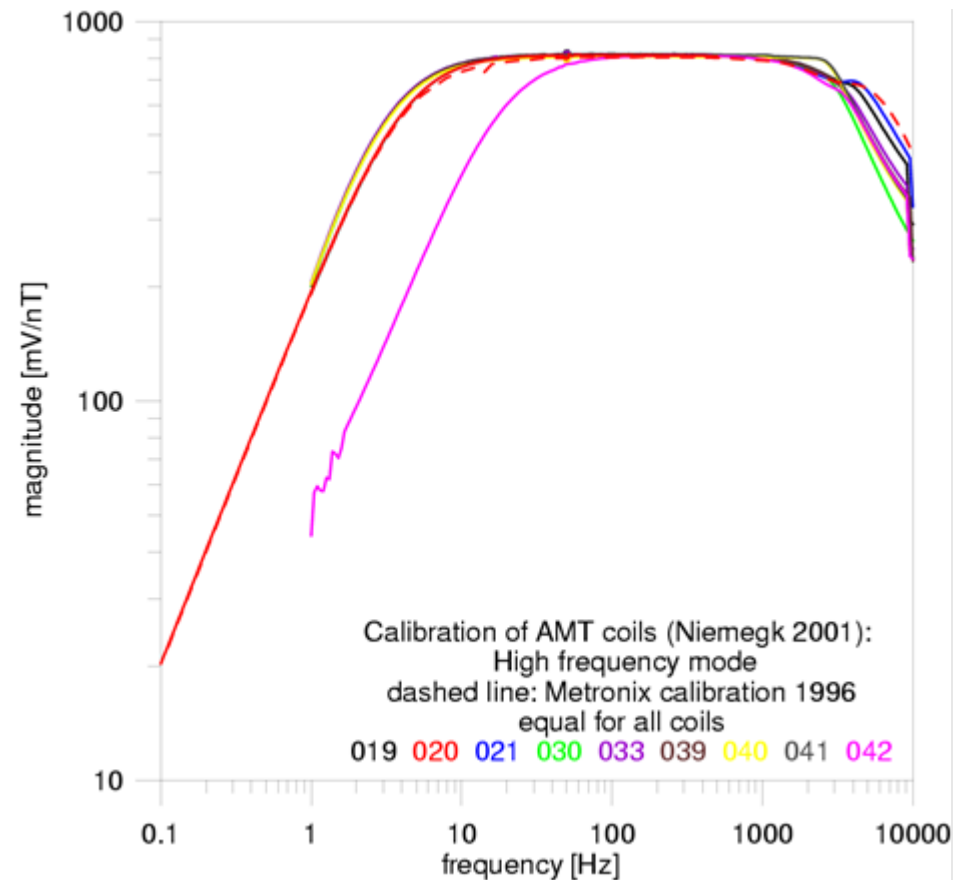


Fig. 4.4: Example of the calibration of several induction coils. The different coils should have the same transfer function. In coil no. 42 (pink line) one element of the filter seems to be broken down.

For long periods ( $T \approx 10 \text{ s} - \text{DC}$ ) *fluxgate magnetometers* are used. These fluxgate magnetometers have a special method of measuring: the outer magnetic field  $B_0$  is superimposed by a harmonic signal so that the non-linear part of the hysteresis curve of a ferrite core is reached. The resulting field contains harmonics in which one harmonic, that is proportional to  $B_0$ , is filtered out electronically (see Fig. 4.5).

A hysteresis curve can be described as a third-degree polynomial:

$$B(H) = \mu_0(3H - H^3) \text{ for } H \leq 1 = H_s, \quad (4.4a)$$

with  $H$  normalized to the saturation field strength  $H_s$ . If we apply an exciting field  $H_-(t) = a \sin \omega t$  to a coil then the resulting field is

$$H(t) = H_e + H_-(t) = H_e + a \sin \omega t \quad ; \quad (4.4b)$$

with  $H_e$  indicating the relevant external field. Then the voltage in a coil around the excitation coil is induced

$$U_{\text{ind}} \sim \frac{\partial B}{\partial t} = 3a(1 - H_e^2 - \frac{1}{4}a^2)\omega \cos \omega t - 3H_e a^2 \omega \sin 2\omega t + \frac{3}{4}a^3 \omega \cos 3\omega t \quad (4.4c).$$

The second harmonic only occurs in the case of  $H_e = 0$ . It is filtered out and measured. The frequency of the excitation field is around several kHz. The excitation coils are wrapped in opposite direction around a double core (or a ring core). The induction coil encloses both and the harmonics with odd numbers complement each other to zero.

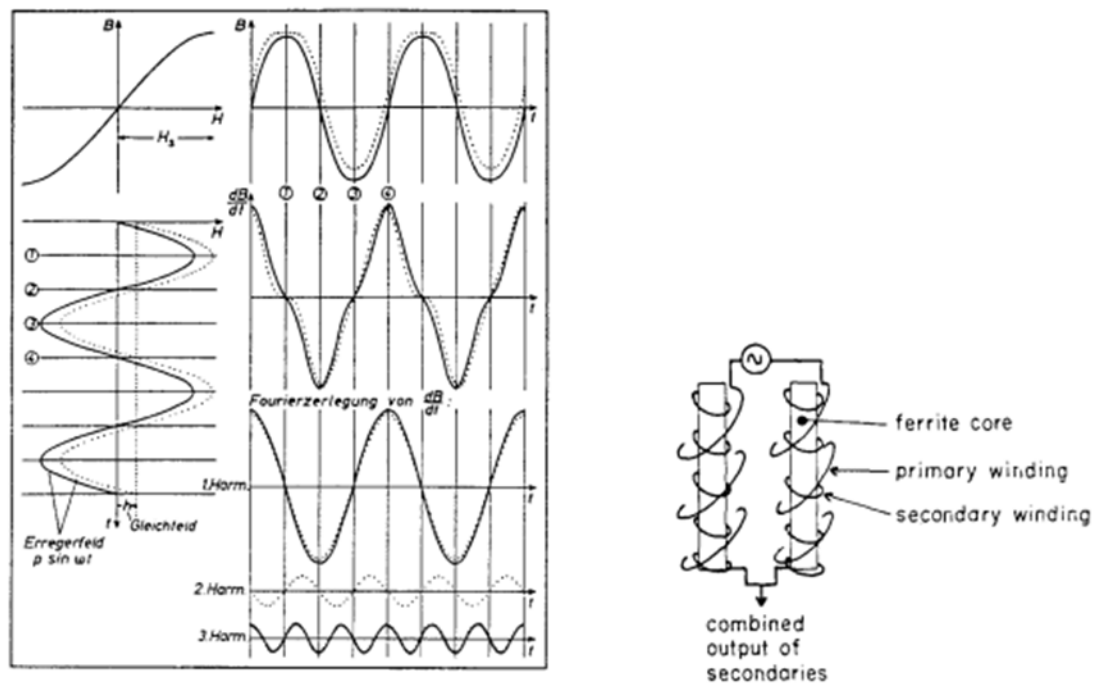


Fig. 4.5: Principle of a fluxgate magnetometer.

## Digging hole for vertical induction coil





As it should be and should not be...



# 1-D subsurface

Recursion formula by Wait (1953) and Lipskaya (1954)

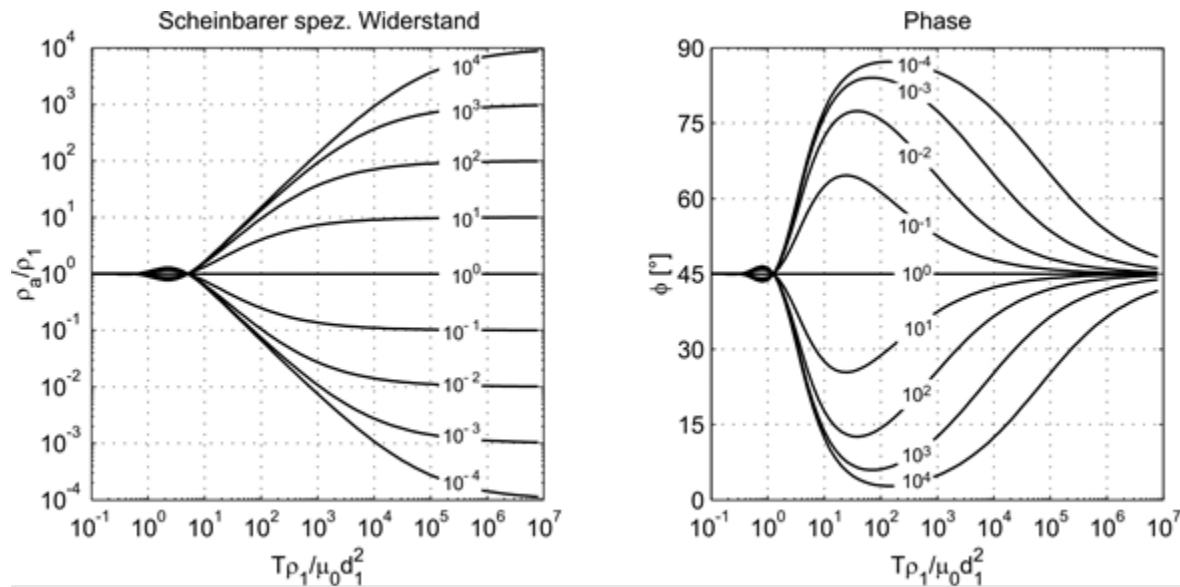
$$C_m = \frac{\gamma_m C_{m+1} + \tanh(\gamma_m d_m)}{\gamma_m (1 + \gamma_m C_{m+1} \tanh(\gamma_m d_m))}$$

$$\gamma_m = \sqrt{i\omega\mu_0\sigma_m + v^2}$$

With  $Z = i\omega C$ ,  $d$  layer thickness,  $\gamma$  wavenumber

- Apparent resistivity  $\rho_a$
- Phase between  $0^\circ$  and  $90^\circ$

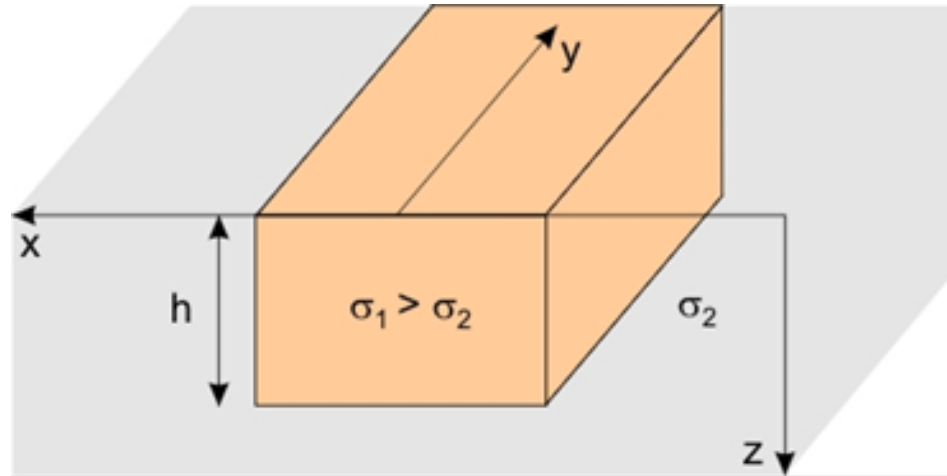
# MT curves for layered media



<http://userpage.fu-berlin.de/~mtag/mt1d/MT-Java.html>



The earth is not 1-D, but perhaps 2-D



E-polarization (TE mode)

$$\frac{\partial B_x}{\partial z} - \frac{\partial B_z}{\partial x} = \mu_0 \sigma E_y$$

$$\frac{\partial E_y}{\partial x} = -\frac{\partial B_z}{\partial t}$$

$$\frac{\partial E_y}{\partial z} = \frac{\partial B_x}{\partial t}$$

B-polarization (TM mode)

$$\frac{\partial B_y}{\partial x} = \mu_0 \sigma E_z$$

$$\frac{\partial B_y}{\partial z} = -\mu_0 \sigma E_x$$

$$\frac{\partial E_x}{\partial z} - \frac{\partial E_z}{\partial x} = -\frac{\partial B_y}{\partial t}$$

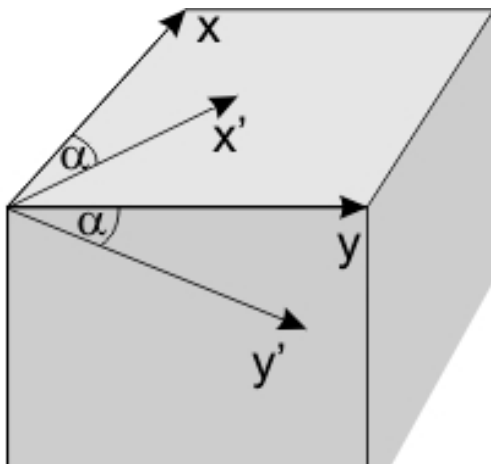


## 2-D MT

First look, if data are really 2-D, e.g. by calculating the skewness (Swift), but note that this is a bad measure:

$$S = \frac{|Z_{xx} + Z_{yy}|}{|Z_{xy} - Z_{yx}|}$$

Then rotate into correct coordinate system



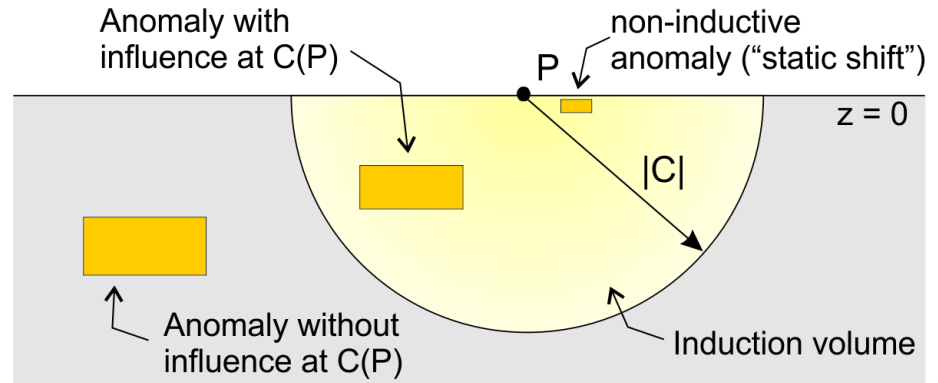
$$\underline{\underline{E'}} = \underline{\underline{R}} \underline{\underline{E}} \quad , \quad \underline{\underline{B'}} = \underline{\underline{R}} \underline{\underline{B}} \quad \text{and}$$

$$\underline{\underline{Z'}} = \underline{\underline{R}} \underline{\underline{Z}} \underline{\underline{R}}^T \quad \text{with } \underline{\underline{R}} = \text{matrix of rotation:}$$

$$\underline{\underline{R}} = \begin{pmatrix} \cos \alpha & \sin \alpha \\ -\sin \alpha & \cos \alpha \end{pmatrix} \quad \text{with } \det \underline{\underline{R}} = 1$$

## 2-D MT

Better to use measures which do not depend on the magnitude of  $Z$  because of static shift problems:



*Definition of the induction space at a given frequency.*

- Phase-sensitive skew (Bahr)
- Phase tensor (Caldwell et al. 2004)
- Multi-site multi-frequency algorithms (Smith 1995, MacNeice and Jones 2004)

Then 2-D inversion, which is standard today. Most common codes are from Rodi and Mackie (2001) and Siripunvaraporn et al. (2000). They make use – in the one or other way – of Tikhonov regularization:

$$\|\underline{G}\underline{m} - \underline{d}\|^2 + \alpha^2 \|\underline{L}\underline{m}\|^2 = \text{Min}!$$

# The phase tensor (Caldwell et al. 2004)

Problem: Electric field is distorted by small-scale inhomogeneities

$\underline{E} = D \underline{E}_R$  with  $\underline{E}_R$  the regional (wanted) field and the real distortion matrix  $D$  which leads to a parallel shift of app. resistivity curves (also in VES!) while the phase is not affected. Then also  $Z = D Z_R$ .

$$Z = X + iY$$

$$\Phi = X^{-1}Y = \Phi_R$$

$$\beta = \frac{1}{2} \tan^{-1} \left( \frac{\Phi_{12} - \Phi_{21}}{\Phi_{11} + \Phi_{22}} \right)$$

$$\alpha = \frac{1}{2} \tan^{-1} \left( \frac{\Phi_{12} + \Phi_{21}}{\Phi_{11} - \Phi_{22}} \right)$$

Skew angle  $\beta$  is an indicator for dimensionality,  $\alpha$  is the geoelectrical strike.

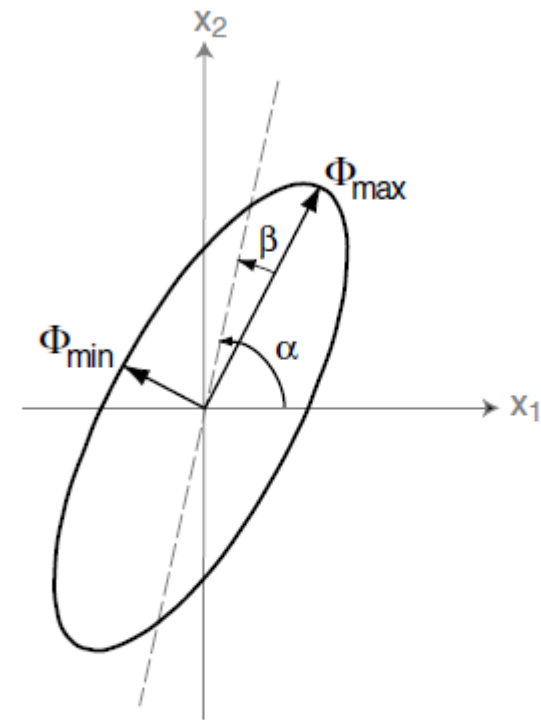


**Figure 1.** Graphical representation of the phase tensor. The lengths of the ellipse axes, which represent the principal axes of the tensor, are proportional to the principal (or singular) values of the tensor. If the phase tensor is non-symmetric, a third coordinate invariant represented by the angle  $\beta$  is needed to characterize the tensor. The direction of the major axis of the ellipse, given by the angle  $\alpha - \beta$ , defines the relationship of the tensor to the observer's reference frame or coordinate system  $(x_1, x_2)$ .

# Induction vectors (or arrows)

Tipper (in TE mode): transfer function between vertical and horizontal magnetic field

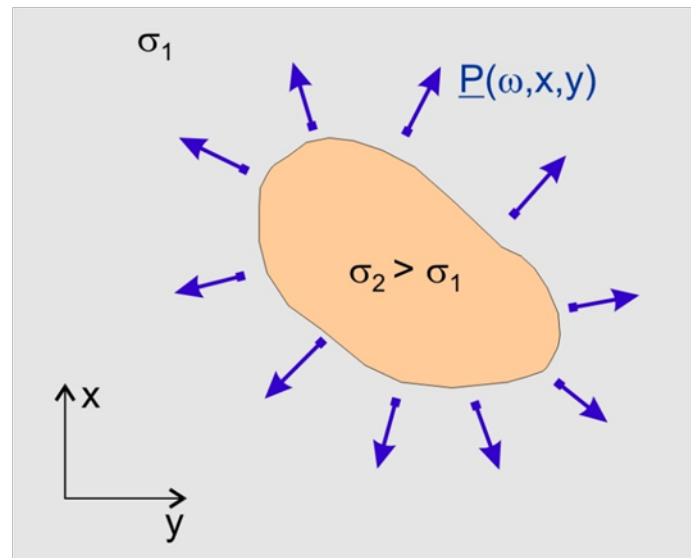
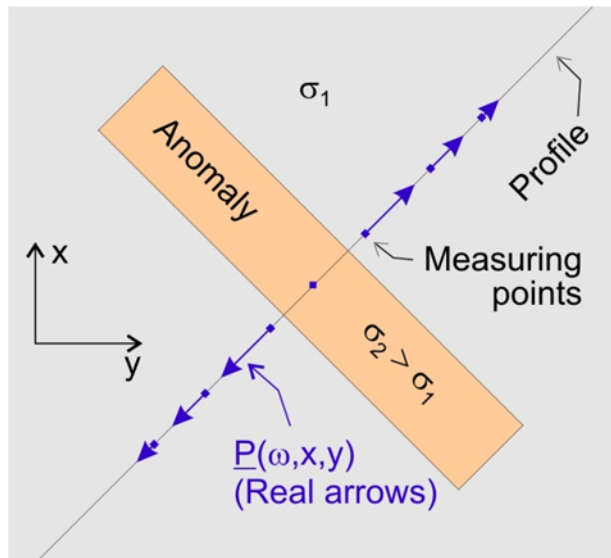
$$\underline{B}_z = T_x \underline{B}_x + T_y \underline{B}_y$$

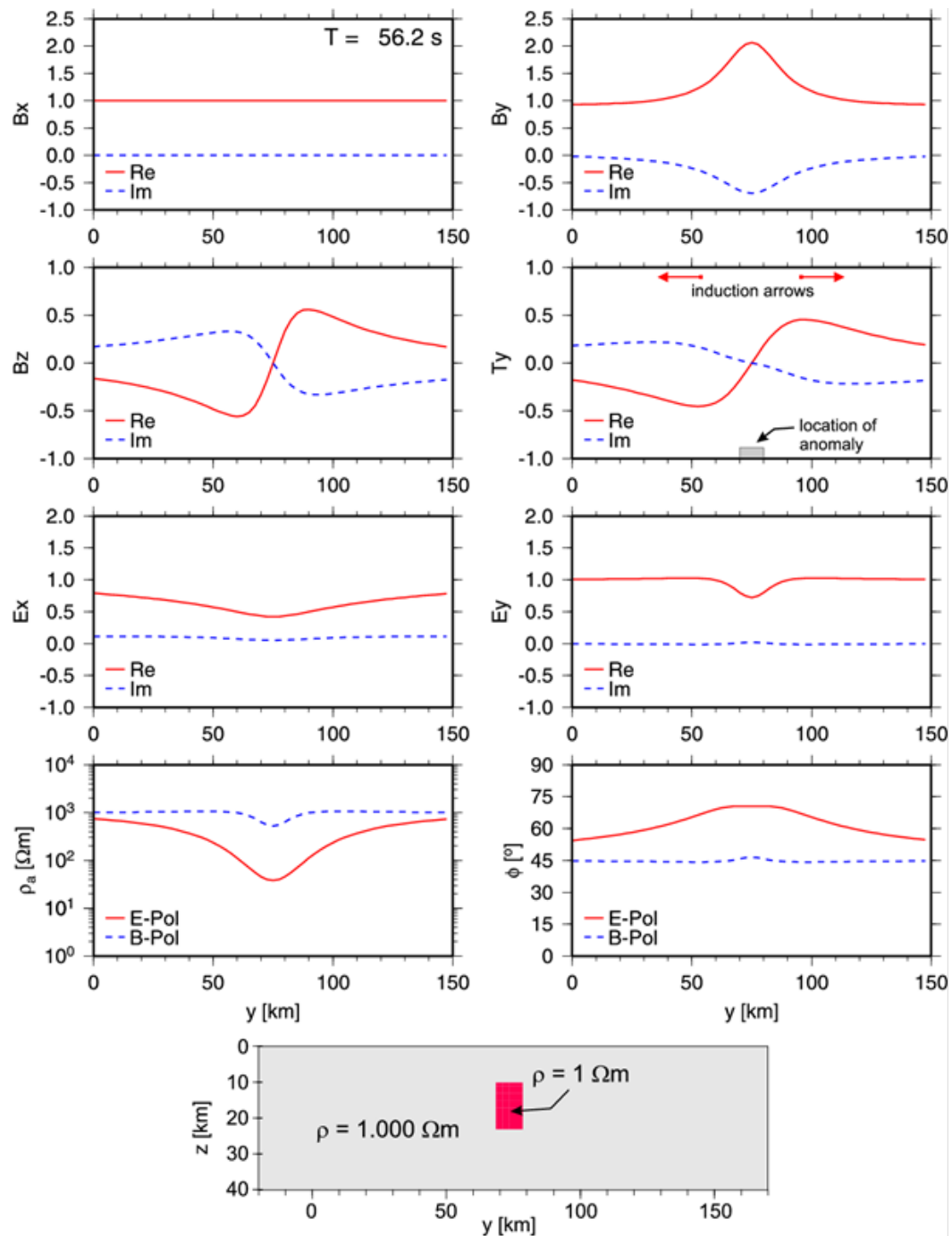
From this, calculate induction vectors and plot them on a map:

$$\underline{P} = \text{Re } T_x \underline{e}_x + \text{Re } T_y \underline{e}_y$$

$$\underline{Q} = \text{Im } T_x \underline{e}_x + \text{Im } T_y \underline{e}_y$$

Wiese or Parkinson convention



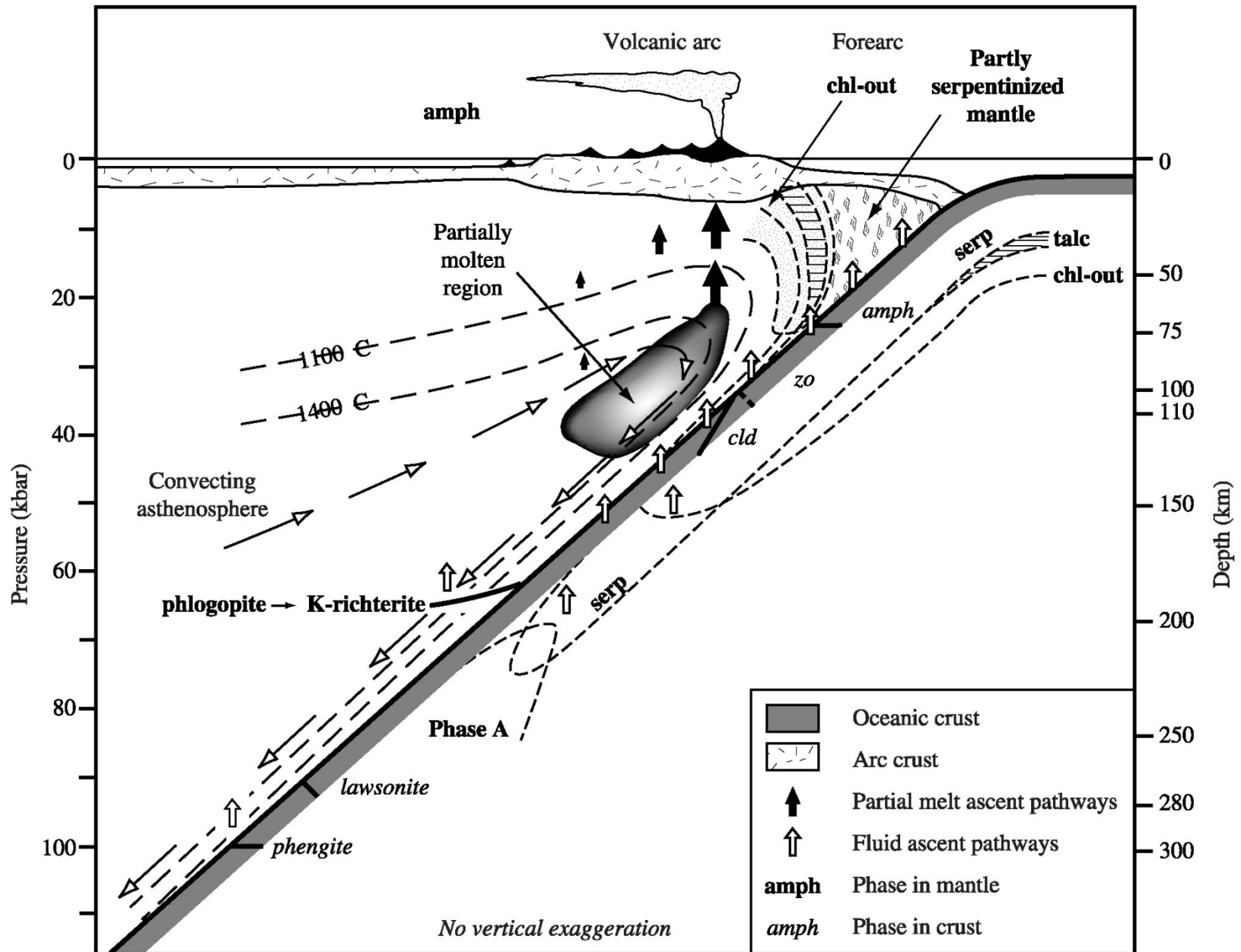


## Example Costa Rica – Nicaragua

Now, 3-D inversion is evolving. Free codes by Siripunvaraporn et al. (2005) and Egbert & Kelbert (2012).

New codes are for multi-core architecture  
(with, e.g., open MPI, open MP)

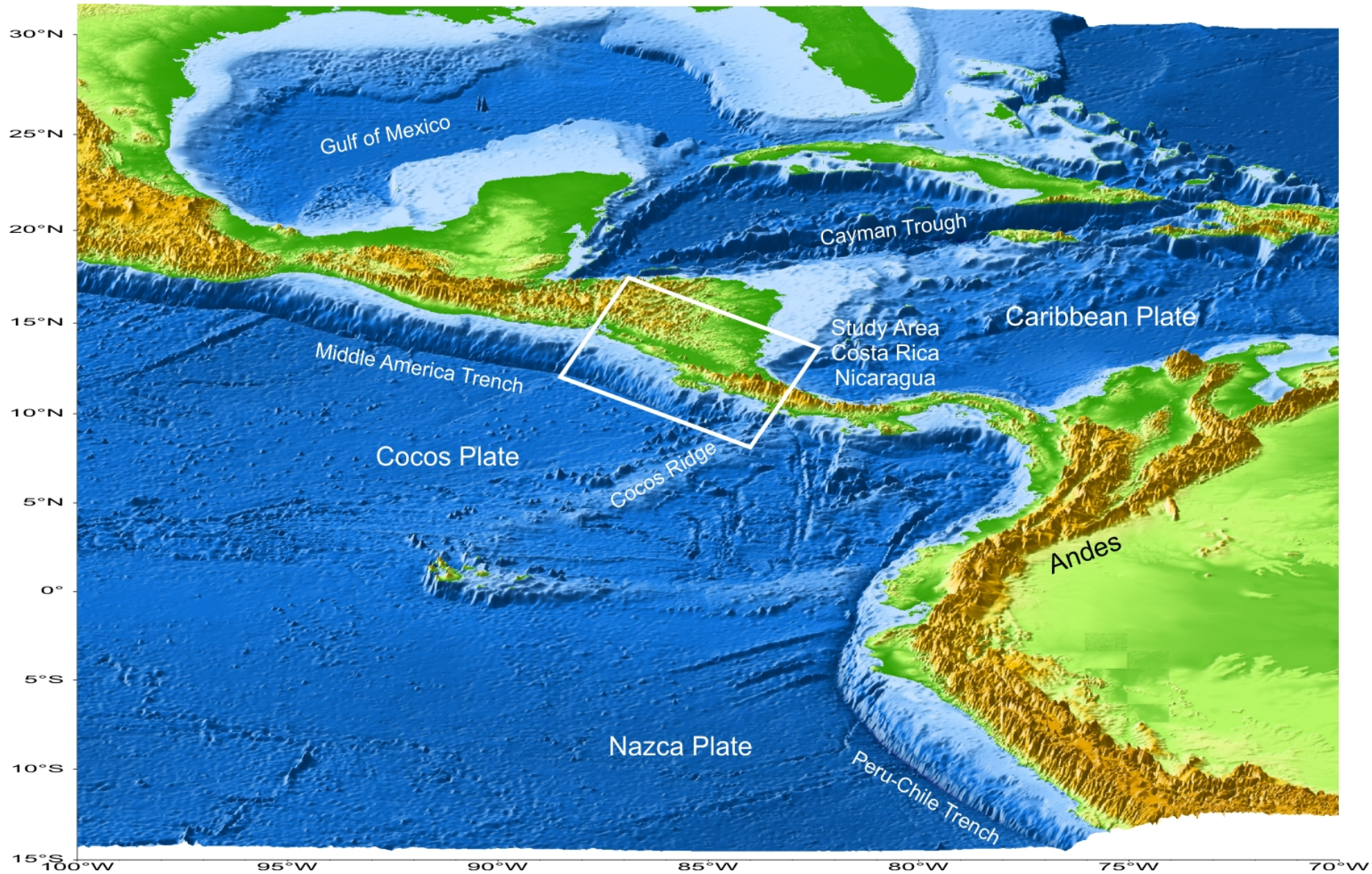
# Standard model of subduction: fluids and melts should appear in images of electrical conductivity



from: Stern, Rev. Geophys. 2002; similar scenario for Andean subduction at larger depths



# Setting of the Central American Isthmus





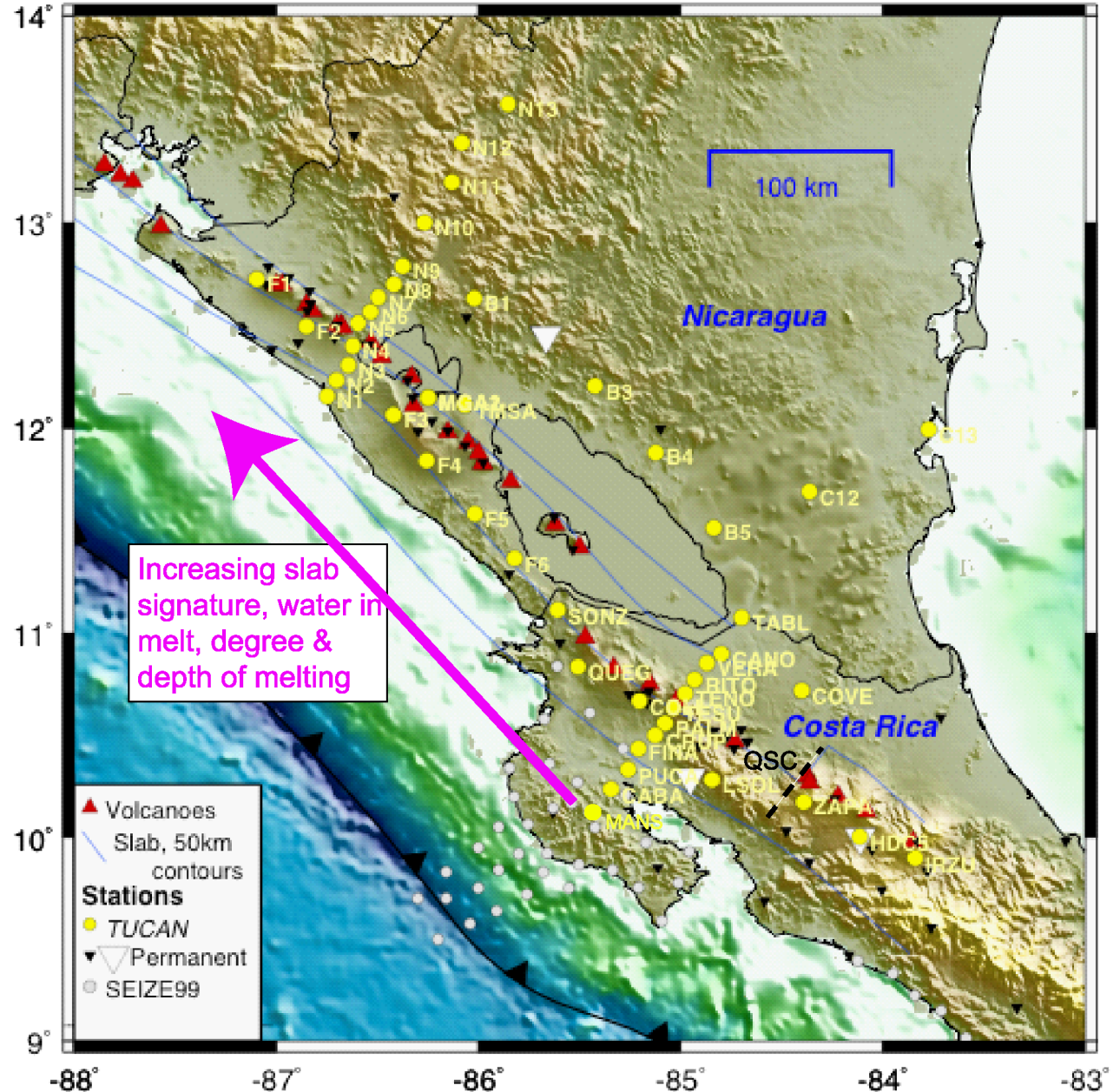
## Some plate-tectonic characteristics

From NW to SW depth of Middle America Trench decreases from  $> 5$  km to  $< 2$  km

Very active volcanism,  
with sharp offset of  
volcano line at border  
between NI and CR;  
significant differences in  
lava chemistry.

NI volcanoes sit on a  
much deeper part of the  
W-B zone.

Large number of active and passive seismic experiments. Latest: TUCAN network (G. Abers et al., Columbia University). Plot from: Rychert et al. 2008

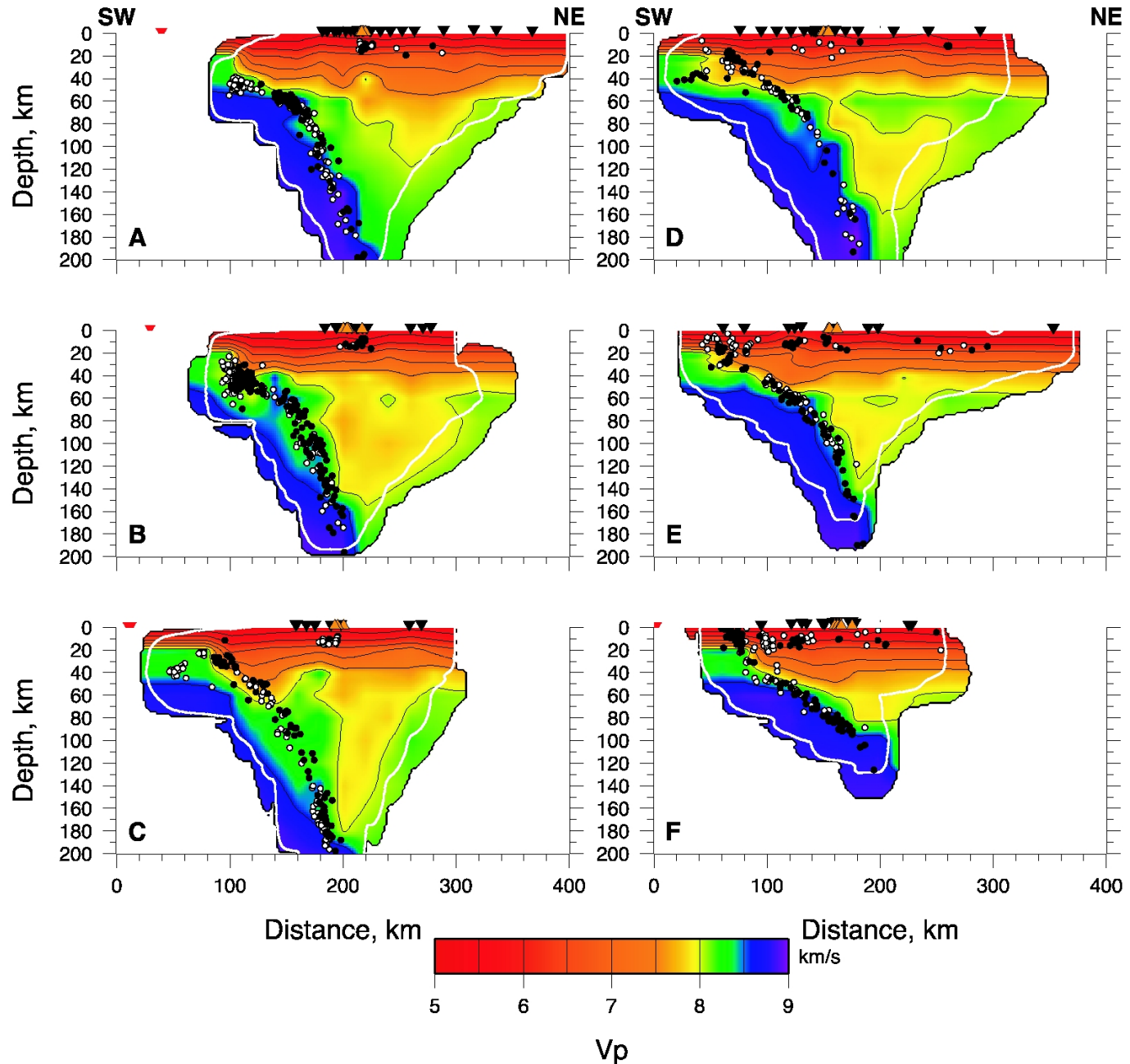


# TUCAN seismology

Sections A-F:  
NW Nicaragua to  
Central Costa Rica  
(Syracuse et al. 2008)

Steepening of the  
slab from the SE to  
the NW

Variations of crustal  
structures not  
resolved by  
seismology

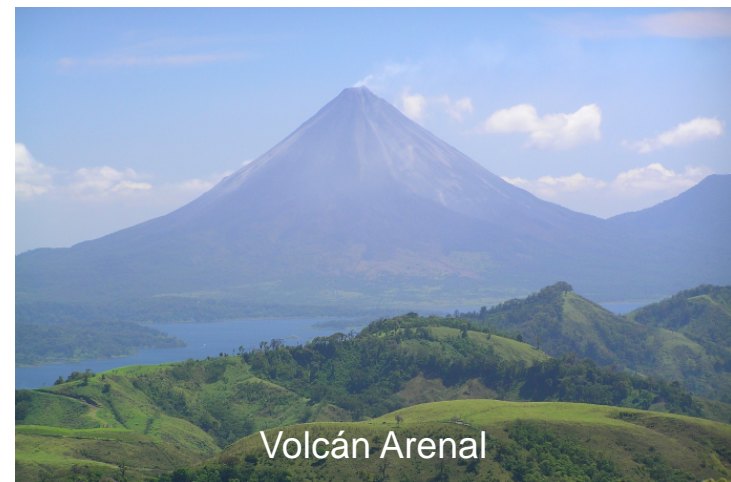




# Study area in Central America

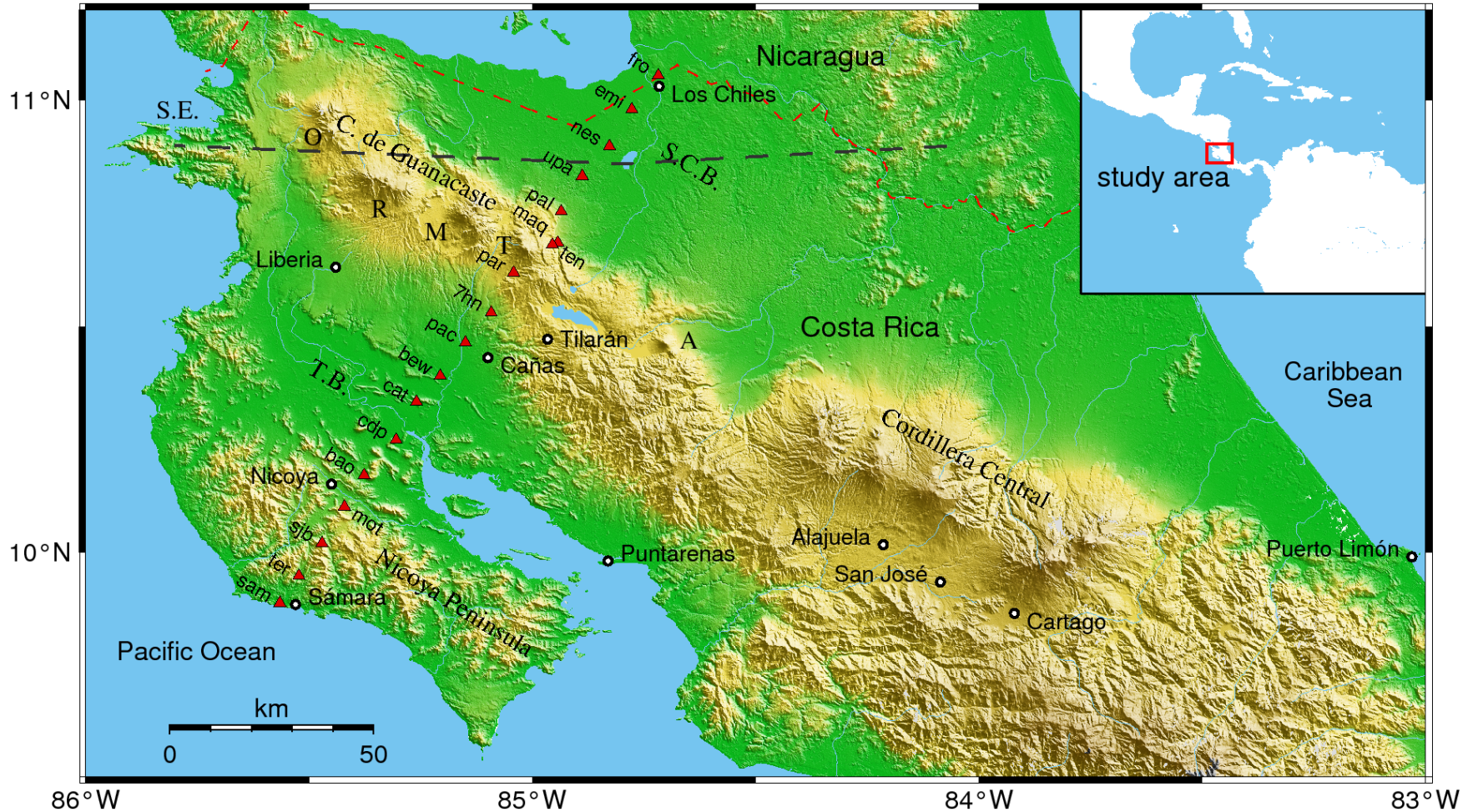


- Ca. 50 LMT stations (period range 10-10.000 s) and some broadband
- Offshore stations by IFM-Geomar, Kiel (Costa Rica) in 2007





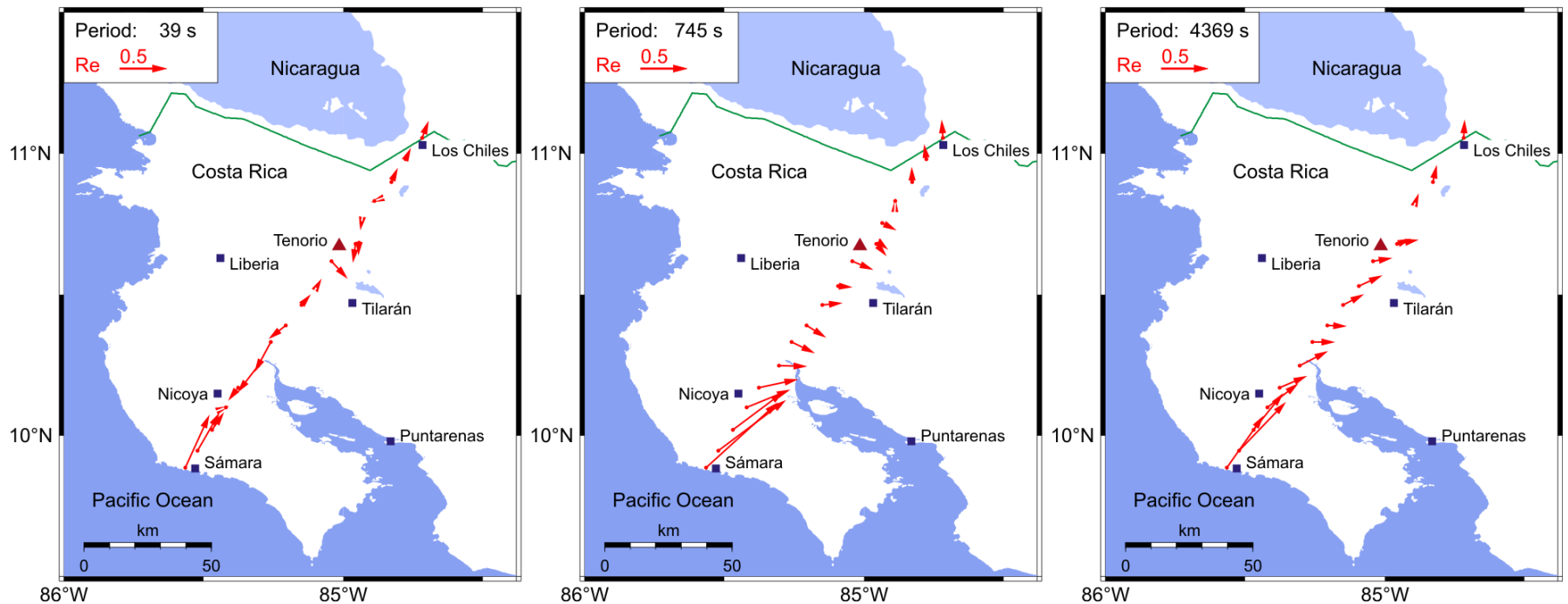
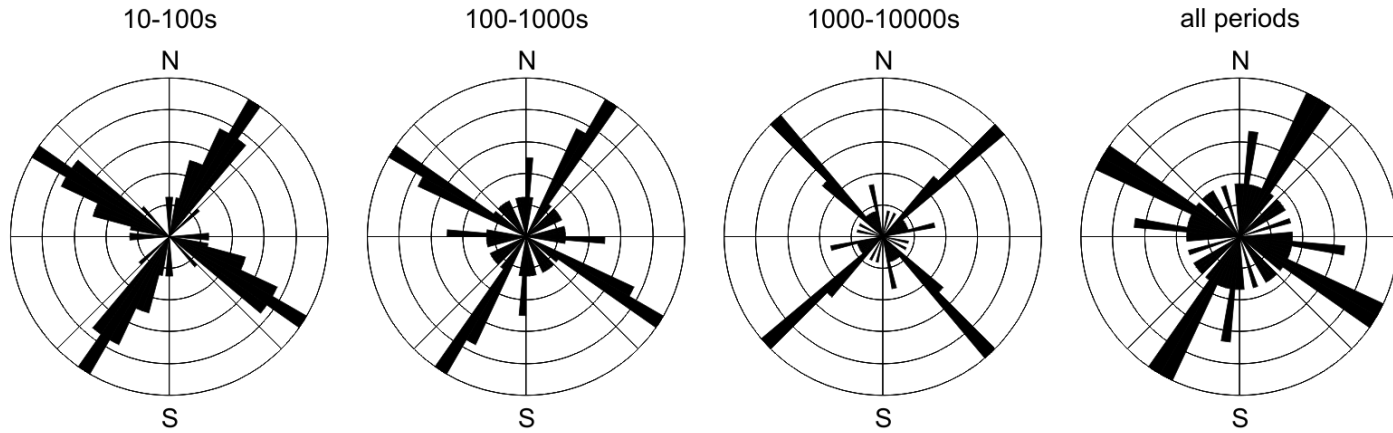
# Costa Rica MT in early 2008



Offshore continuation (IFM-Geomar): data not modeled yet

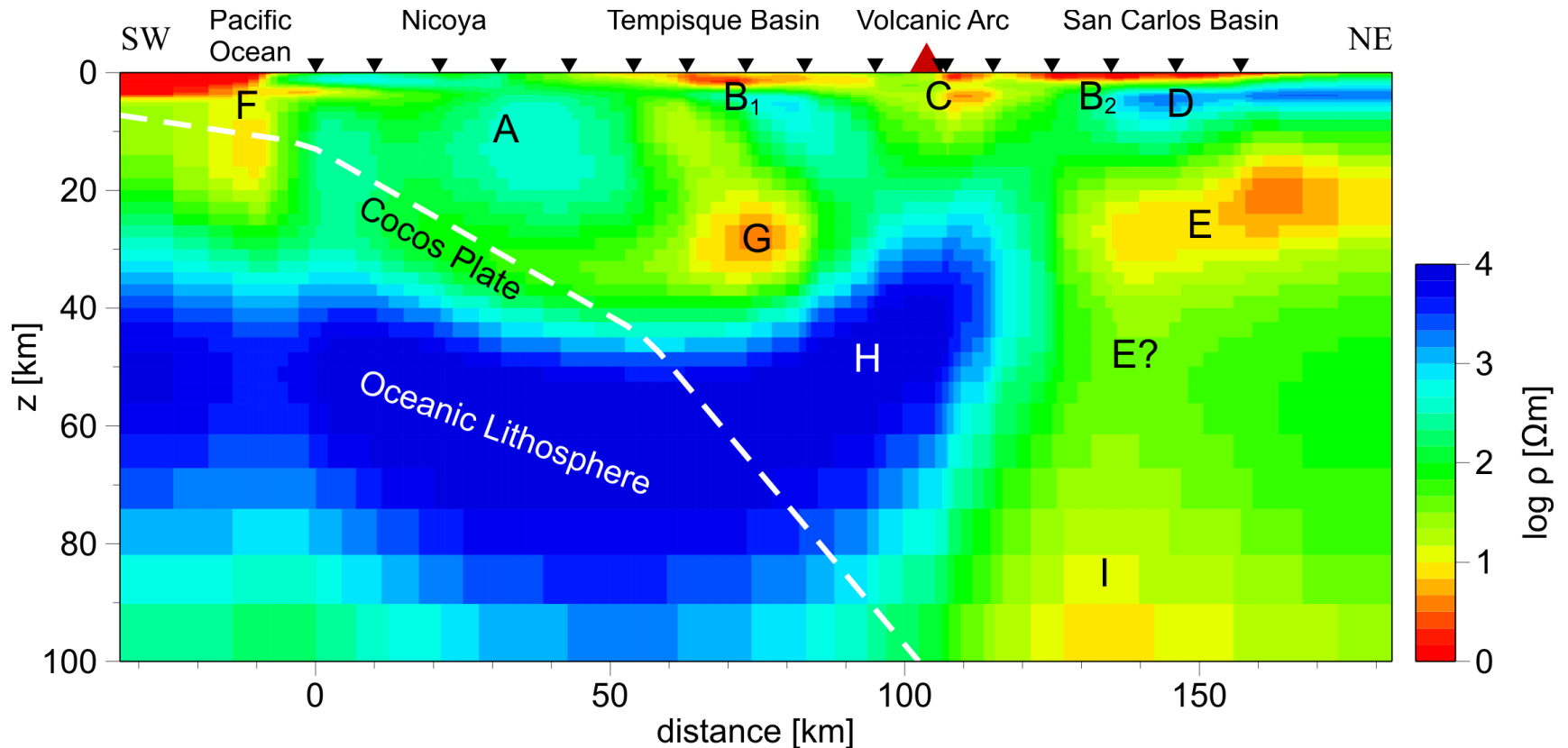
Dashed line: Proposed Santa Elena suture between Paleozoic Chortis (beneath Nicaragua) and Chorotega (Costa Rica) blocks, allochthonous mafic/ultramafic rocks on Nicoya and Santa Elena Peninsula (peridotite outcrops)

# Impedance strikes and induction vectors



Common strike of  $-53^\circ$  assumed, but note 3-D effects in tippers

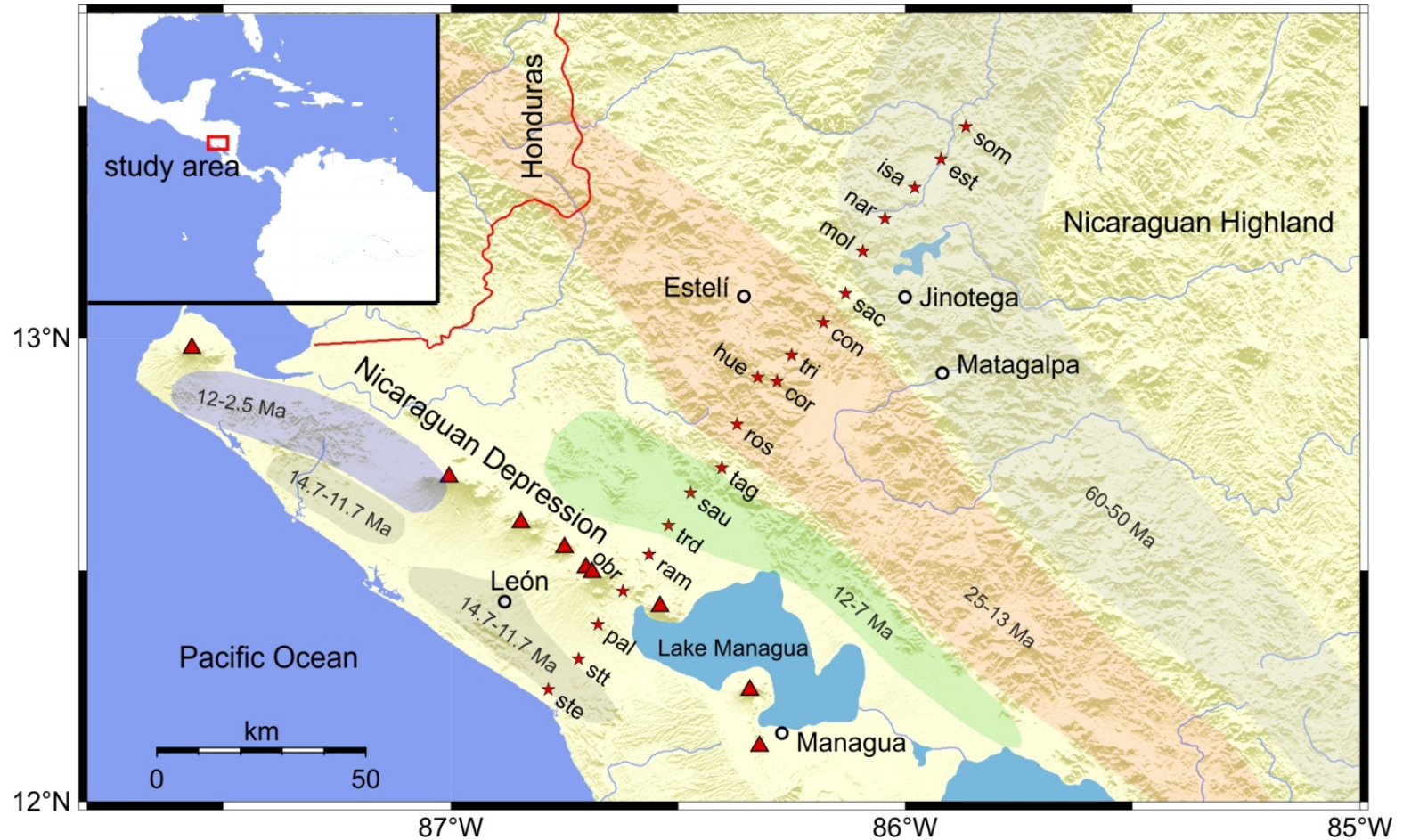
# 2-D model approximation of NW Costa Rica



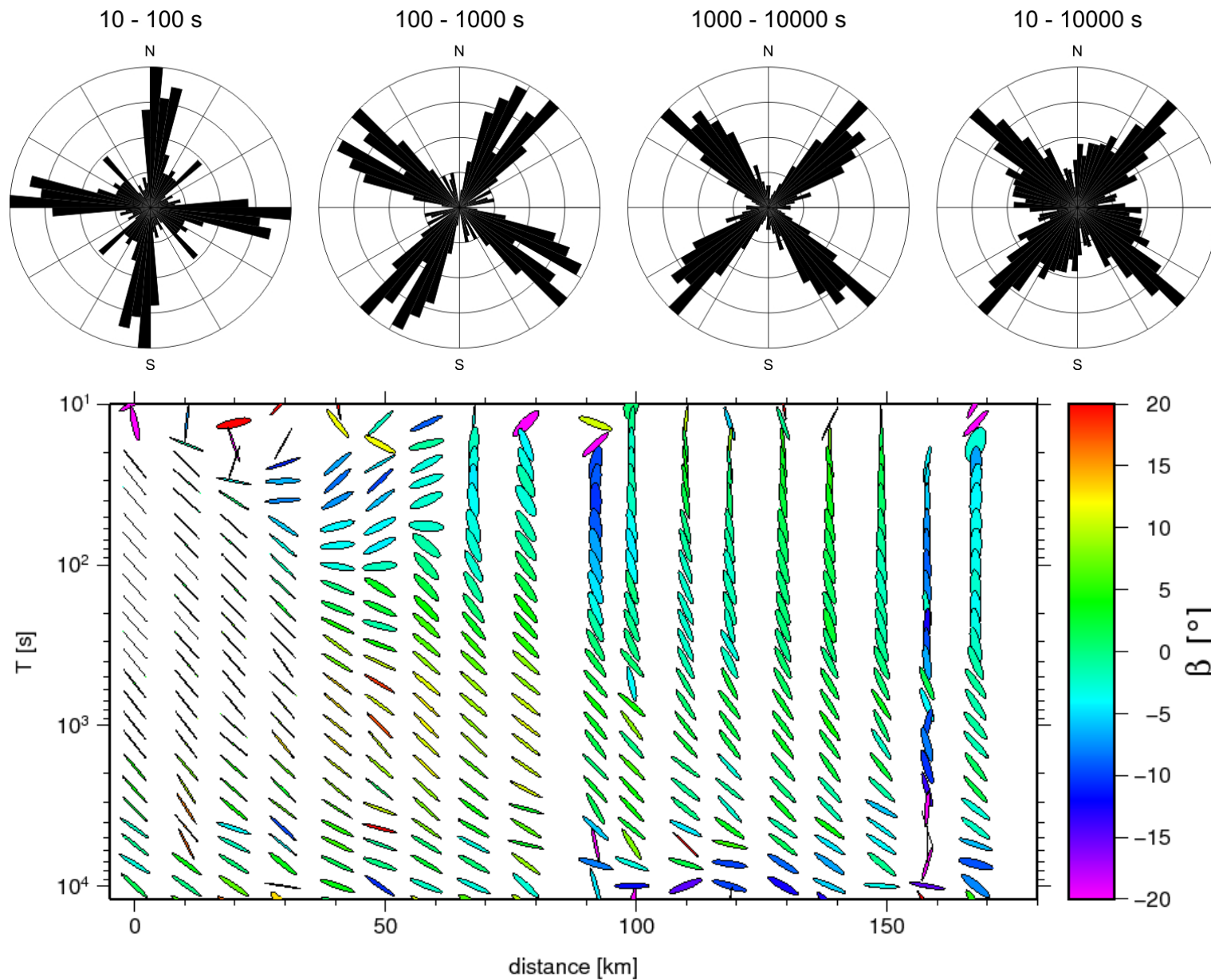
A: Nicoya mafic and ultramafic rocks.  $B_1$ ,  $B_2$ : Tempisque and San Carlos basins.  
C: Tenorio volcano. D: Chortis block. E: Melt from the asthenospheric wedge to the backarc? F: Fluids above plate interface? Not resolved, offshore data needed.  
G: Serpentinization of forearc mantle + fluids (!).  
H: Mantle sliver. I: Asthenospheric wedge.



# MT sites in Nicaragua, crossing the current and the Paleogene-Neogene arcs

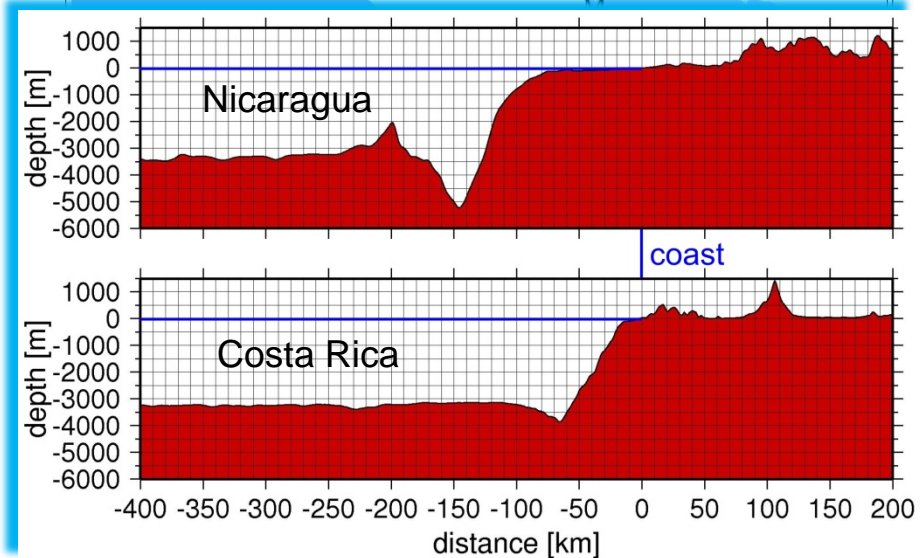
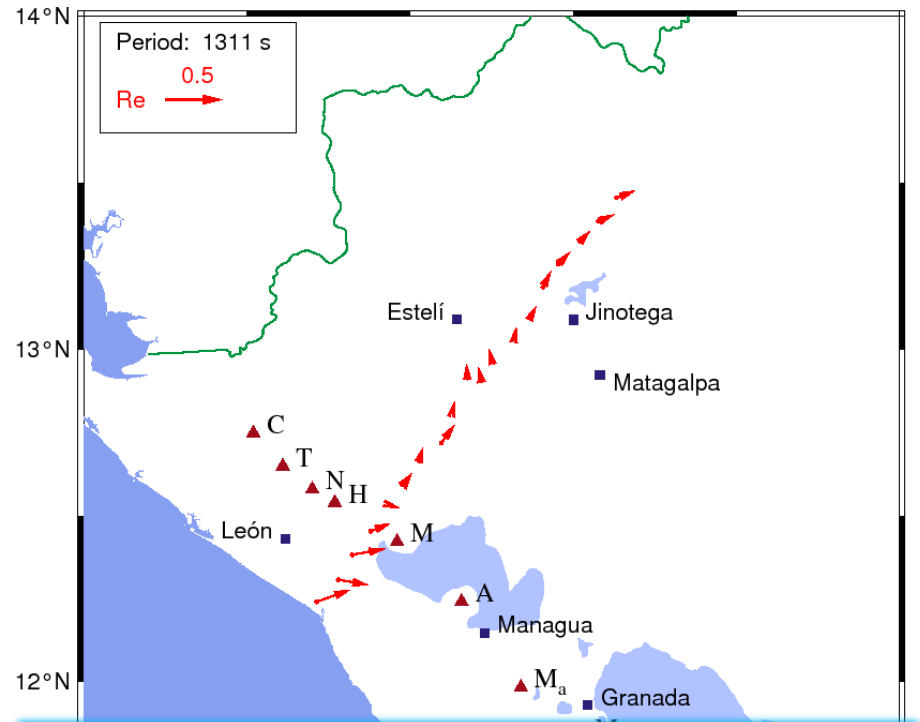
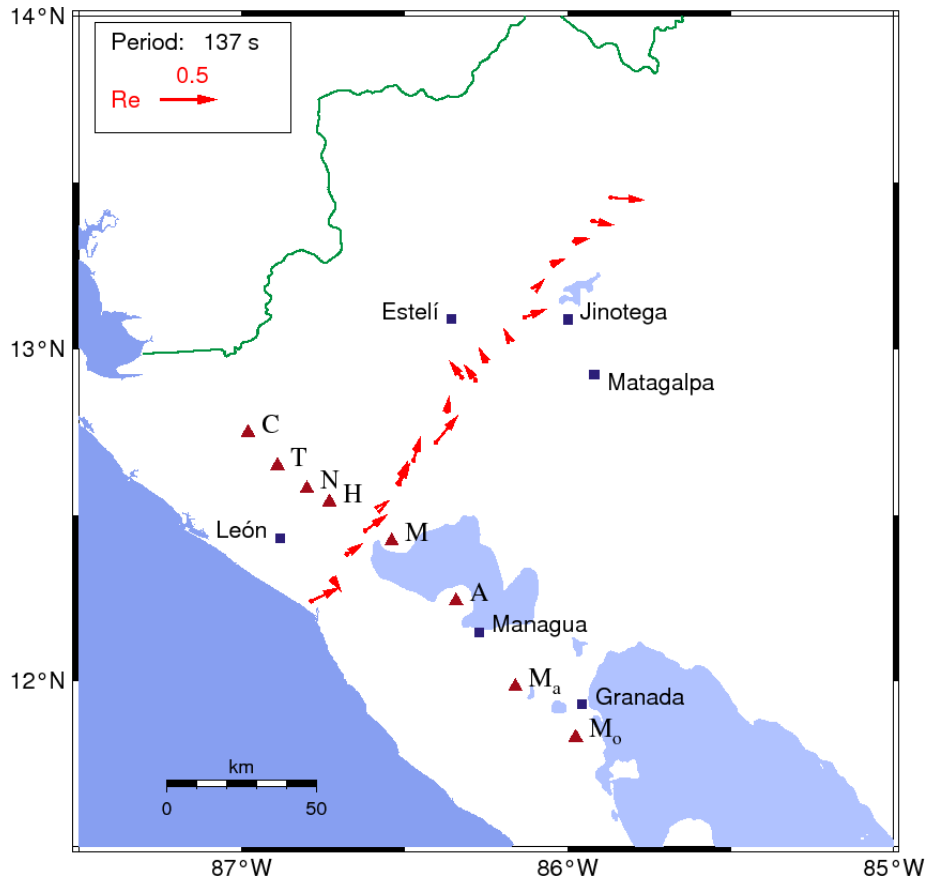


# Strike directions in Nicaragua



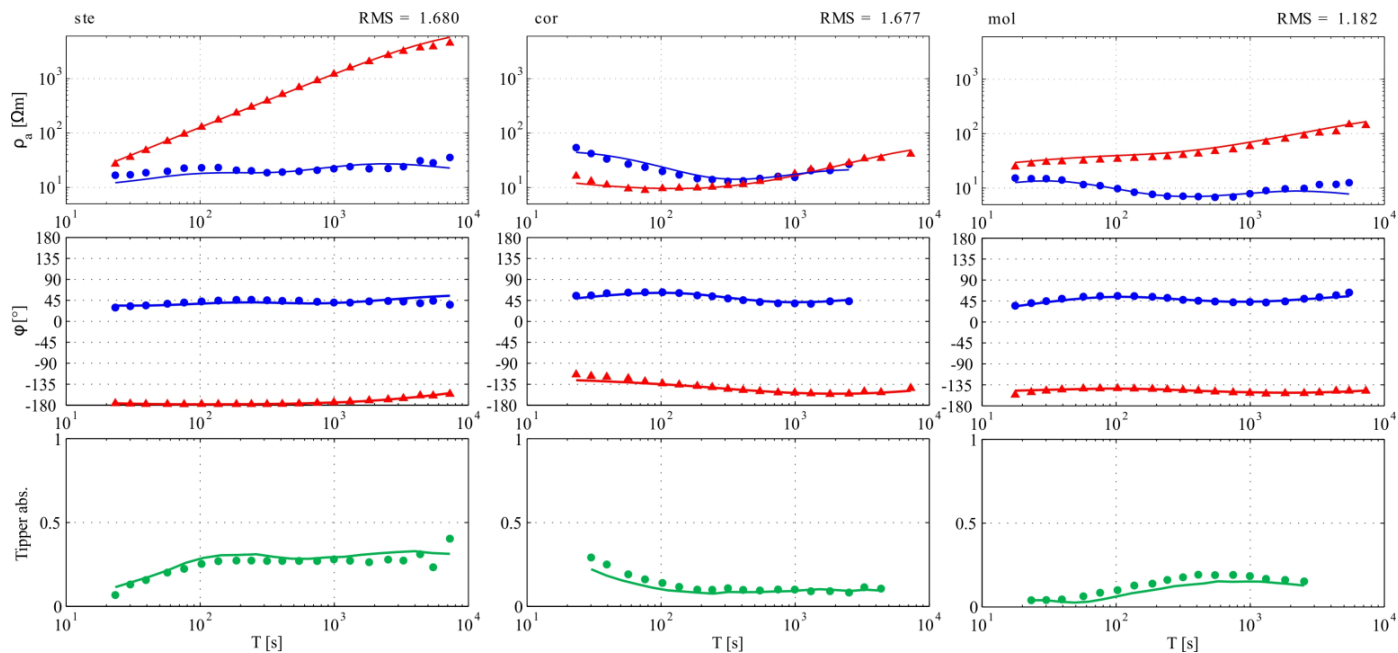
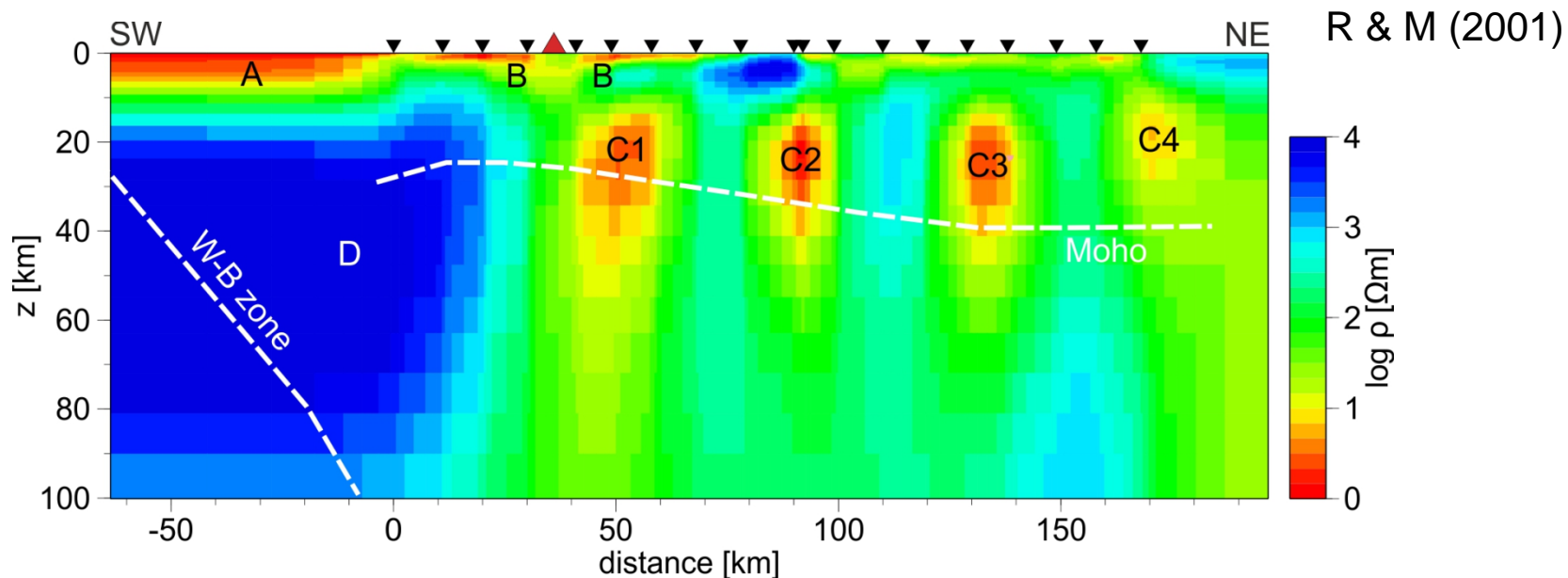


# Very small induction vectors in Nicaragua

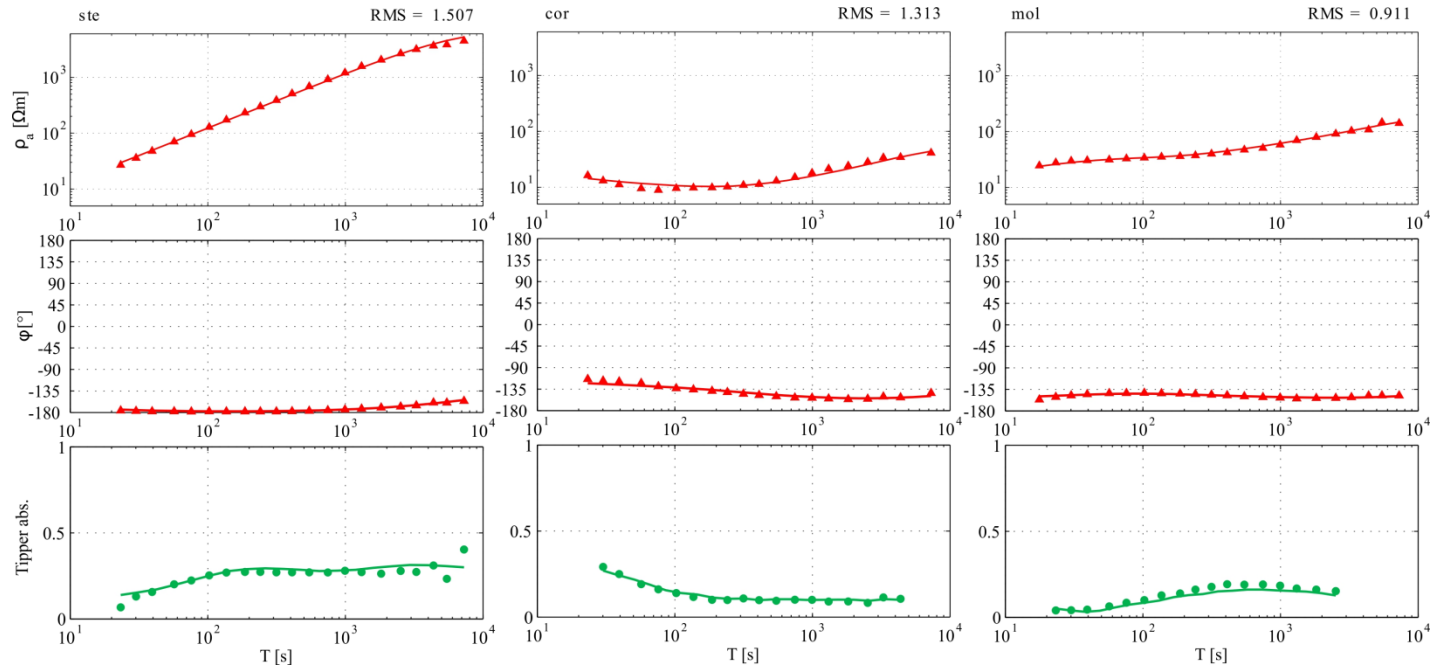
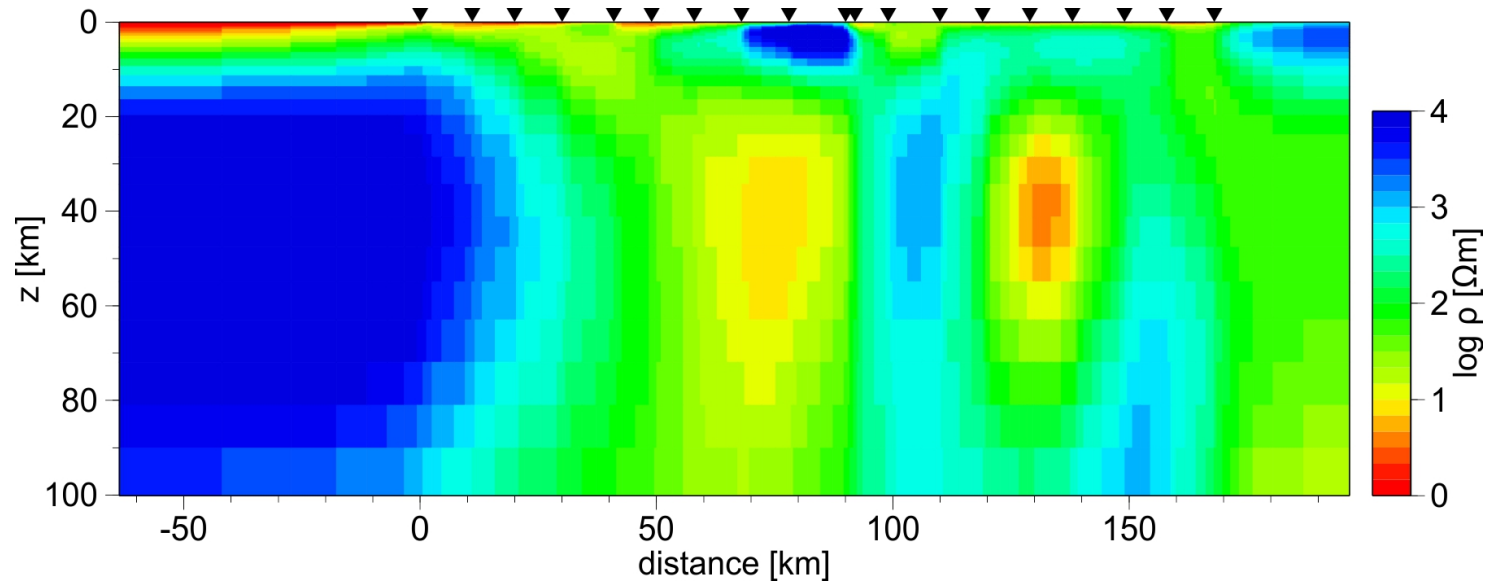


Partly explainable by bathymetry  
(shelf off Nicaragua - Sandino Basin)

# Ambiguous 2-D model (TE, TM, tipper)



# 2-D model (TM, tipper): overcomes TE distortion

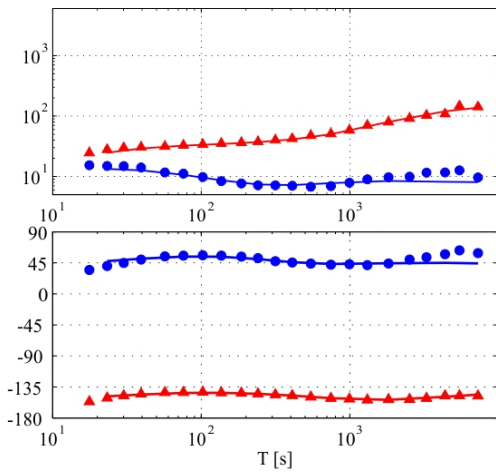
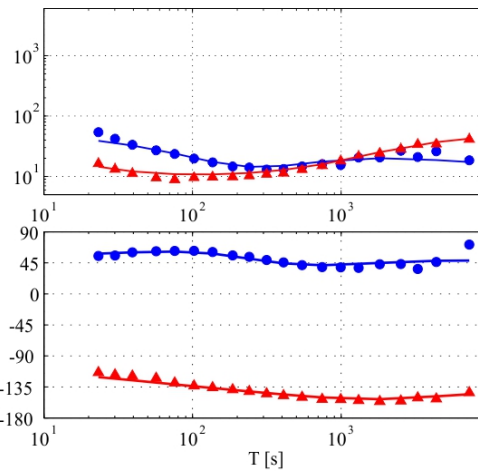
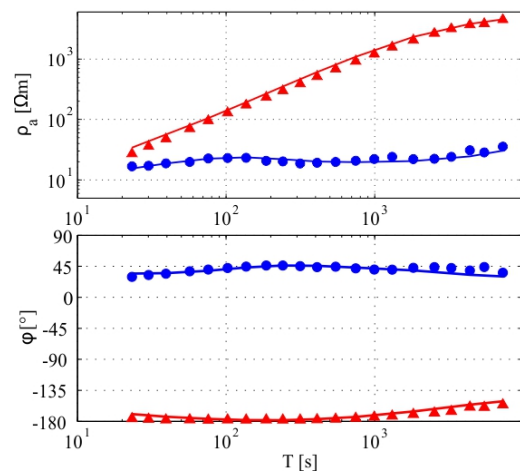
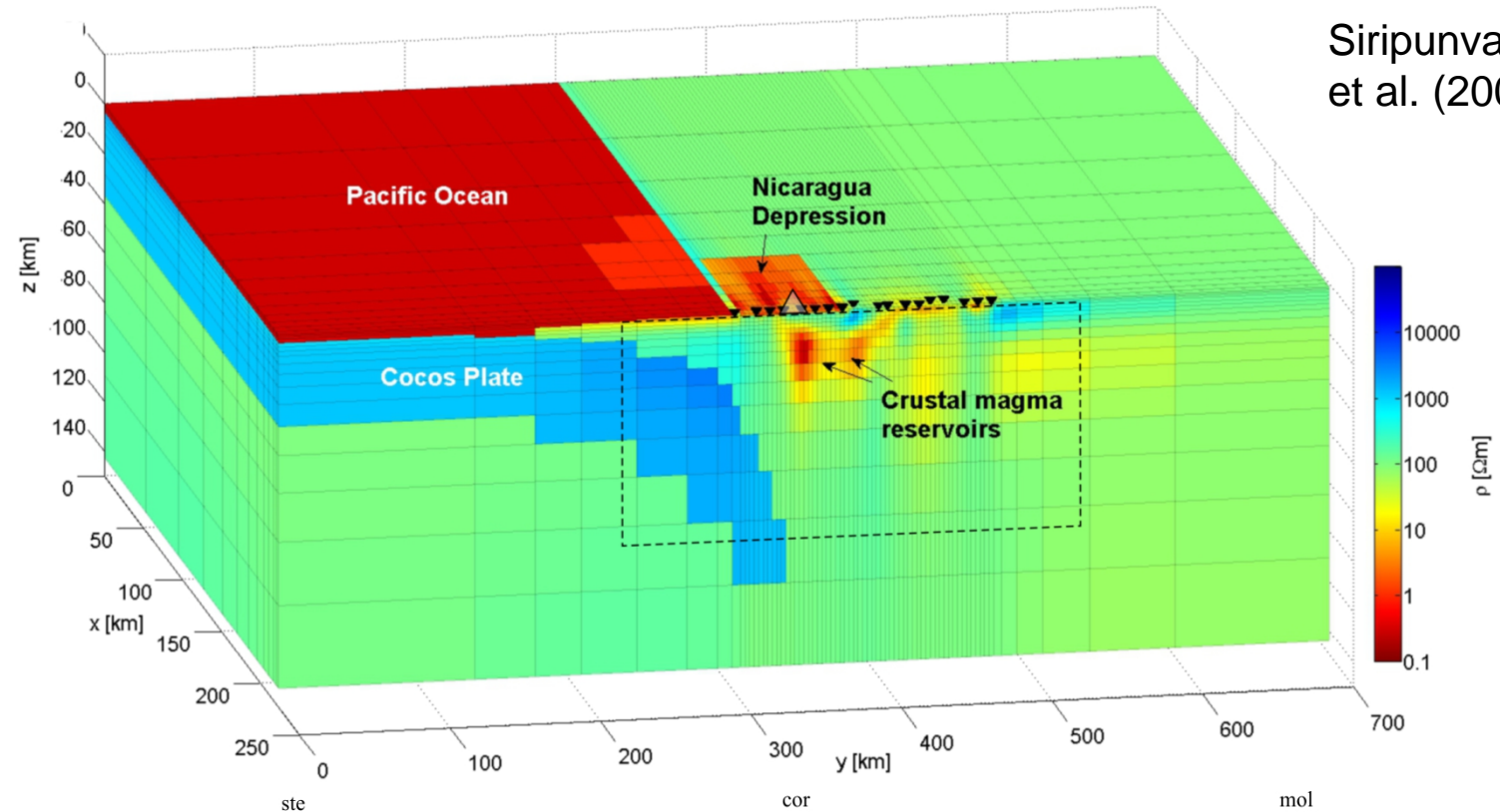


# First 3-D inversion attempts

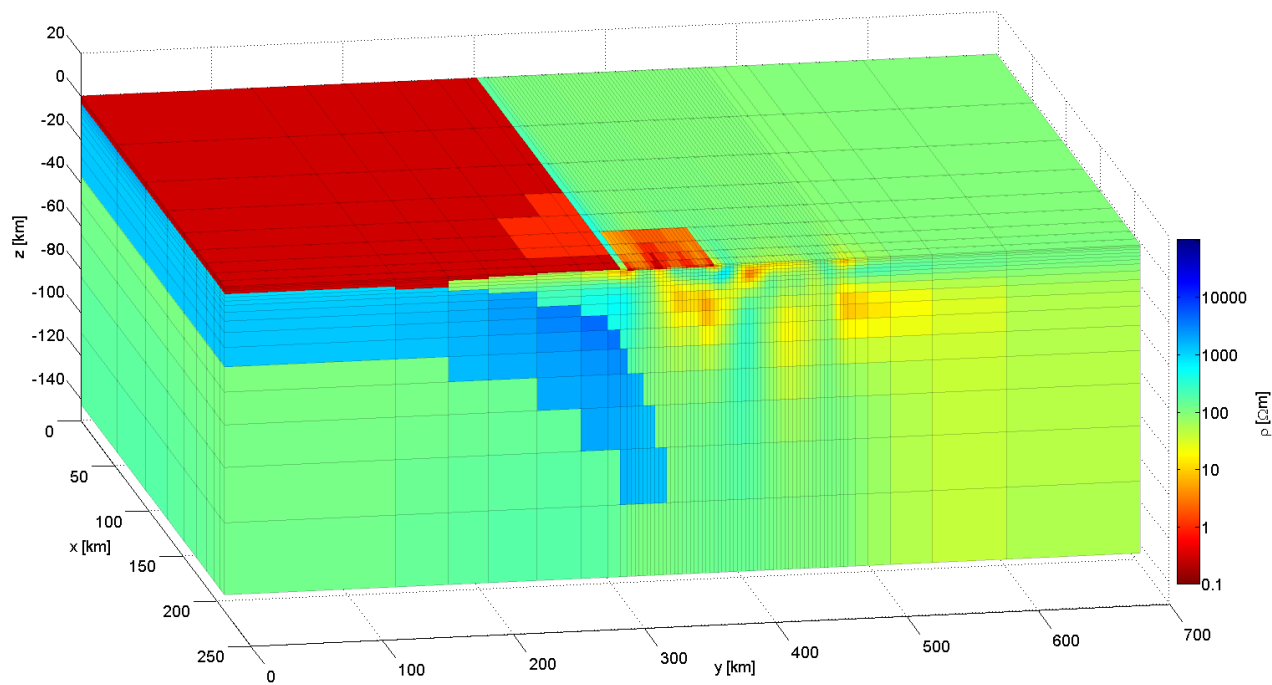
- Serial code of Siripunvaraporn et al. (2005)
- Inverts impedances, not tipper
- Rotate data and coordinate system by  $-50^\circ$  ( $x' \rightarrow$  NW,  $y' \rightarrow$  NE)
- Starting model incorporates Pacific Ocean with crude bathymetry, resistive Cocos slab, well-conducting sediments of the Nicaraguan Depression
- Inversion of full tensor (failed due to poor data quality of the main diagonal) and of minor diagonal (successful, rms =1.14)
- Removes artifacts (backarc conductors) and relocates the main anomaly directly beneath the volcanic arc
- Rather small side effects, conductivity highest beneath highly-active Momotombo volcano

# 3-D model (impedance only, rotated, minor diagonal)

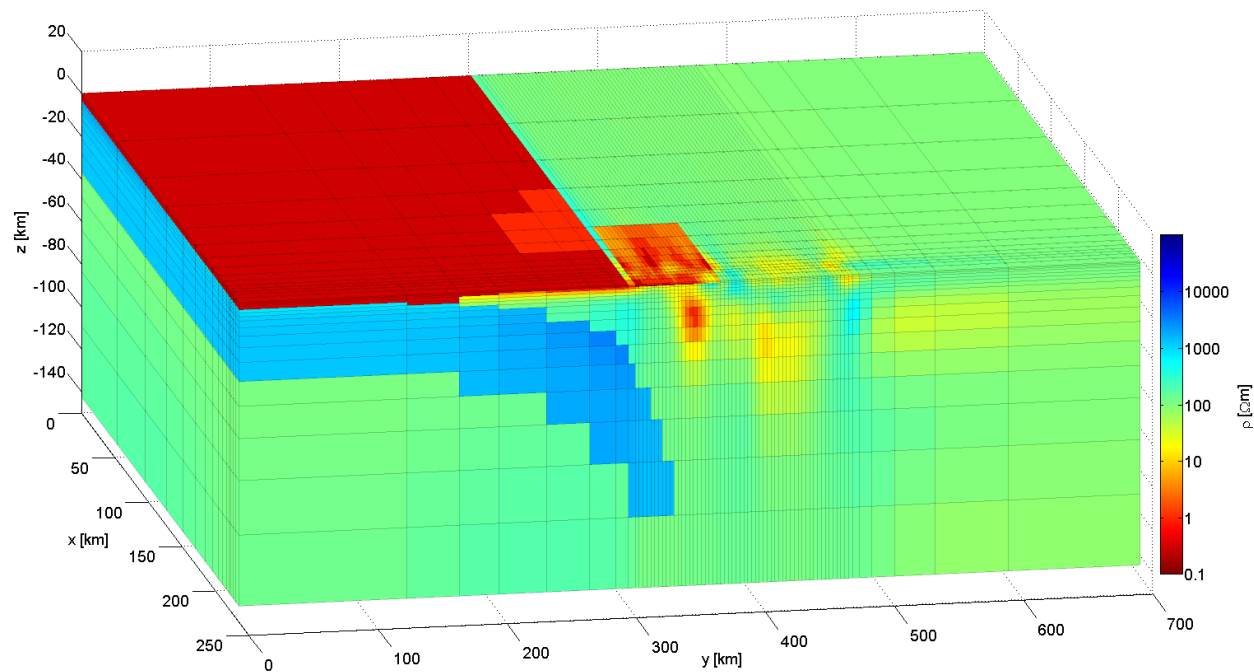
Siripunvaraporn  
et al. (2005a,b)



3-D model  
(10 km NW and SW)



No unrealistic major  
side effects.  
Anomaly greatest  
directly beneath  
Momotombo volcano



## Conclusions:

- No really clear strike from impedances and tipper
- Although yielding a very good fit, 2-D model is ambiguous, strong distortion in TE
- Anisotropy modeling failed
- 3-D inversion improves the 2-D model with geologically meaningful structures

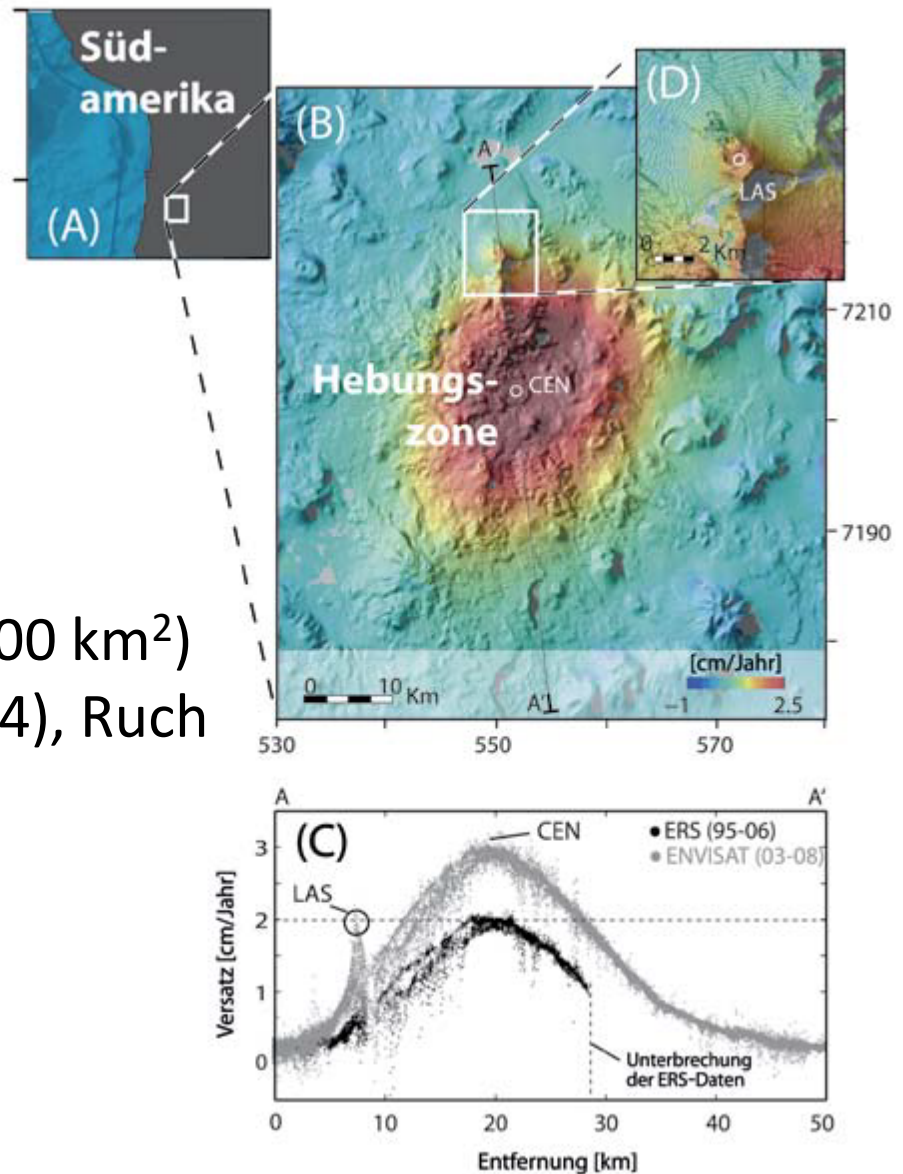
## To do:

- Integrate tipper
- More sites between 2 main profiles
- Prolong Scripps offshore profile into Nicaragua



# Surface deformation at Lazufre volcanic complex from InSAR measurements

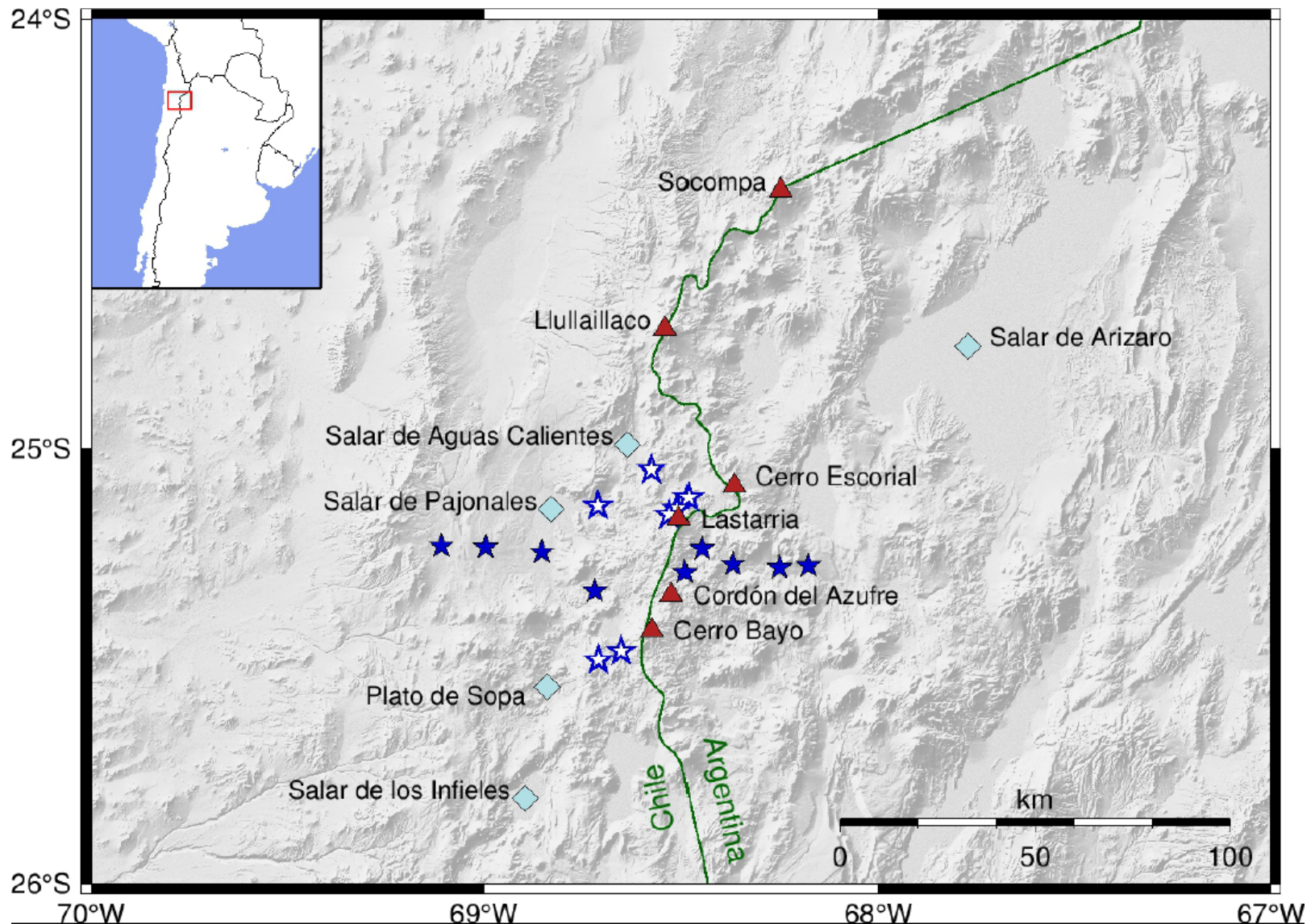
(3 cm/a uplift over an area of 1000 km<sup>2</sup>)  
Pritchard and Simons (2002, 2004), Ruch  
and Walter (2010)



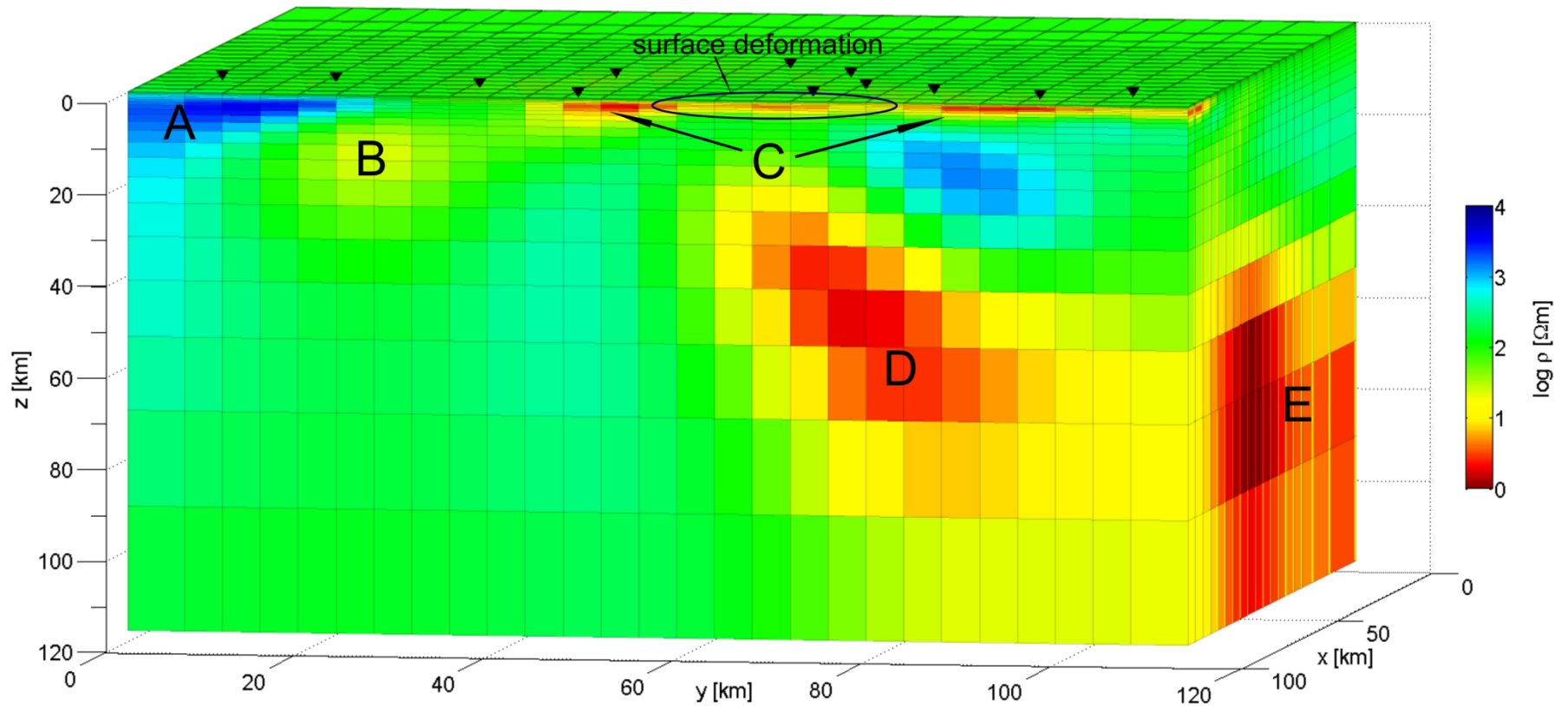
Walter (2011)



# MT sites at Lazufre volcanic complex, Chile/Argentina

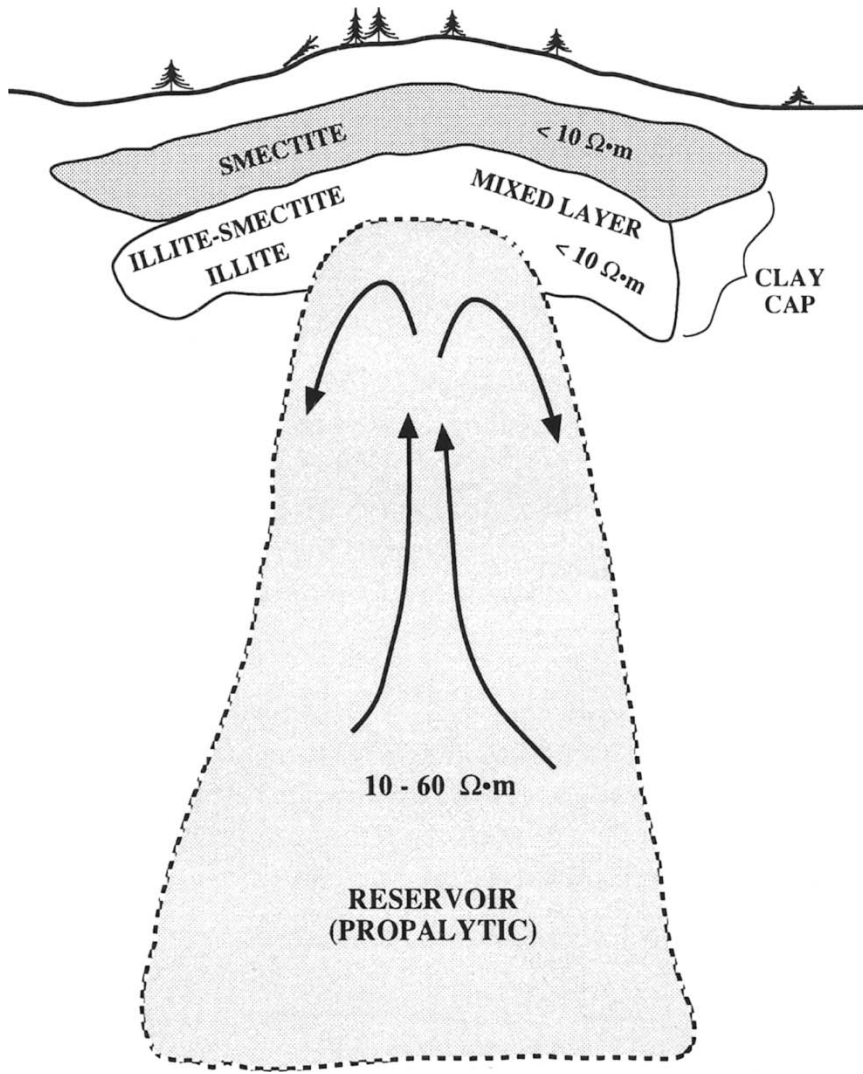


# 3-D model of Lazufre volcanic complex in the Central Andes



Budach et al., submitted to Tectonophysics

# MT and geothermal exploration

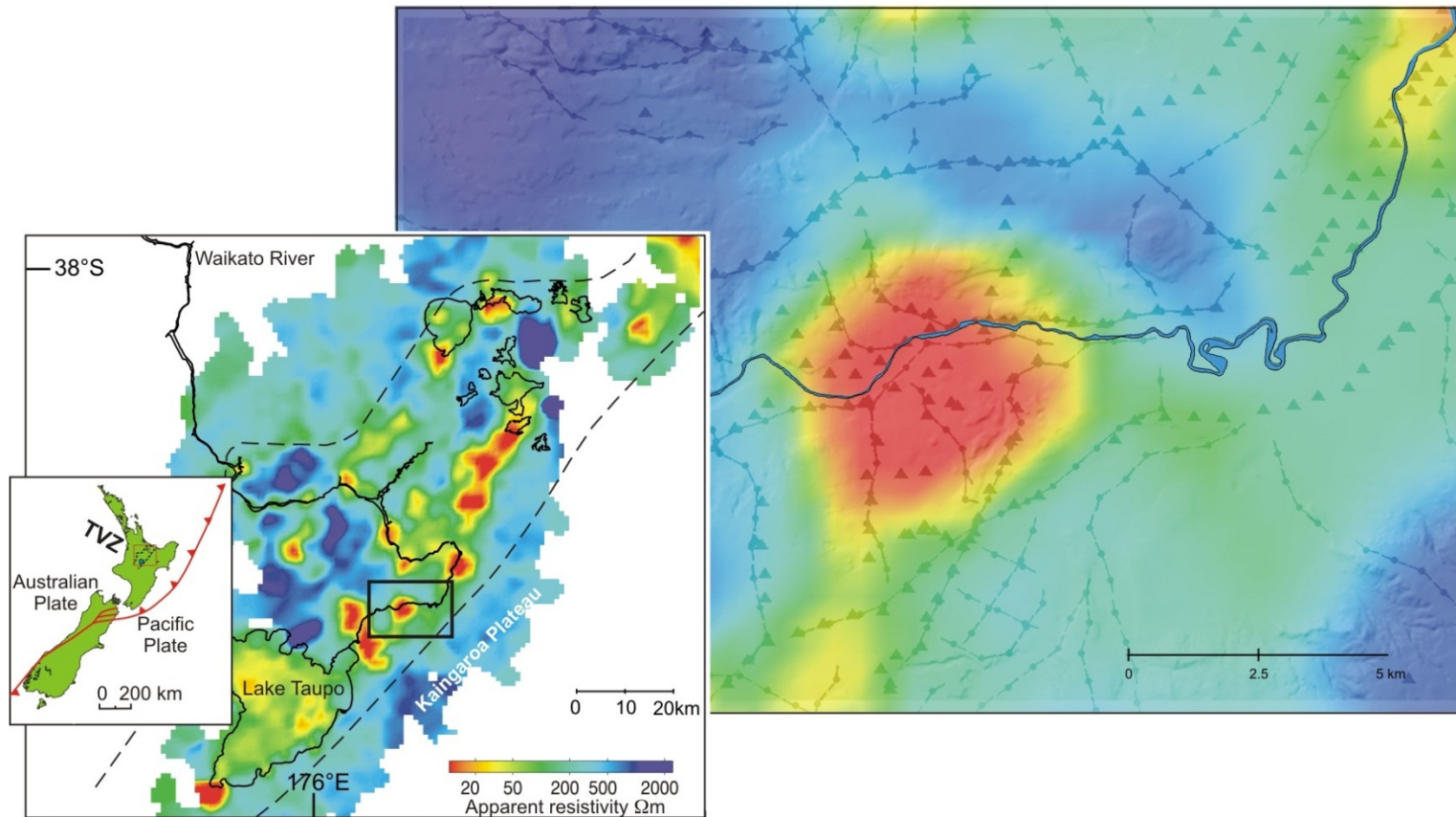


Major problem: resolving the not so well-conducting hydrothermal system beneath the conductive clay cap

Propylitic Alteration is caused by iron and sulfur-bearing hydrothermal fluids, and typically results in epidote-chlorite-pyrite alteration, often with hematite and magnetite facies

Conceptual model of a geothermal system (Pellerin et al. 1996)

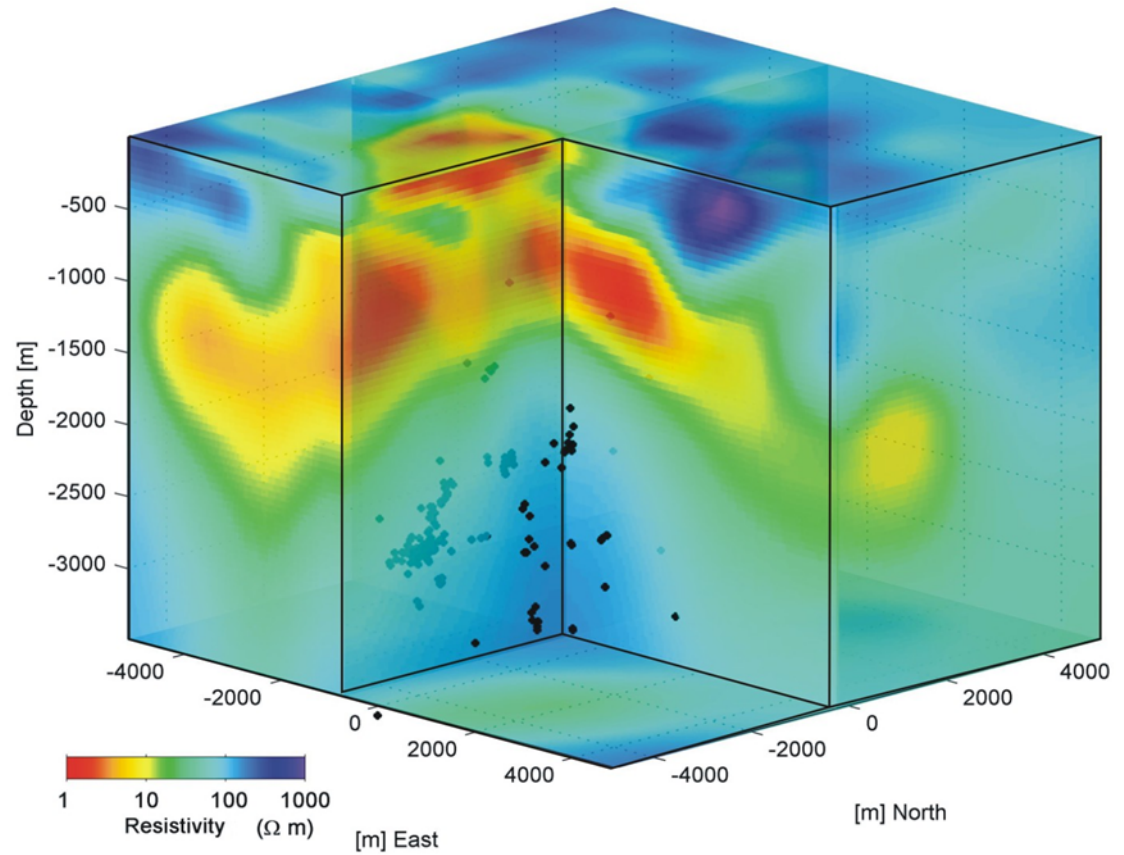
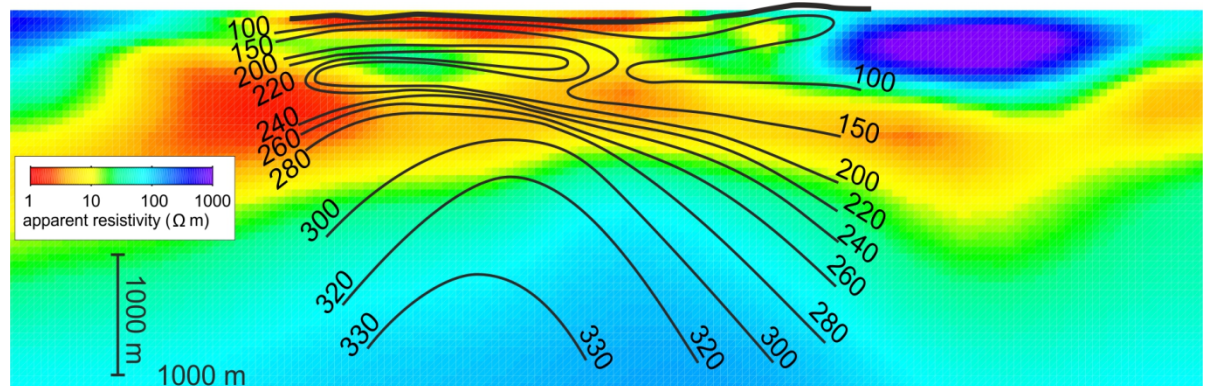
# Geothermal exploration in New Zealand (Heise et al. 2008)



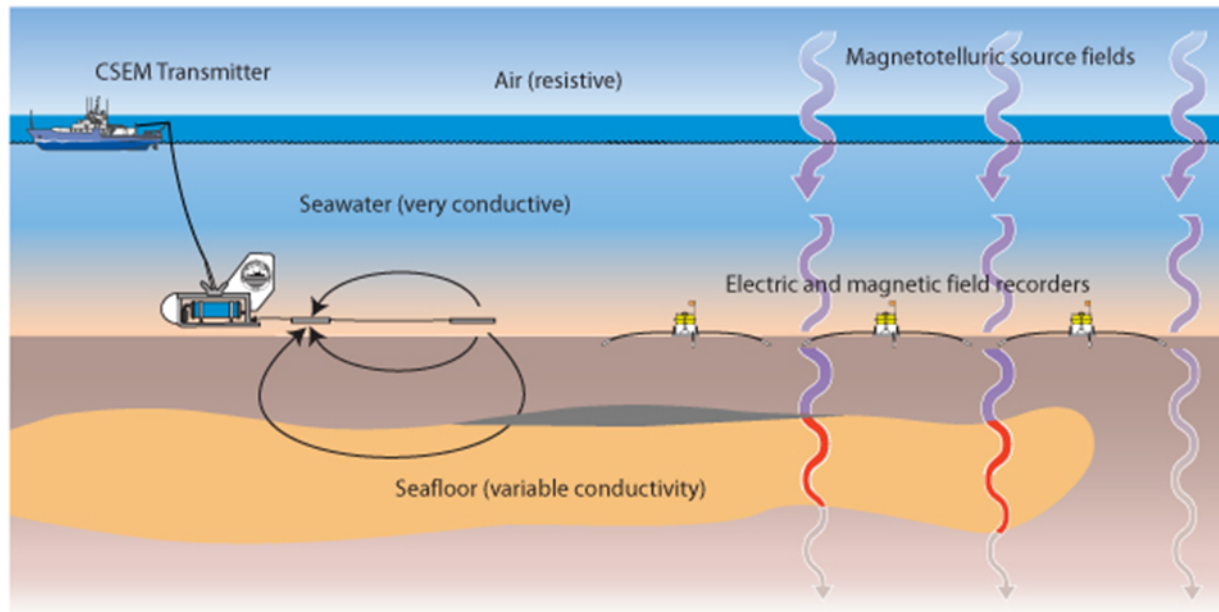
DC app. resistivity map (Schlumberger  $L/2 = 500\text{m}$ ) in the Taupo Volcanic Zone



# 3-D MT inversion model

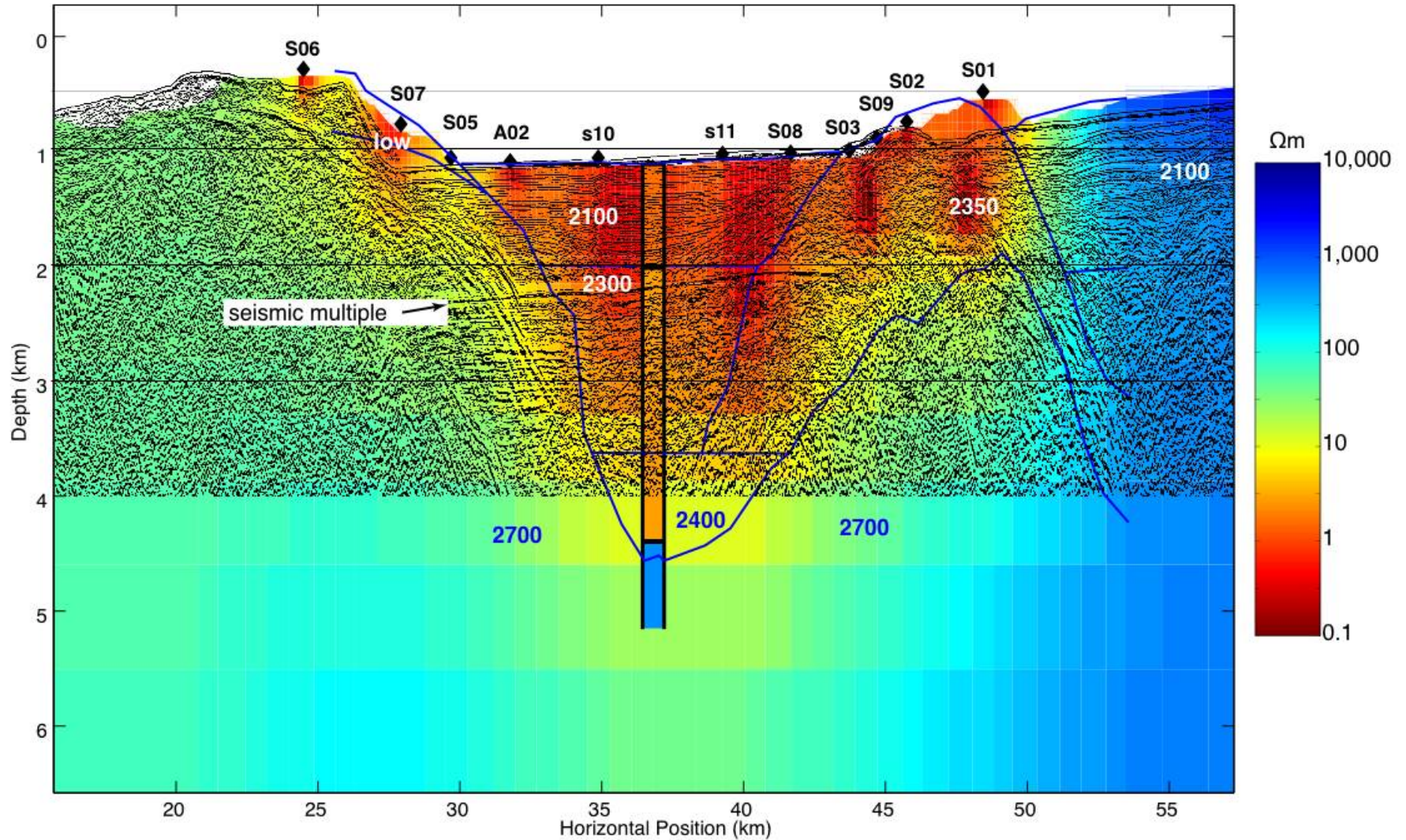


# Offshore MT - Examples



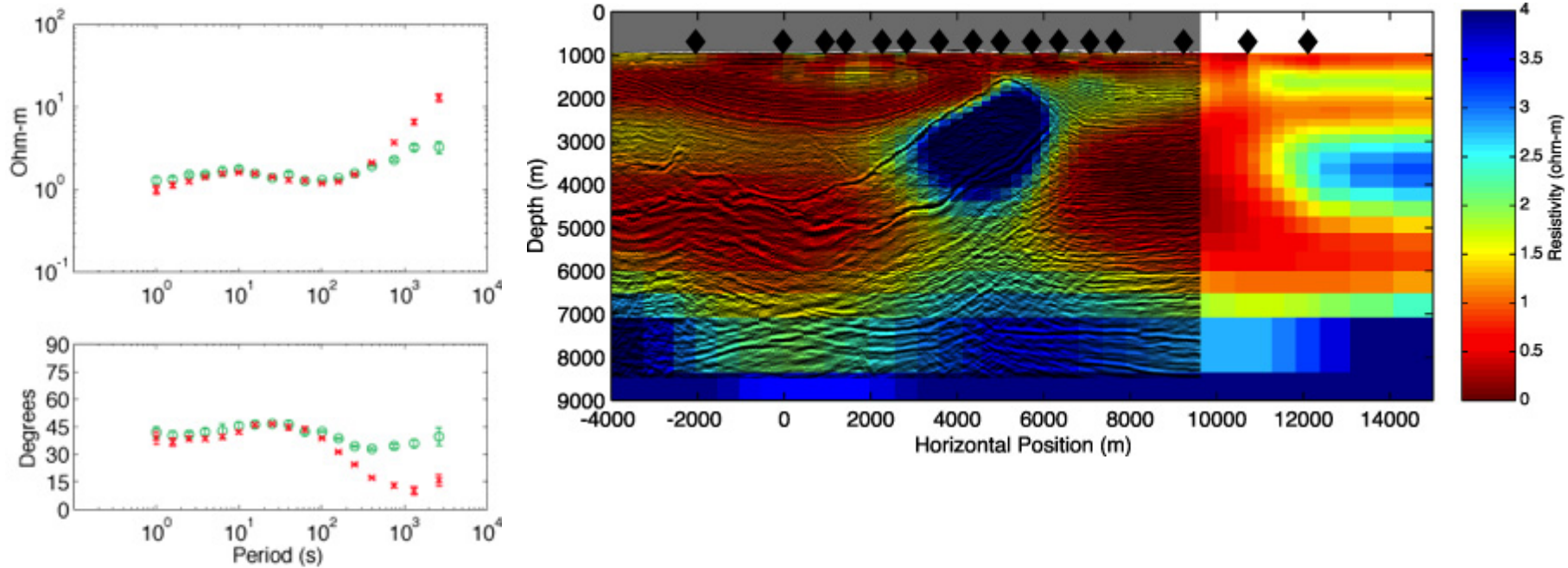
Hybrid (passive and active) experiment at Scripps (S. Constable, K. Key)

# San Diego Trough





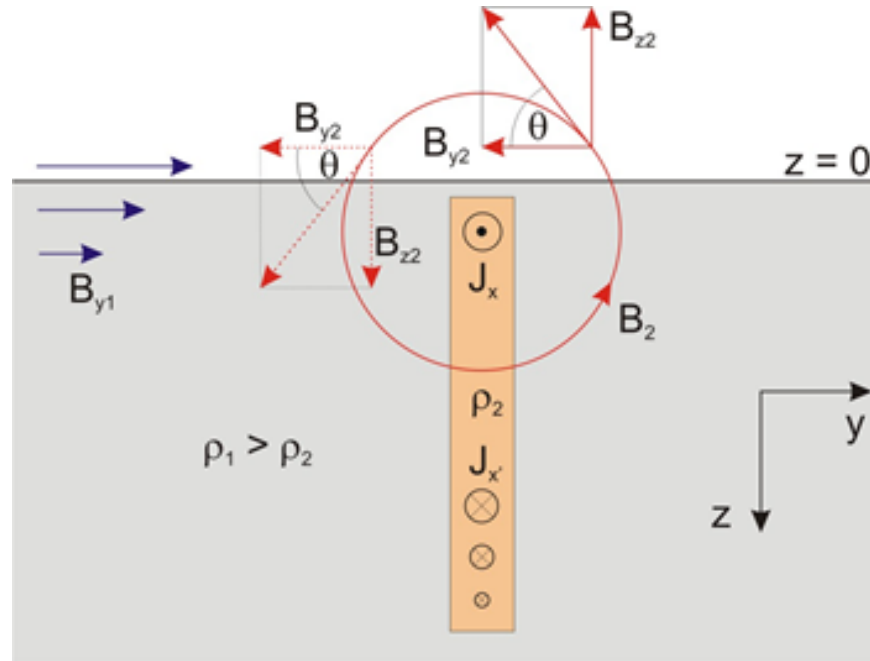
# Salt structures in the Gulf of Mexico



This is a rare example where MT successfully mapped a resistive (salt) structure. Small indication in app. resistivity curve at 10s.



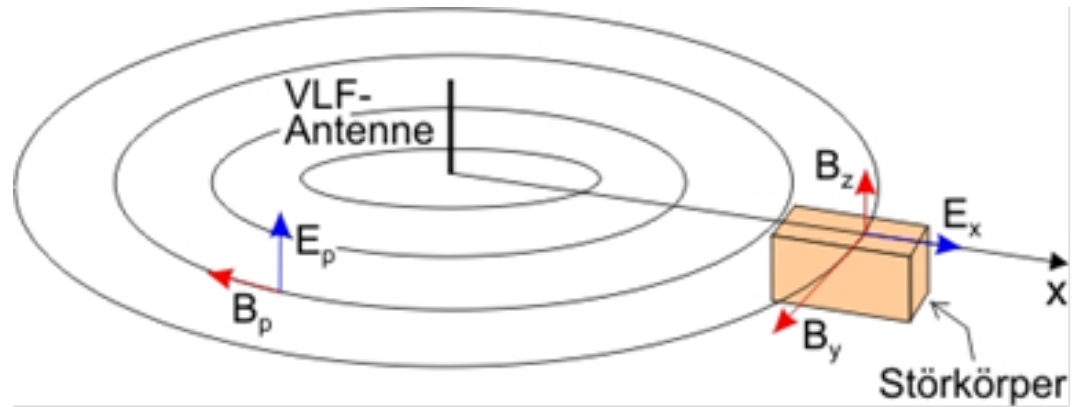
## Some remarks on the VLF/R method as a MT special case



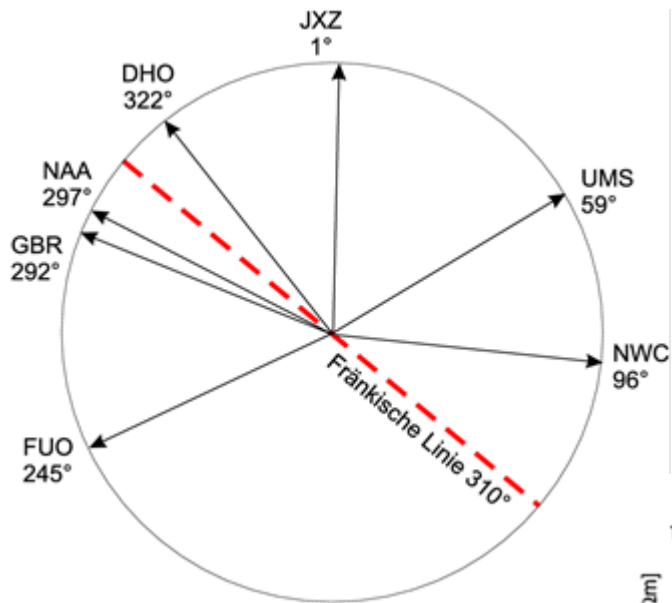
The magnetic fields of a well-conductive plate in homogeneous subsoil.  $B_{y1}$  is the normal field,  $B_{y2}$  and  $B_{z2}$  are the components of the secondary field  $B_z$  caused by the anomalous body on the left and right side. The plate is extended in x-direction which corresponds to E-polarization as well as to the direction of the transmitter here.  $\theta$  is the corresponding tilt angle.

# Distribution of VLF transmitters

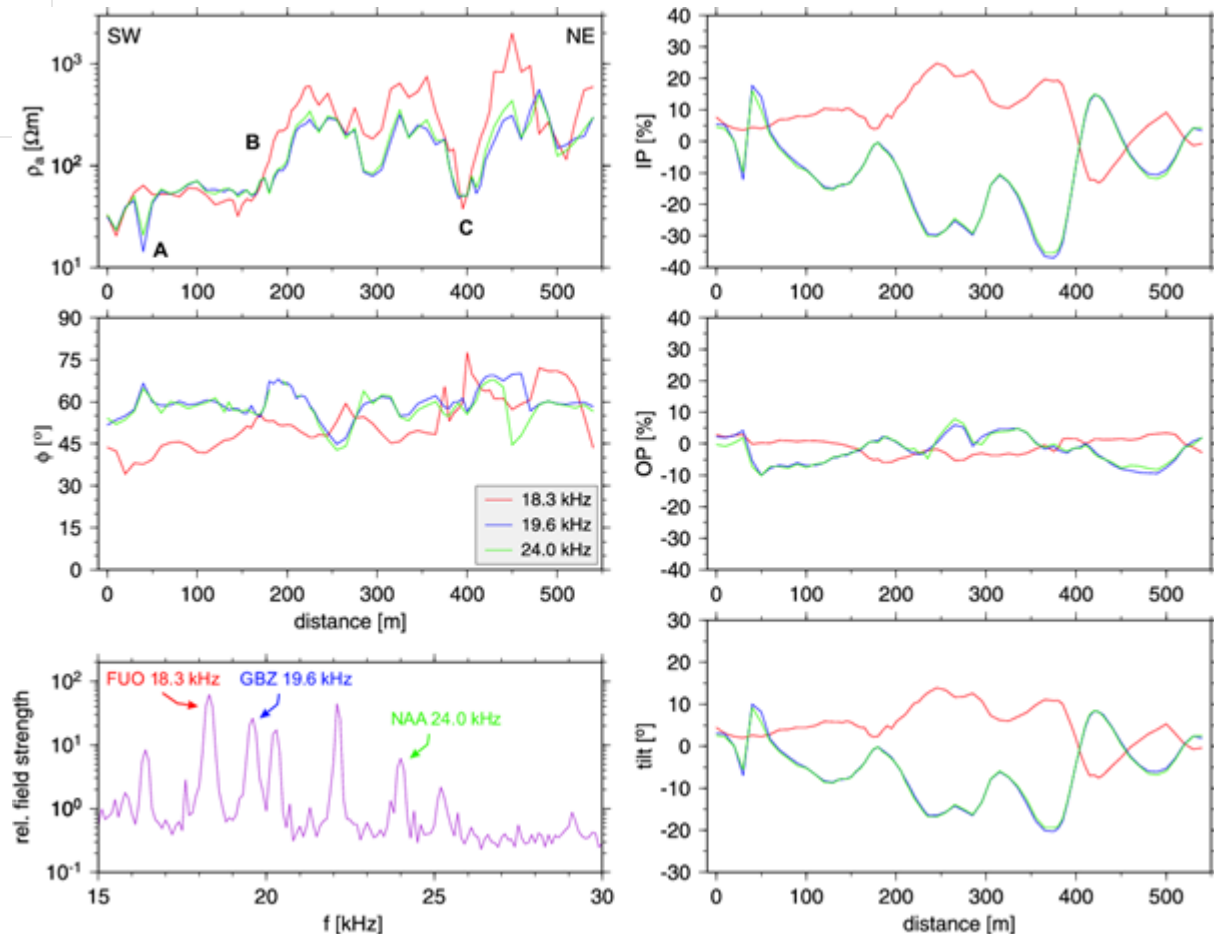
Communication with  
submarines, frequencies  
 $15 < f < 25$  kHz



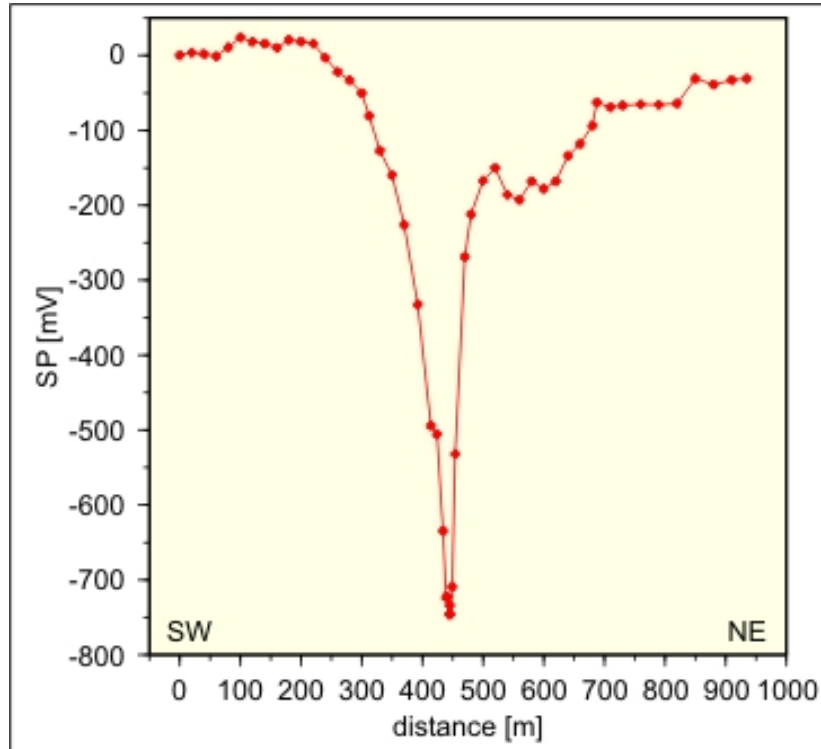
# Example: Franconian Line, Bavaria



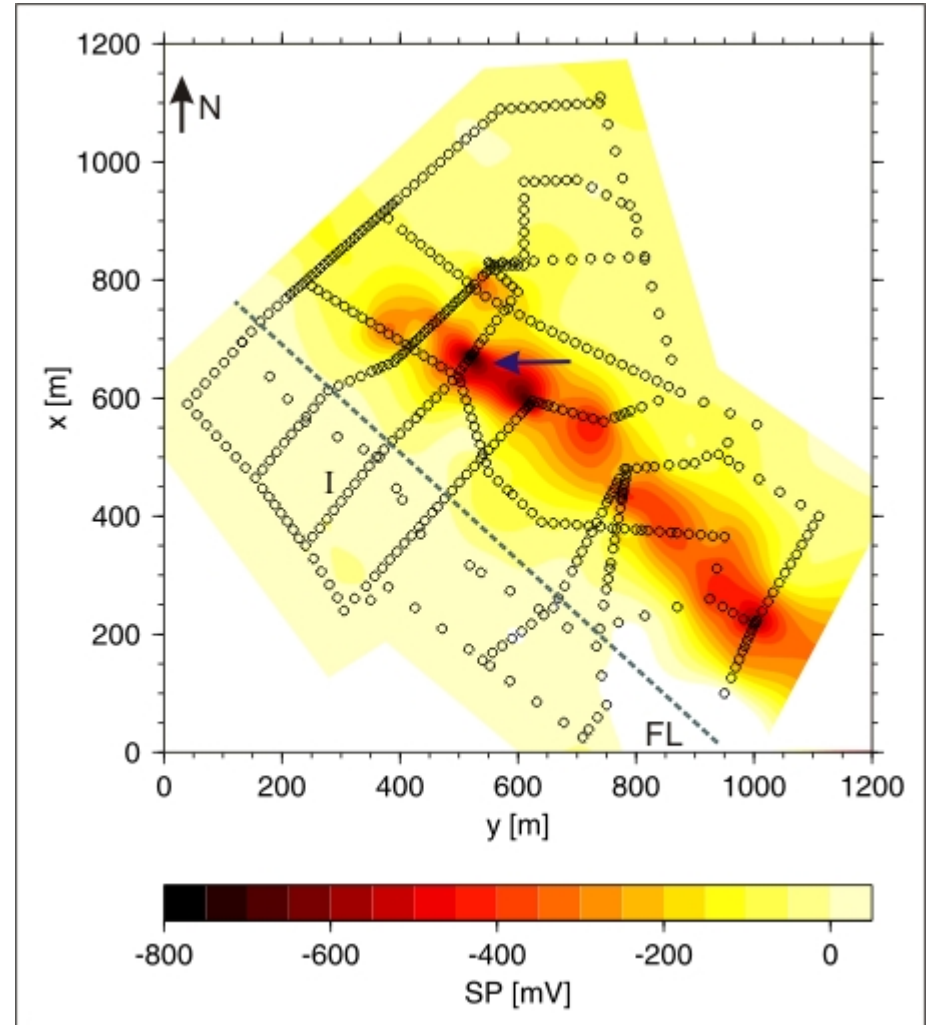
Anomaly C at same location  
as VES conductor



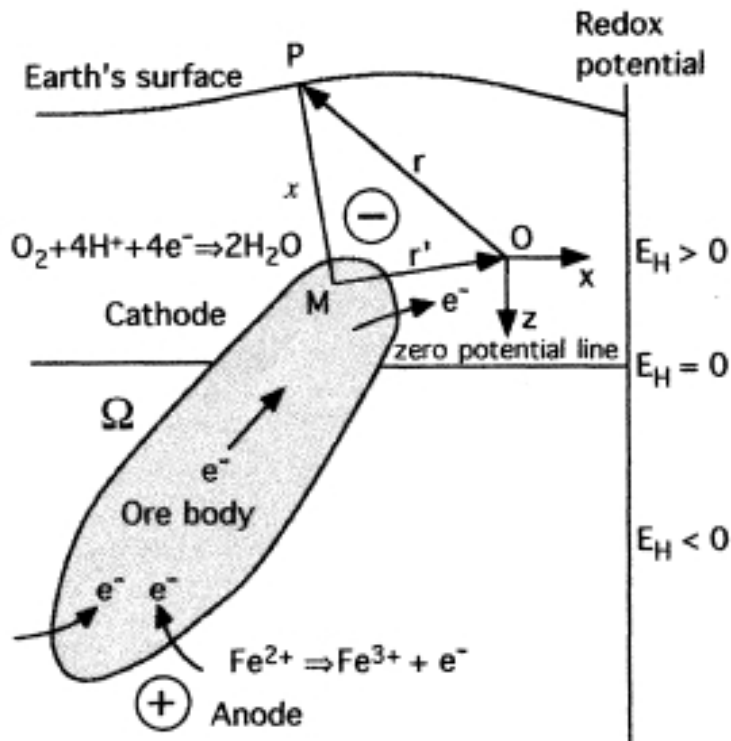
# Location of geoelectric and VLF anomaly also shows large self potential



SP measurements are easy to realize:  
2 non-polarizable electrodes,  
a voltmeter and 2 cables, that's all.



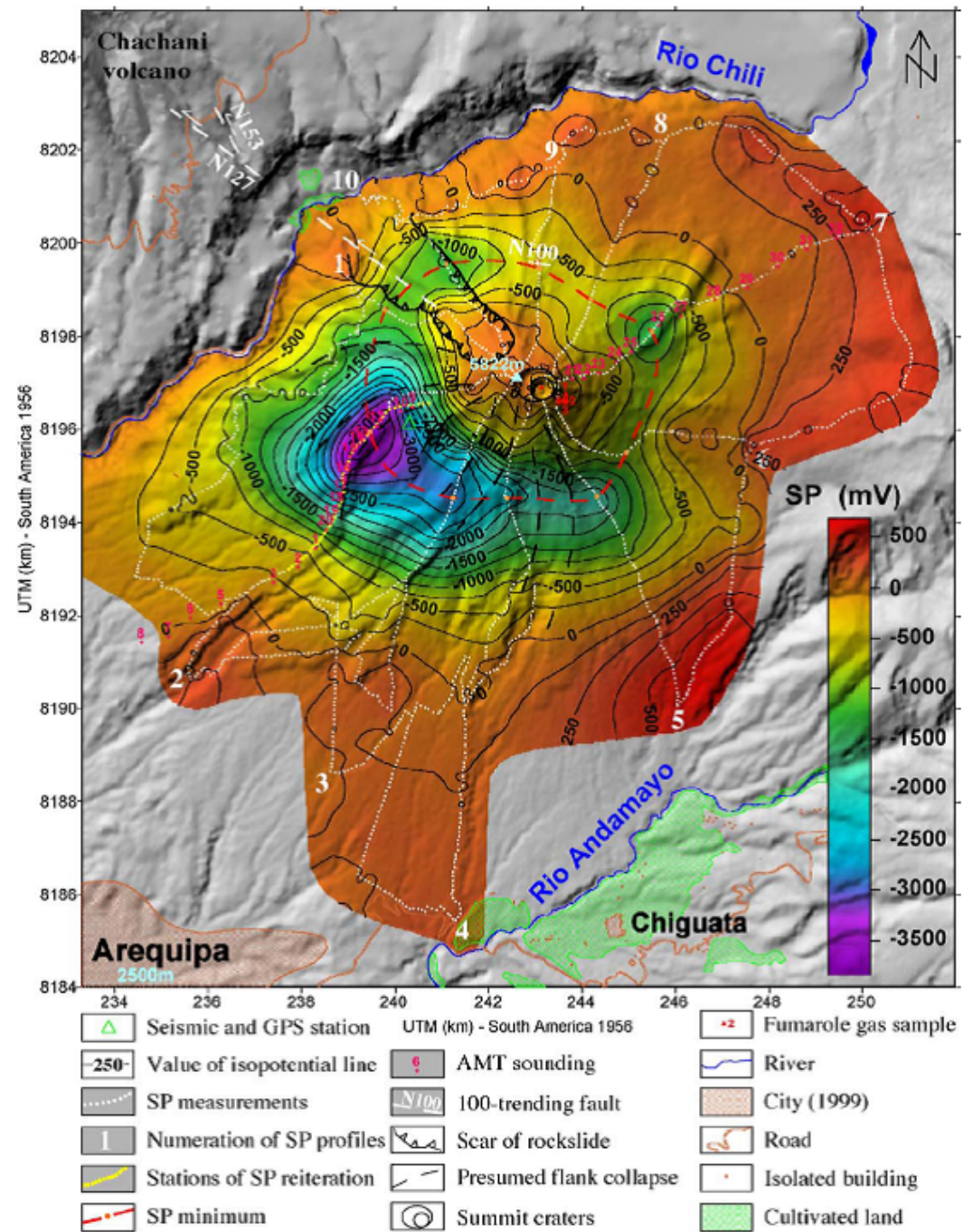
# The geo-battery



Revil (2001)

For an SP anomaly to develop at ore bodies it is decisive according to Sato & Mooney (1960) that an electronic conductor intersects domains of different redox potential. Above the groundwater surface the environment is oxidizing (through penetration of atmospheric oxygen), below it is reducing. The redox potential  $E_H$  is positive in the oxidation zone, negative in the reduction zone. Are there now – not connected – electronic conductors in the ground, and one measures the potential against a non-polarizable probe close by, the potential difference is identical to zero. However, if one connects these individual bodies through the aquifer top, a compensating electron current will flow in the conductor. In the upper part of the conductor (cathode) electrons pass into the surrounding medium, in the lower part (anode) they enter again. At the surface this current is measured as a voltage drop against a distant reference point.

Self potential  
(streaming potential) at  
Volcán Misti (Perú)  
indicates hydrothermal  
circulation and high  
risk for the city of  
Arequipa



Finizola et al. (2004)



Thanks to all Latin American colleagues, those hard-working students and to German Science Foundation who made the Andean research possible!



Lecture notes online:

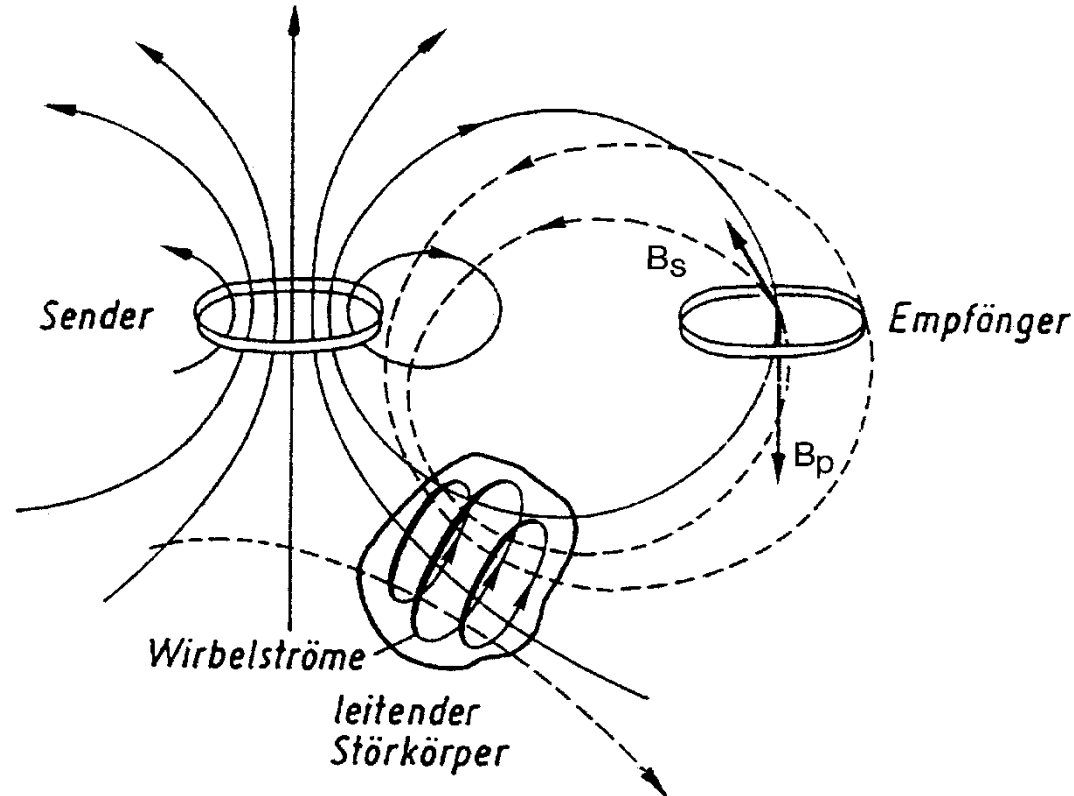
[http://userpage.fu-berlin.de/~hbrasse/EM-methods\\_part-I.pdf](http://userpage.fu-berlin.de/~hbrasse/EM-methods_part-I.pdf)

[http://userpage.fu-berlin.de/~hbrasse/EM-methods\\_part-II.pdf](http://userpage.fu-berlin.de/~hbrasse/EM-methods_part-II.pdf)

Password for all documents: "mt-fu"



# Controlled source methods in frequency and time domain



magnetic field lines in the HLEM layout.  $B_p$  is the primary,  $B_s$  the secondary field at the location of the receiver coil.

# Possible configurations

Horizontal coplanar (HLEM)



Vertical coaxial (VLEM)



Perpendicular



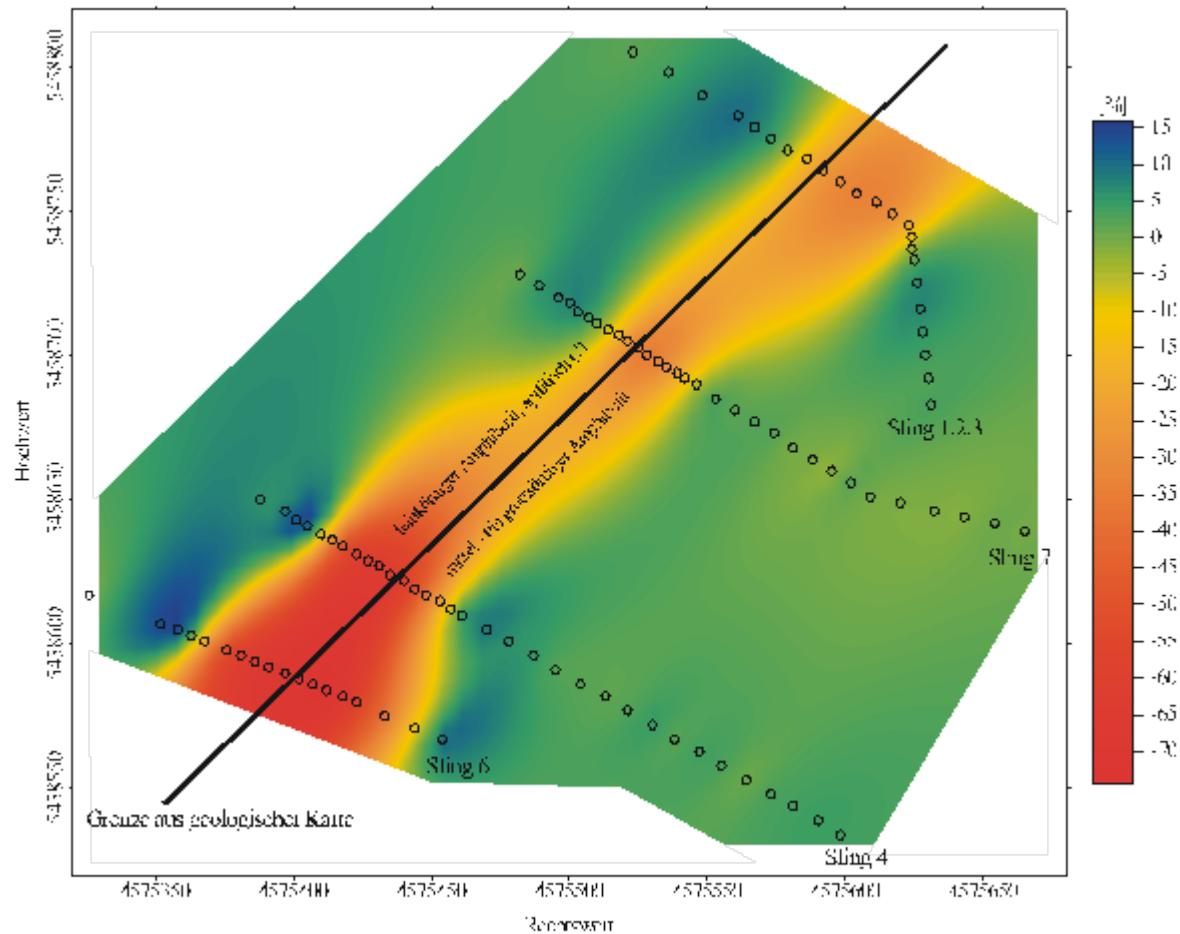
Vertical coplanar



Wire-loop



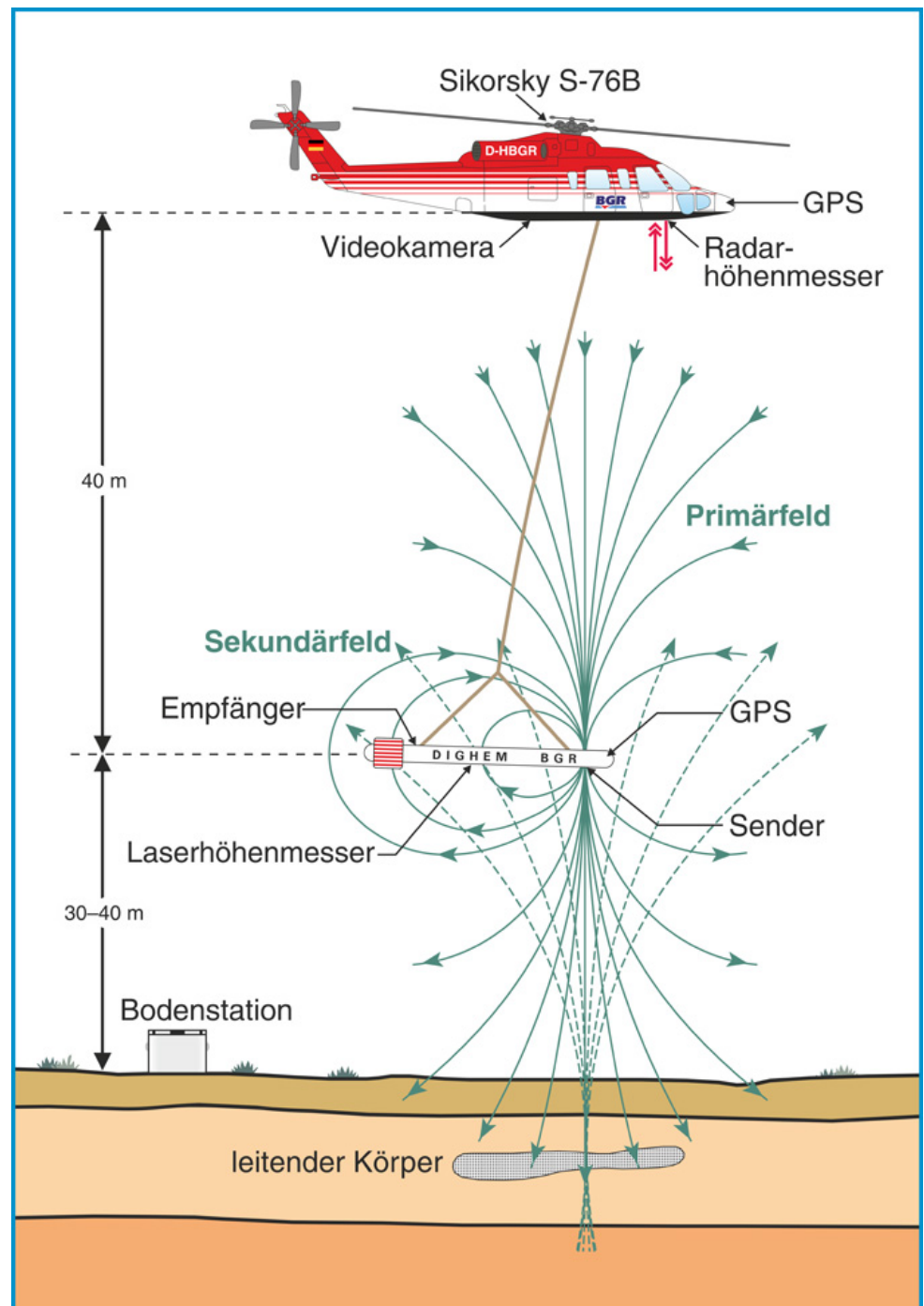




Example of a Slingram anomaly (in-phase) along a fault zone in the Bohemian Forest near the border Germany/Czech Republic. Excursion report FU Berlin 1998.



# Helicopter EM





Layout of aero-electromagnetic devices. Links: Bird at a helicopter, right top: TEM-System (Fugro Airborne Surveys, [www.fugroairborne.coft.au/index.shtml](http://www.fugroairborne.coft.au/index.shtml)), right below: Helicopter-TEM to detect UXO (unexploded – also unexplored – ordnance) (Oak Ridge Airborne Geophysical System, from: Beard et al., Geophysics, 69, 2004).

Figure 1 is a map of the Florida Bay area showing apparent resistivity. The map is bounded by 81° to 80° 30' longitude and 25° to 25° 30' latitude. A color scale on the right indicates apparent resistivity in ohm-m, ranging from 1 (blue) to 200 (dark red). The map shows various geographical features including Cape Sable, Taylor Slough, Barnes Sound, and Key Largo. A legend in the bottom left corner identifies river (pink), canal (blue), and road (red) features. A scale bar at the bottom indicates distances from 0 to 10 km. The map displays a complex pattern of resistivity values, with higher resistivity (red/orange) concentrated in the central and eastern parts of the bay, and lower resistivity (blue) in the western and southern parts.

# Salt water intrusion in Florida

